TotalControl

TotalControl

Advanced integrated supervisory and wind turbine control for optimal operation of large Wind Power Plants

Validation of controller adaptations
Deliverable no. D3.7

Delivery date: (31.05.2022)
Lead beneficiary: ORE
Dissemination level: Public

This project has received funding from the European Union's Horizon 2020 Research and Innovation Programme under grant agreement No. 727680

Author(s) information (alphabetical):		
Name	**Organisation**	**Email**
Ervin Bossanyi	DNV	ervin.bossanyi@dnv.com
Ian Browne	DNV	Ian.Browne@dnv.com
Morven Fraser	ORE	morven.fraser@ore.catapult.org.uk
Will Keogh	DNV	william.keogh@dnv.com
Elliot Simon	DTU	ellsim@dtu.dk
Nick Skeen	DNV	Nicholas.Skeen@dnv.com

Document information

Version	Date	Description		
		Prepared by	**Reviewed by**	**Approved by**
1	31.05.2022	Authors as above	Alasdair MacLeod Ervin Bossanyi	Ervin Bossanyi

TABLE OF CONTENTS

EXECUTIVE SUMMARY

Work Package 3 of the TotalControl project is concerned with developing and testing adaptations of the wind turbine controller which could be beneficial in the context of wind farm control. In Task 3.1, various controller adaptations were developed, and tested in simulations, while in Task 3.2, controller adaptations were implemented and tested on a real turbine in the field, namely the 7MW Levenmouth Demonstration Turbine (LDT) just off the coast of Eastern Scotland. This document is a report on those field tests, covering the implementation of all the different tests and the data collected, together with some preliminary analyses of the experimental results.

The following experiments were performed:

- Yaw misalignment tests, useful for wake steering control for wind farms
- Delta control tests, useful for axial induction control for wind farms, power curtailment and some grid ancillary services
- Derating tests, for power curtailment and load minimisation
- LiDAR-assisted control tests, using wind preview information from a forward-facing LiDAR to improve the control action and reduce loads
- Enhancements to the individual pitch control, to further reduce loads and allow the use of cheaper sensors
- Fast frequency response tests, intended to help enhance grid stability in the presence of a high penetration of renewables

The experiments have yielded a large amount of valuable data, including concurrent inflow and wake flow data from two scanning LiDARs which were installed for the project, as well as met mast data and turbine performance and loading data. The data will continue to be analysed well beyond the end of the TotalControl project, and further results will be published in due course.

INTRODUCTION

Work Package 3 of the TotalControl project is concerned with developing and testing adaptations of the wind turbine controller which could be beneficial in the context of wind farm control.

In Task 3.1, a number of controller adaptations were developed, and tested in simulations. The results are reported in the following Task 3.1 deliverables:

- D3.1 [1] reports on the aeroelastic model and design loads of the 7MW turbine, which was used for the controller adaptations developed as part of Work Package 3.
- D3.2 [2] describes several adaptations concerned with active power control and the provision of grid ancillary services.
- D3.3 [3] is concerned with active damping of tower loads.
- D3.4 [4] covers the development of a Model Predictive Controller (MPC).
- D3.5 [5] describes algorithms for LiDAR-assisted control (LAC) and individual pitch control (IPC), both aimed at reducing tower loads, and also blade loads in the case of IPC.

In Task 3.2, a number of these adaptations were tested in the field, using the 7MW demonstration turbine at Levenmouth on the East coast of Scotland. This report, deliverable D3.7, is the last deliverable from Work Package 3, and is a report on these field tests. The deliverables from Task 3.2 are as follows:

- D3.6 [6] describes the LiDARs which installed on the 7MW turbine for the field tests.
- D3.7 is this report, describing the field tests of controller adaptations on the 7MW turbine.
- D3.8 [7] further develops the MPC controller of D3.4 to the point of being ready for implementation on the 7MW turbine, taking account of all real-world practicalities.
- D3.9 [8] reports on the use of the LiDAR and turbine measurements together with CFD analysis to model the flow in the induction zone in front of the turbine.

The 7MW turbine controller was modified to include a number of different field tests, as follows:

- Yaw misalignment tests – with particular application to wake steering control on a wind farm, the turbine was run at different yaw misalignment settings in order to measure the power and thrust of the turbine, with the rear-facing LiDAR used to measure the downstream wake development. This required no significant changes to the turbine controller, needing only an offset to be introduced to the wind vane signal to induce a yaw misalignment.
- Delta control tests – with application to axial induction control on a wind farm, and also any grid-mandated power curtailment, this algorithm allows the power and thrust to be reduced by a defined amount at any operational wind speed. The rear-facing LiDAR was again used to measure the effect on the turbine wake. The algorithm is described in Appendix 1.
- Derating tests: for curtailment purposes, two different ways to reduce the turbine rated power, which have different effects on the turbine loads, were developed as described in D3.2 [2].

- LiDAR-assisted control: using the forward-facing LiDAR to provide a preview of the approaching wind, a feed-forward term is added to the controller to help reduce pitch duty and tower loading, as described in D3.5 [5].
- Individual pitch control tests: the turbine already uses 1P-IPC to reduce 1P blade fatigue loads, using blade root load measurements. Two additional features are tested here, as reported in D3.5 [5], namely the use of potentially cheaper and more robust tower-top strain gauges instead of blade root gauges, and the addition of 2P-IPC to reduce the 3P non-rotating fatigue loads.
- Delta control tests – with application to axial induction control on a wind farm, and also any grid-mandated power curtailment, this algorithm allows the power and thrust to be reduced by a defined amount at any operational wind speed. The rear-facing LiDAR was again used to measure the effect on the turbine wake. The algorithm is described in Appendix 2.

This deliverable is a report on all of these field tests.

1. THE 7MW LEVENMOUTH DEMONSTRATION TURBINE

This section describes the turbine on which the controller adaptations were tested.

1.1. The Levenmouth site

The Offshore Renewable Energy (ORE) Catapult's Levenmouth Demonstration Turbine (LDT) is located off the coast of Methil, Fife. The turbine is the world's most advanced, open-access offshore wind turbine dedicated to research and development. The company Wood. operates as the operations and maintenance (O&M) contractor at the site and were present to facilitate all testing carried out.

1.2. Description of the turbine

Table 1 summarises some of the key information about the turbine.

Table 1 LDT Parameters

Parameter	Specification
Original Equipment Manufacturer (OEM)	Samsung Heavy Industries (SHI)
Capacity	7 MW
Hub Height	110.6 m
Rotor Diameter	171.2 m

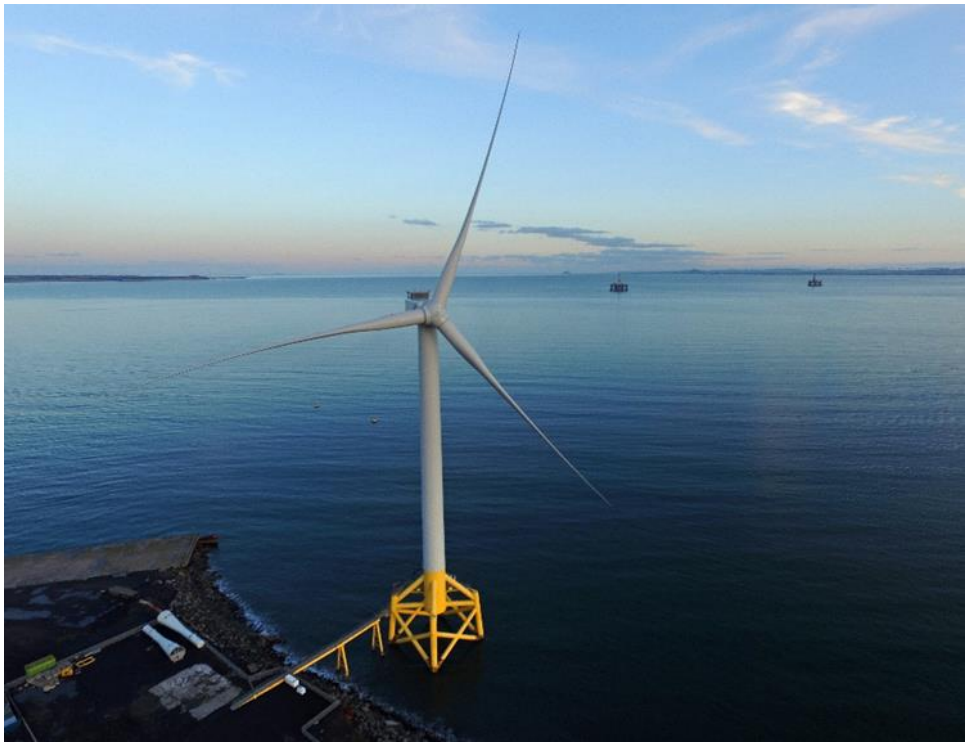

Figure 1 Levenmouth Demonstration Turbine

1.2.1.1. Turbine controller

With the exception of the yaw misalignment tests, the testing of controller adaptations inevitably needed modifications to the controller software, to implement each of the new features and associated testing modes (such as toggling a feature on and off at regular intervals). The turbine controller was software had originally been provided by DNV, who were therefore able to make the necessary changes, and test them against a real-time turbine simulator using the *Bladed* hardware test module. The changes for most of the tests were incorporated into a single controller version upgrade. Once the fast frequency response algorithm had been implemented, this was incorporated into a second version upgrade.

1.2.1.2. Safety considerations

Tests involving changes to the turbine controller clearly involve some risks. To minimise any danger of damaging the turbine, the following precautions were taken:

- The controller already includes a comprehensive set of alarms and safety features designed to ensure that the turbine always operates safely, or shuts down in a safe way if any abnormal conditions are detected which could compromise safety. Care was taken to ensure that these features, which override the controller, remained in place.
- Every controller modification was tested using detailed aeroelastic simulations with the *Bladed* code, in which the simulated turbine communicated through a DLL interface to the actual turbine controller software compiled to run on a PC. Simulations were run for a suitable range of wind conditions, so that any potential performance or loading issues could be identified and rectified before the software was installed in the turbine.

- For each test, the test design and simulation results were reviewed and approved by the PAC committee charged with ensuring the safety of the turbine.

1.3. Instrumentation

1.3.1. Met mast

The Meteorological (MET) Mast is located on top of a small hill at the Fife Energy Park, shown in Figure 2. The mast was installed in 2012 to order to provide reference data for the prototype Samsung 7 MW turbine (now Levenmouth Demonstration Turbine) which was commissioned in January 2015. The MET mast sensors measure wind speed, wind direction and air temperature at various heights. Each sensor provides a data value at 1Hz frequency. MET mast data was recorded and used throughout testing.

Figure 2 Onshore Met Mast at LDT site

1.3.2. SCADA system / data collection

The turbine SCADA (supervisory control and data aquisition) condition monitoring system collects data from the wind turbine controller. The SCADA system consists of 574 OEM sensors, each providing data at 1Hz frequency. SCADA data was recorded and used throughout testing.

1.3.3. Additional turbine sensors

As part of an OREC project to create a clone of the Levenmouth wind turbine (CLOWT), additional instrumentation was installed to measure loads on the jacket, transition piece, tower and turbine blades at LDT. Additional instrumentation was also installed to monitor the electrical

equipment of the PCS and pitch system. The CLOWT data monitoring system was used to gather data throughout testing for monitoring and assessing the different test strategies.

1.3.4. LiDAR measurements

For the purposes of this project, the turbine was equipped with two nacelle-mounted LiDAR systems developed by DTU: a forward-facing continuous-wave spinner LiDAR used to measure the wind inflow, and a long-range rear-facing pulsed scanning LiDAR to measure the turbine's downstream wake effects. Full details of the LiDAR systems are provided in Deliverable D3.6 [6][6].

Figure 3 Forward-facing DTU spinner LiDAR installed on turbine nacelle

Figure 4 Rear-facing DTU Long-range WindScanner installed on turbine nacelle

2. YAW MISALIGNMENT TESTS

The yaw misalignment tests were carried out in order to validate model predictions about the effect of yaw misalignment on turbine performance and the behaviour of the turbine wake. This would be important in the context of using the turbine for wake steering control on a wind farm.

Turbine yaw position is controlled by wind direction measurement on the nacelle. The nacelle wind direction measurement is a record of wind direction with respect to North. The signal from the wind direction measurement is used in the turbine controller to control nacelle orientation. The signal has an offset that can be set to account for any offset between the measured yaw misalignment and the actual yaw misalignment. Yaw misalignment is the angle between the incoming flow and the turbine nacelle orientation. Yaw misalignment and wake steering are illustrated in Figure 5.

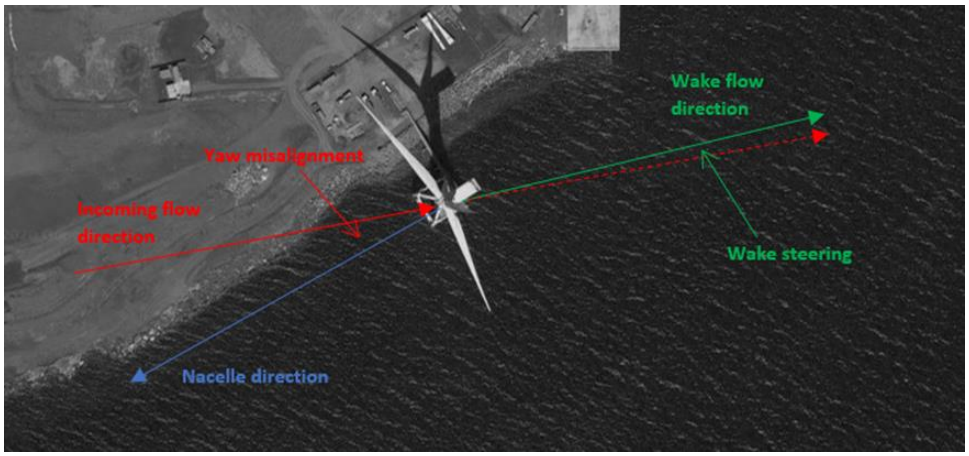

Figure 5 Yaw Misalignment and Wake Steering Image

To artificially yaw the turbine with respect to the incoming wind flow the yaw misalignment offset was adjusted. No further changes to the turbine controller were required.

The aim of the tests was to determine the effect of different yaw misalignments on turbine power, rotor thrust and loads as well as on the turbine's wake, since the wake deficit is affected by the rotor thrust, and the wake itself is deflected laterally as a result of the yaw misalignment.

The measured effect on the turbine power and loads is useful for comparing to *Bladed* predictions, to validate the use of Blade Element Momentum theory for yawed rotors, and the wake deflection is useful for validating the predictions from engineering models of wakes.

2.1. Aeroelastic simulations

To gain approval for these yaw misalignment tests, aeroelastic simulations performed using *Bladed* were used to show that the yaw misalignments would not be expected to cause any unacceptable increase in loading.

2.2. Yaw misalignment test setup

The yaw misalignment tests aimed to:

- misalign the turbine, to the incoming flow, by up to 30 degrees in both directions
- operate in wind speeds up to rated wind speed (11m/s)
- operate at a range of turbulence intensities (5-15%)

The rear-facing LiDAR was set to perform repeating PPI (plan position indicator) scans at zero-elevation angle to provide horizontal cross sections of the wind field downstream of the turbine rotor (i.e. measuring the turbine wake effects). The azimuth range was first set to +/- 30 degrees along the rotor centreline, which was expanded to +/- 60 degrees during the later stages of testing. The pulse length was set to 200 nanoseconds, FFT size of 128 points, accumulation time of 500 milliseconds, scanning speed of 2 degrees per second, and range gates spanning 100 to 2000 meters spaced equally at intervals of 20 meters. This provides an angular resolution of 1 degree, and sampling rate (i.e. 1 complete PPI scan) of 2 Hz for the +/- 30 degrees scans, and 1 Hz for the +/- 60 degrees scans.

The test schedule for the yaw misalignment tests was owned and defined by the ORE Catapult. Testing was undertaken by WOOD. as per ORE Catapult instruction.

2.2.1. Yaw Misalignment Test Stages

To reduce risk of damage to the turbine the tests were performed in a structured and staged manner. The test stages for the yaw misalignment tests are outlined in Table 2.

Table 2 Yaw Misalignment Test Stages

Test Stage	Yaw Misalignment	Stage wind speed limit
Stage 1	+/- 10 degrees	< 8 m/s average
Stage 2	+/- 10 degrees	< 11 m/s average
Stage 3	+/- 20 degrees	< 8 m/s average
Stage 4	+/- 20 degrees	< 11 m/s average
Stage 5	+/- 30 degrees	< 8 m/s average
Stage 6	+/- 30 degrees	< 11 m/s average

2.2.1.1. Yaw misalignment test stage limits

Before advancing to the next test day and test stage, previous test data was analysed to monitor and compare blade loading with test stage limits. Stage gate limits were based on historic loading and turbine design information, these were considered for the following loads:

- Maximum and mean blade flapwise bending
- Equivalent fatigue from flapwise bending
- Maximum and mean blade edgewise bending
- Equivalent fatigue from edgewise bending

If blade load thresholds were exceeded, a full review of the test stage would be performed, and a load analysis done to assess risk of advancing to the next test stage.

2.2.2. Yaw Misalignment Daily Test Procedure

The daily test process involved:

1. Review forecast and identify suitable test period
2. Confirm target yaw misalignment for testing with Wood, recorded in Yaw Misalignment test log
3. Set turbine parameters to adjust yaw error signal to test stage yaw requirement, record yaw offset in test log
4. Start-up turbine, record start time in test log
5. Test for 2hrs
6. Review weather forecast, record in log
7. Repeat steps 6 and 7 until end of test period
8. Shutdown turbine, record time in test log
9. Reset yaw error signal to default offset, checked by operator and 2nd competent person, record value set in the test log and sign and date.
10. Test end

2.3. Yaw misalignment data collected

Yaw misalignment tests were carried out between June 2020 and December 2020. These tests were carried out first as a controller update was not required to implement these tests. Testing was influenced by suitable weather windows and operator availability.

SCADA and MET data were recorded for all tests. CLOWT and LiDAR data were also recorded during tests when the respective systems were not experiencing issues. During tests, accurate measurement of yaw misalignment and incoming flow was taken by the installed front-facing LiDAR. This information was used to validate yaw misalignment readings.

For each of the yaw misalignment targets, the tests aimed to fill the bins of the occurrence matrix presented in Table 3, to monitor test progress. Bins shown in the table are bin centres, each bin was 1 m/s wide. Bin counts were increased when a 10-minute period of data met the bin conditions.

Table 3 Yaw Misalignment test condition occurrence matrix

		Wind Speed bin centre (m/s)								
		3	4	5	6	7	8	9	10	11
Turbulence intensity bin centre (%)	5									
	10									
	15									

Table 4 summarises the bin count and overall test time for each of the test stages carried out for the yaw misalignment tests. Testing was not carried out for the target yaw misalignment angle of

+/- 30 degrees. This was due to the project timeline considerations, and it was agreed that it would be more beneficial to the project to progress to the next test strategy. It was also agreed that once the initial analysis of the test data was complete, that additional testing could be carried out if the results suggested that it would be valuable to test at these additional yaw misalignment angles, and if the project timeline allowed.

Table 4 Yaw Misalignment Test Summary

Test Stage	Yaw Misalignment Target (degrees)	Bins of 10 mins data	Test time (hours)
1&2	+10	109	26.25
1&2	-10	70	22
3&4	+20	109	36.5
3&4	-20	126	24.75
All Testing		**414**	**109.5**

2.4. Results

The test data was grouped into experimental periods corresponding to all the test data collected during each day of testing for this experimental mode. The experimental periods vary according to the day of testing and how much data was able to be collected on the day. For each experimental period, the rear facing Lidar data was time-averaged over the over the whole period, producing an individual spatial wind speed scan at hub height behind the turbine. The example in Figure 6 is an averaged scan plot for one of the experimental periods, with 10° yaw offset. The lateral deflection of the wake is clearly visible.

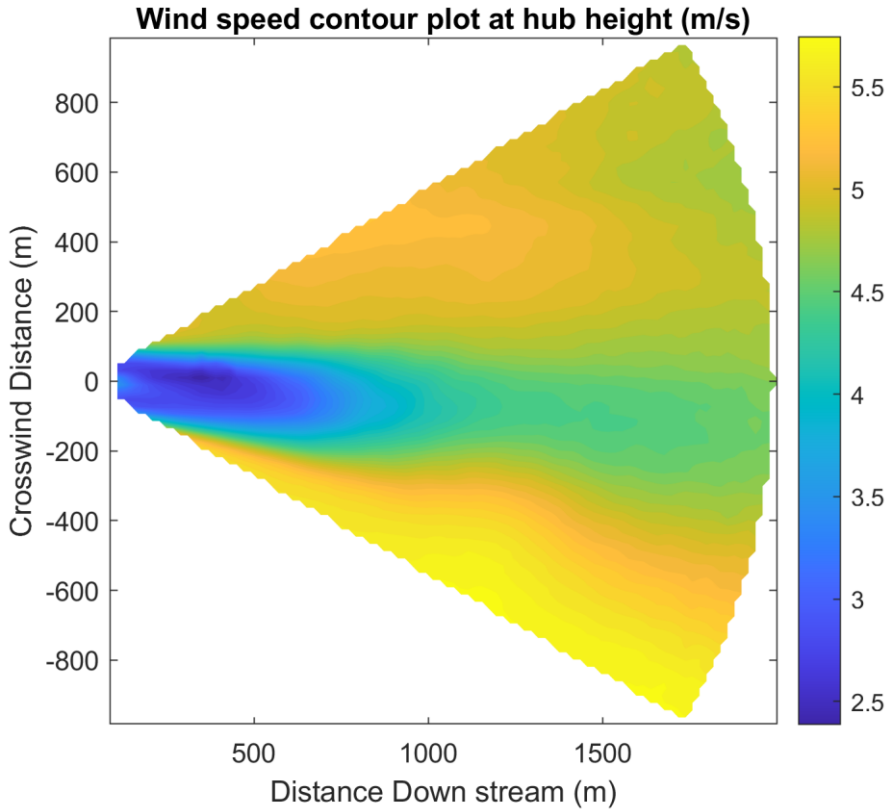

Figure 6 Averaged lidar scan at hub height for yaw offset 10 degrees, run time 390 minutes, 744 LiDAR scans used

For each experimental period, the line-of-sight LiDAR wind speed data was resolved into the mean wind direction (assuming zero mean lateral flow) and time-averaged over the period. Wind field 'slices' from one to eleven diameters downstream were taken, and a Gaussian profile fitted to each slice. The Gaussian parameters defined the ambient wind speed (allowing for any underlying linear variation), the centreline deficit, wake width, and the centreline lateral deflection. Figure 7 below shows the gaussian fits for a given experimental period. The distances downstream are normalised in terms of rotor diameters. Plots like Figure 7 below for the full set of experimental periods used for this analysis are shown in Appendix 3.

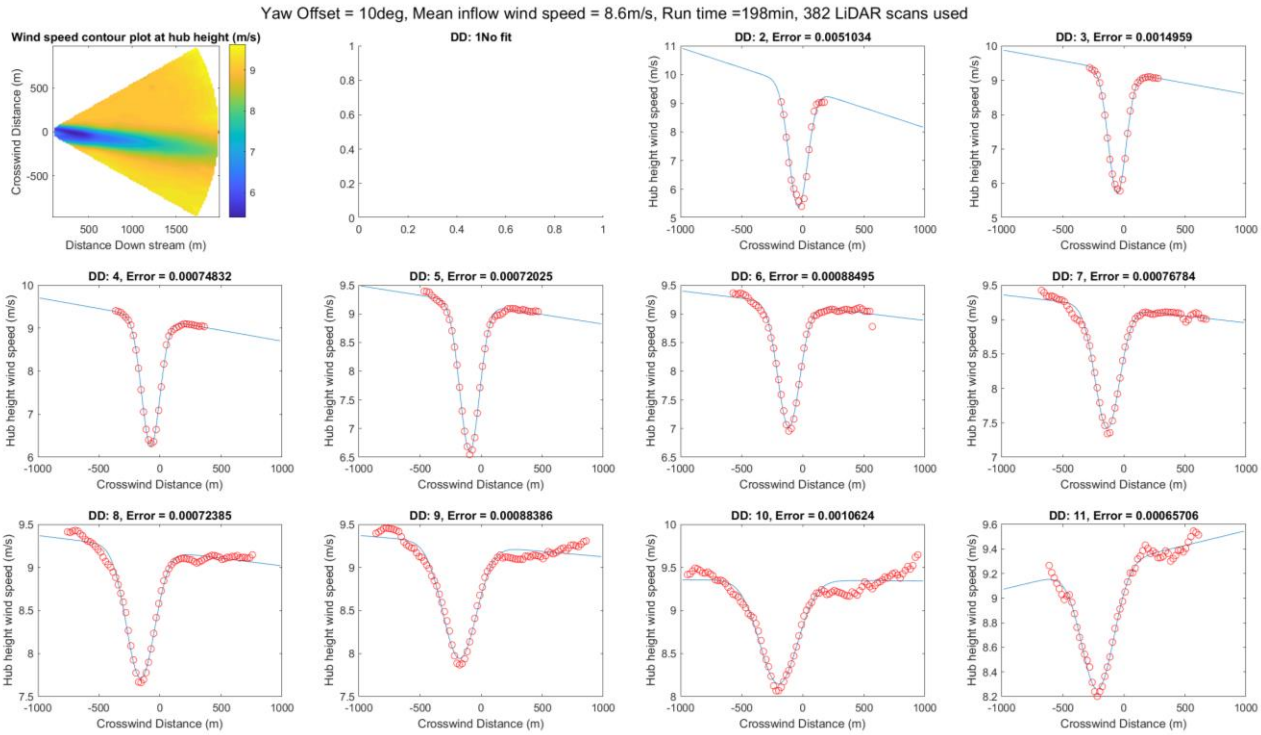

Figure 7 Gaussian fits applied at each downstream distance for a given experimental period

The Gaussian fits provide a centre deficit crosswind displacement at each distance downstream for each of the experimental periods used. This crosswind displacement was extracted and binned according to the yaw offset used. For each yaw offset, the crosswind displacement was plotted against downstream distance to show the resultant wake deflection. Figure 8 below shows the wake deflection for each yaw offset tested. The mean centre deficit crosswind displacement was used for each downstream distance. Only a single experimental period for the minus 20-degree yaw offset condition was collected. The Gaussian fit error on this experimental period was relatively high, therefore the resultant wake deflection for this yaw offset condition has high uncertainty. The other yaw offset conditions had multiple experimental periods with low error Gaussian fits. This increases the confidence in the wake deflection observed for those experimental conditions.

It can be seen that the wake is indeed deflected as a result of the applied offset. These results will be very useful for comparing the measured wake deflections against candidate wake deflection models so that the accuracy of different wake deflection models can be validated.

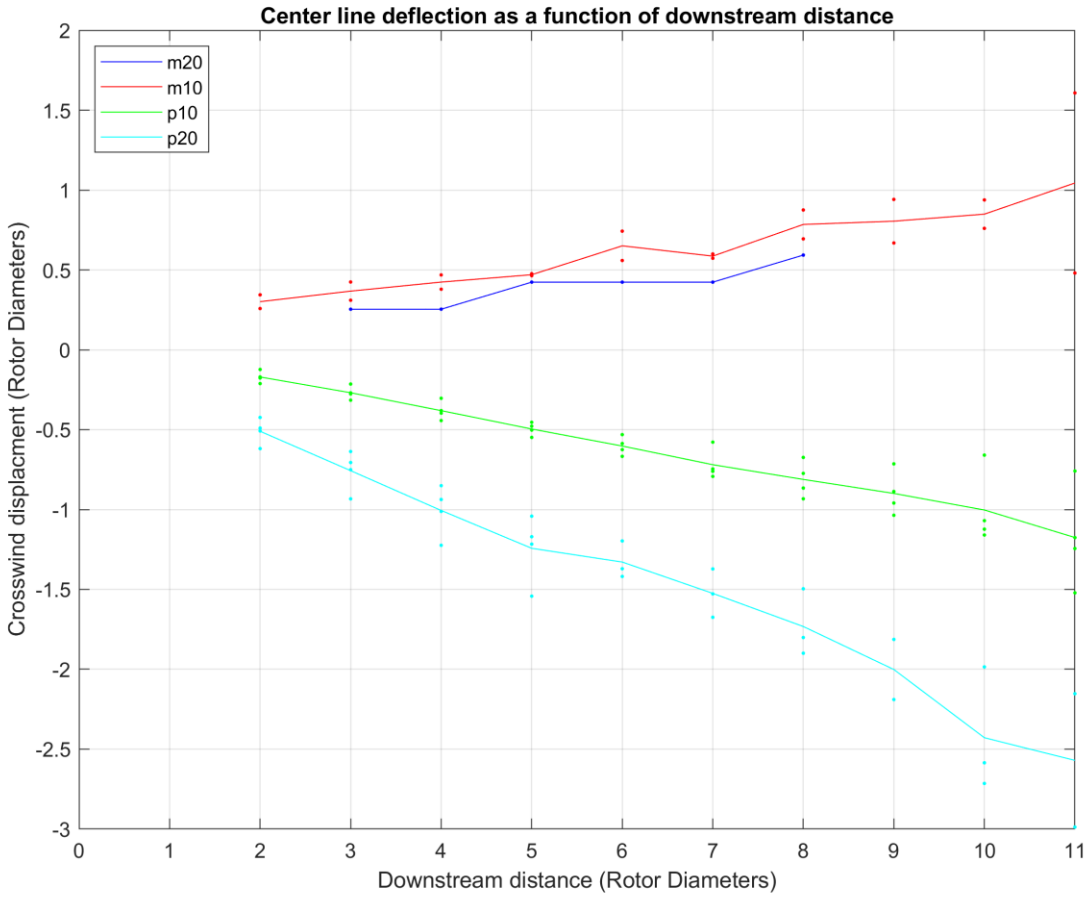

Figure 8 Centre line wake deflection for each yaw offset tested

3. DELTA CONTROL TESTS

Here, delta control refers to a deliberate reduction in power output by a given amount at any operational wind speed. The name delta control originates from the possibility to continually generate less than physically possible, so as to have a margin of 'spinning reserve' available to the grid at short notice (in situations where that might be valuable enough to compensate for the lost generation). However, it also has application for axial induction control on a wind farm, since by reducing the power at an upstream turbine, the thrust will also decrease, weakening the wake, and hence allowing wake-affected turbines further downstream to experience higher wind speeds, potentially increasing the total wind farm power, and lower levels of added turbulence, resulting in reduced fatigue loading.

Delta control is achieved by a combination of increasing the fine pitch angle and changing the torque control so that torque is increased and rotor speed consequently reduced. For axial induction control, it is advantageous to reduce the thrust as much as possible while reducing the power as little as possible, as explained (and illustrated for the Lillgrund turbines) in deliverable D2.3 [18], and although the settings tested here were not actually optimised in that way, their effect should be similar.

Appendix 1 presents the design of the algorithm and the simulation results demonstrating its operation.

The delta control tests are intended to demonstrate the correct operation of a delta control algorithm, and also confirm model predictions of reduced velocity deficits in the wake by making use of measurements from the rear-facing LiDAR.

3.1. Delta control test setup

The delta control tests aimed to:

- Test at the following blade fine pitch angle (FPA) setpoints:
  - -0.5 degrees (default)
  - 2.9 degrees
  - 5.7 degrees
  - 10 degrees
- operate in wind speeds up to rated wind speed (11m/s)
- operate at a range of turbulence intensities (5-15%)

The test schedule for the delta control tests was owned and defined by the ORE Catapult. Testing was undertaken by WOOD. as per ORE Catapult instruction.

3.1.1. Delta Control Test Stages

To reduce risk of damage to the turbine the tests were performed in a structured and staged manner. The test stages for the delta control tests are outlined in Table 5.

Table 5 Delta Control Test Stages

Test Stage	Fine Pitch Angle	Stage wind speed limit
Stage 1	-0.5 degrees	< 8 m/s average
Stage 2	-0.5 degrees	< 11 m/s average
Stage 3	2.9 degrees	< 8 m/s average
Stage 4	2.9 degrees	< 11 m/s average
Stage 5	5.7 degrees	< 11 m/s average
Stage 6	10 degrees	< 11 m/s average

3.1.2. Delta Control Test Stage Limits

Before advancing to the next test day and test stage, previous test data was analysed to monitor and compare blade loading with test stage limits. Stage gate limits were based on historic loading and turbine design information, these were considered for the following loads:

- Maximum and mean blade flapwise bending
- Equivalent fatigue from flapwise bending
- Maximum and mean blade edgewise bending
- Equivalent fatigue from edgewise bending

If blade load thresholds were exceeded, a full review of the test stage would be performed, and a load analysis done to assess risk of advancing to the next test stage.

3.1.3. Delta Control Daily Test Procedure

Before daily delta control tests could proceed, commissioning tests were carried out to ensure the necessary controller updates had been implemented correctly and ran without issue. These tests were carried out successfully.

The daily test process involved -

1. Review forecast and identify suitable test period
2. Confirm target FPA for testing with Wood, recorded in Delta Control test log
3. Set turbine parameters to adjust the FPA to test stage requirement, record FPA in test log
4. Start-up turbine, record start time in test log
5. Test for 2hrs
6. Review weather forecast, record in log
7. Repeat steps 6 and 7 until end of test period
8. Shutdown turbine, record time in test log
9. Reset FPA to default, checked by operator and 2nd competent person, record value set in the test log and sign and date.
10. Test end

3.2. Delta Control Data collected

Delta Control tests were carried out between June 2021 and February 2022. The test schedule was influenced by suitable weather windows and operator availability. There was also significant turbine downtime between October 2021 and February 2022 that prevented testing.

SCADA and MET data were recorded for all tests. CLOWT and LiDAR data were also recorded during tests when the respective systems were not experiencing issues.

For each of the blade fine pitch angle setpoints, the tests aimed to fill the bins of the occurrence matrix presented in Table 6. The occurrence matrix allowed test progress to be monitored and informed the upcoming test schedule. Bins shown in the table are bin centres, each bin was 1 m/s wide. Bin counts were increased when a 10-minute period of data met the bin conditions.

Table 6 Delta Control test condition occurrence matrix

		Wind Speed bin centre (m/s)												
		3	4	5	6	7	8	9	10	11	12	13	14	15
Turbulence intensity bin centre (%)	5													
	10													
	15													

Table 7 summarises the bin count and overall test time for each of the test stages carried out for the delta control tests.

Table 7 Delta Control Test Summary

Test Stage	Blade Fine Pitch Angle Setpoint (degrees)	Bins of 10 mins data	Test time (hours)
1	-0.5 (default)	73	14.5
2	-0.5 (default)	1	10.5
3	2.9	34	6
4	2.9	11	7.5
5	5.7	42	11.25
6	10	39	7.5
All Testing		**200**	**57.25**

Power curves were plotted for each of the fine pitch angles. This allowed for comparison with the modelling work completed, to ensure the derating strategy was operating as expected and as a check of test progress. Figure 9 shows the power curves plotted using 10-minute averages of data gathered during the delta control tests. Figure 10 shows the blade pitch vs windspeed for each fine pitch angle tested.

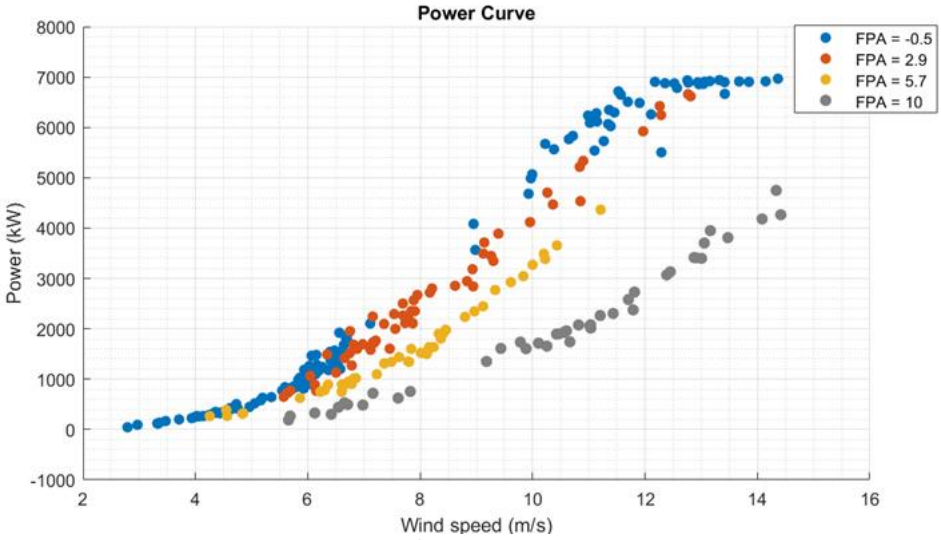

Figure 9 Power vs wind speed for each delta setting (10-minute average points)

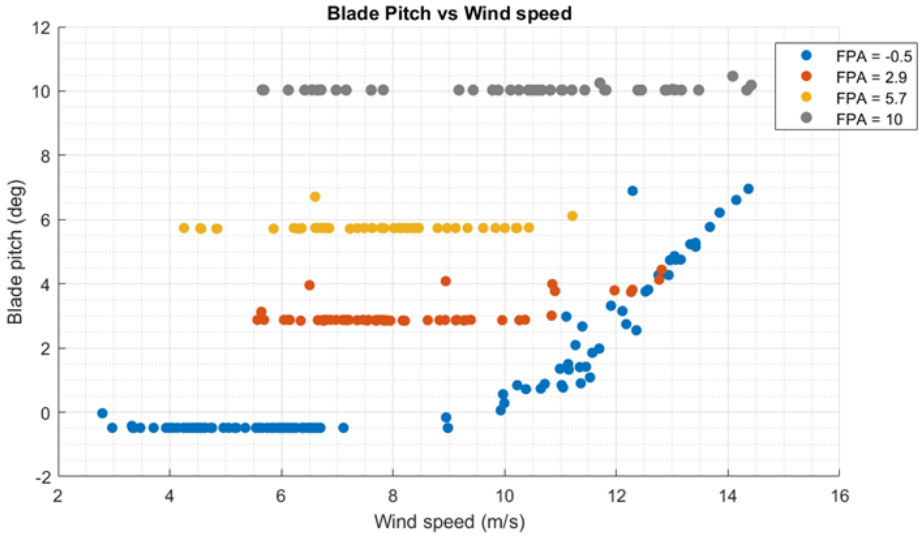

Figure 10 Blade pitch vs wind speed for each delta setting (10-minute average points)

3.3. Results

The following section presents the results of the collected SCADA data following the procedure outlined above. The results include data from each of the four fine pitch angle configurations outlined in the above section. The figures below show the measured power, collective pitch angle, rotor speed and computed thrust vs wind speed for both the collected SCADA data and *Bladed* simulations using the turbine model described in Appendix 1.The data points shown in each figure are 1-minute mean values, and the lines represent the mean values over wind speed bins of 0.5 m/s increments. As described in Appendix 1 there is a speed exclusion zone included in the turbine control algorithm, and in consequence, there are two characteristic curves for speed and thrust, one above the speed exclusion zone and one below the speed exclusion zone. Therefore, two figures are presented for thrust and speed.

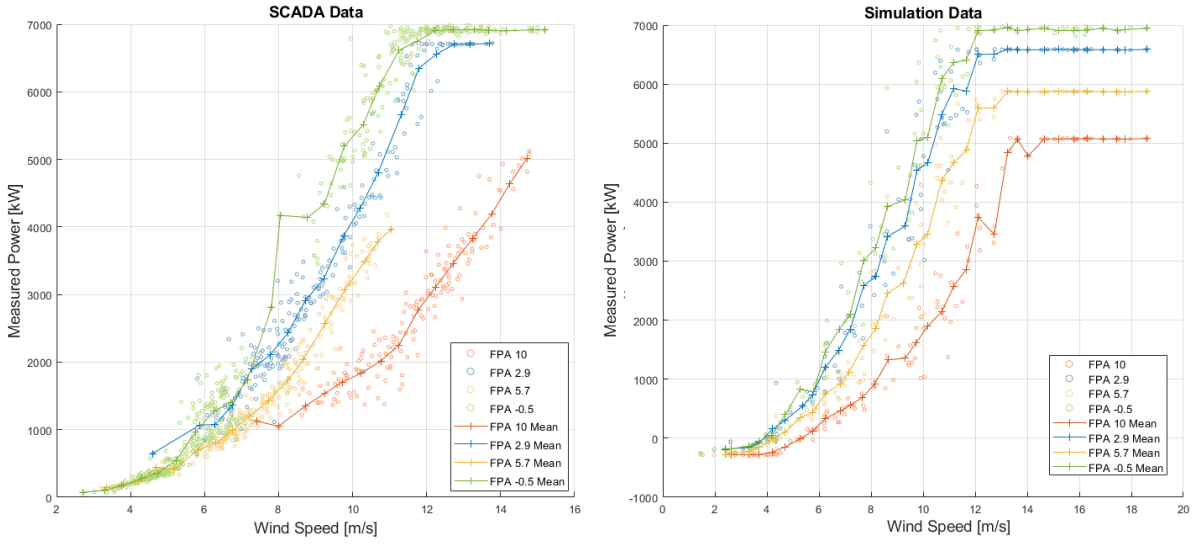

Figure 11 Measured power vs wind speed across each delta control fine pitch angle for SCADA and Simulation data (note different axes: simulation data extends to higher wind speeds)

Figure 11 above shows a comparable relative change in measured power across wind speed for the collected SCADA data and the simulations data. Unfortunately, the spread of collected SCADA data is dependent on the weather conditions during testing, as a result there is no data with high enough wind speed for fine pitch angle configurations of 5.7 and 10 degrees to reach above their respective rated wind speeds. However, there is enough data collected to confirm excellent correspondence between measured and simulated results for all settings, indicating that if the wind speed had been high enough the data for FPA 5.7 degrees and 10 degrees would have produced a rated power level very similar to the simulations as both are producing very similar curves in below rated conditions.

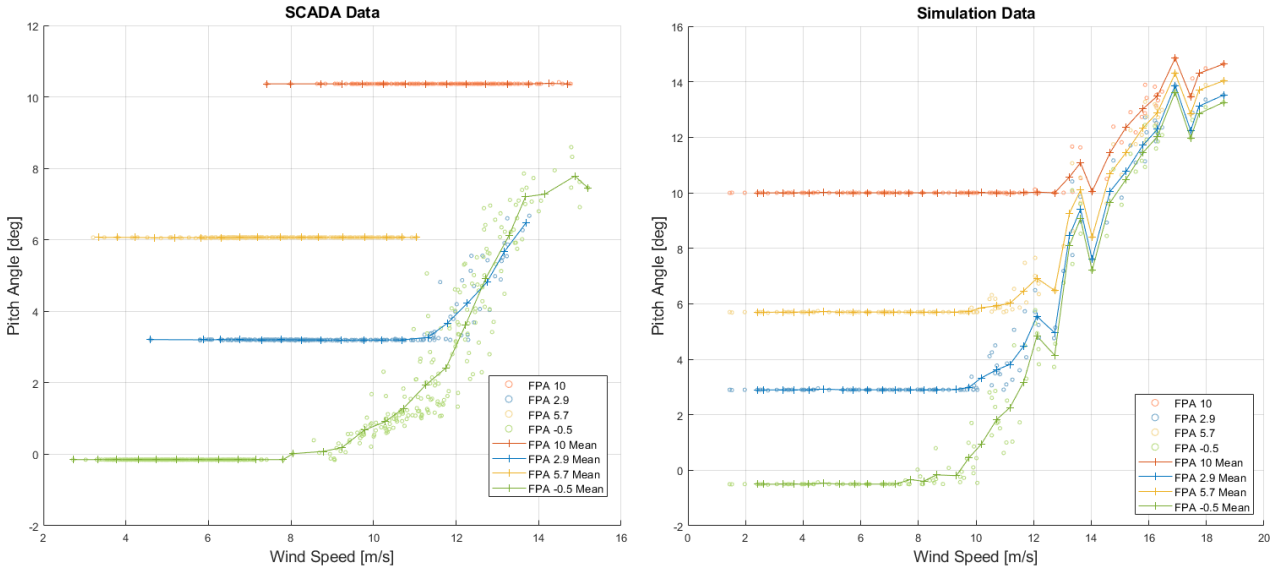

Figure 12 Pitch angle vs wind speed across each delta control fine pitch angle for SCADA and Simulation data

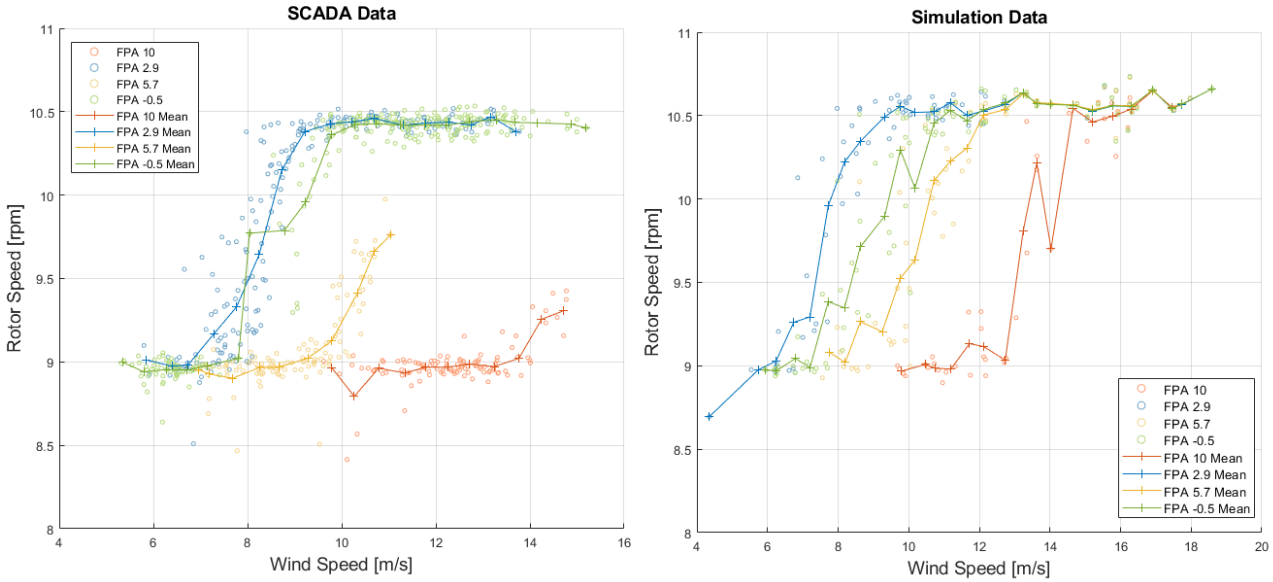

Figure 13 Rotor speed vs wind speed across each delta control fine pitch angle for SCADA and Simulation data (Above speed exclusion zone)

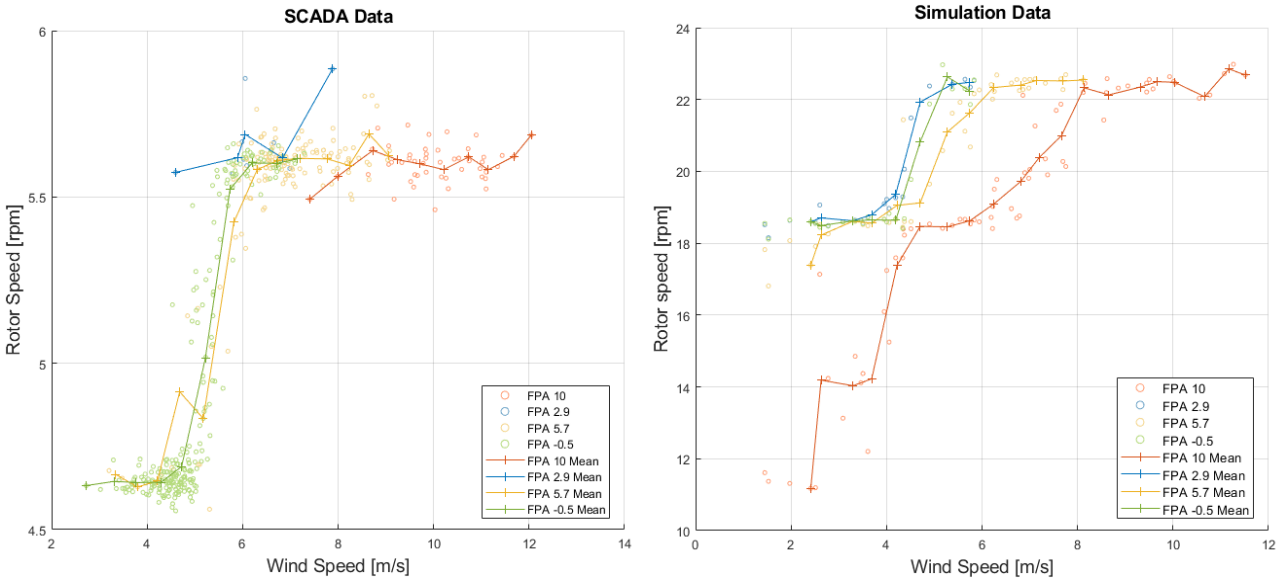

Figure 14 Rotor speed vs wind speed across each delta control fine pitch angle for SCADA and Simulation data (Below speed exclusion zone)

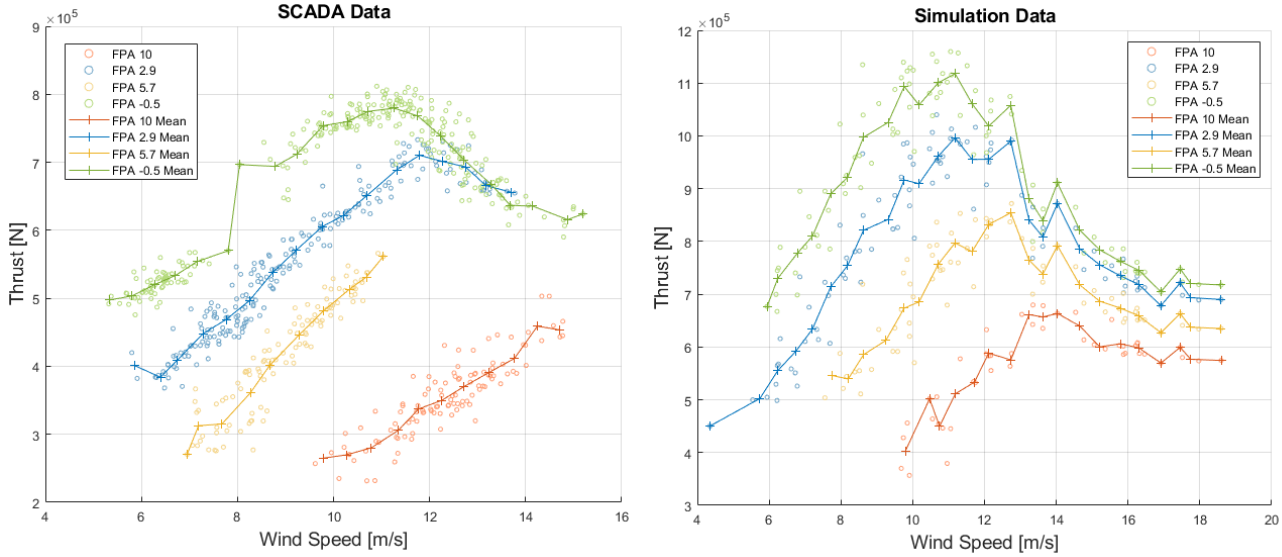

Figure 15 Rotor thrust vs wind speed across each delta control fine pitch angle for SCADA and Simulation data (Above speed exclusion zone)

The relative change in thrust across the different fine pitch angle configurations for the SCADA data and simulations data is very similar, with a drop in thrust of across each fine pitch angle configuration is consistent with the expectations based on the report in Appendix 1. (The absolute values of measured thrust are lower, but this is probably just due to the calibrations applied when calculating the thrust from blade strain gauge measurements.)

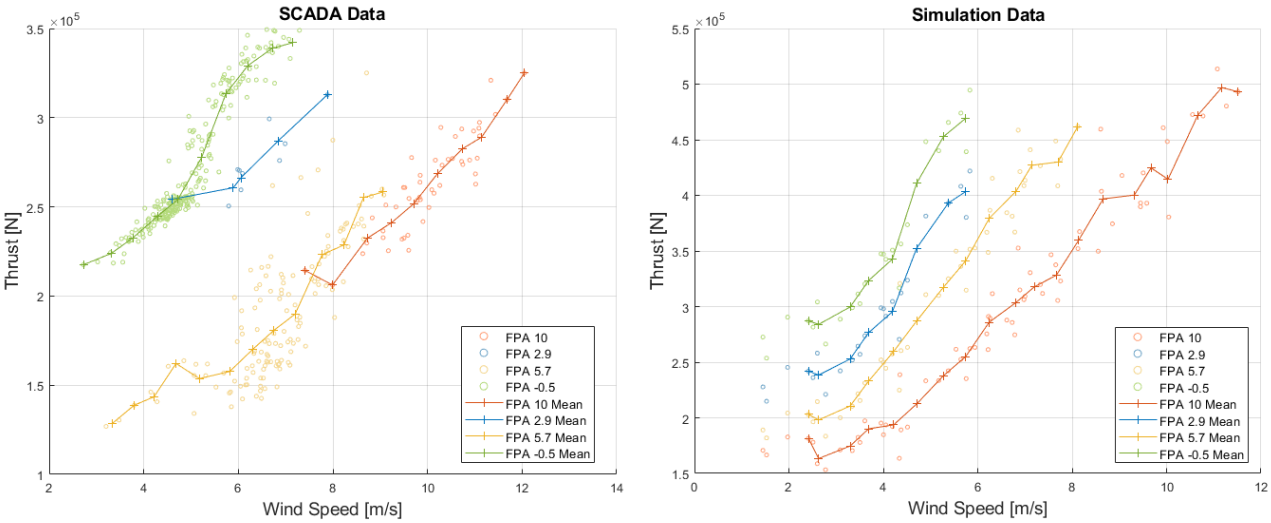

Figure 16 Rotor thrust vs wind speed across each delta control fine pitch angle for SCADA and Simulation data (Below speed exclusion zone)

3.3.1. Wake deficit analysis

The following figures show the wake deficit of the turbine at varying downstream diameters. This data was collected using the rear facing LiDAR, and processed in the same way as for the yaw tests described in Section 2.4.

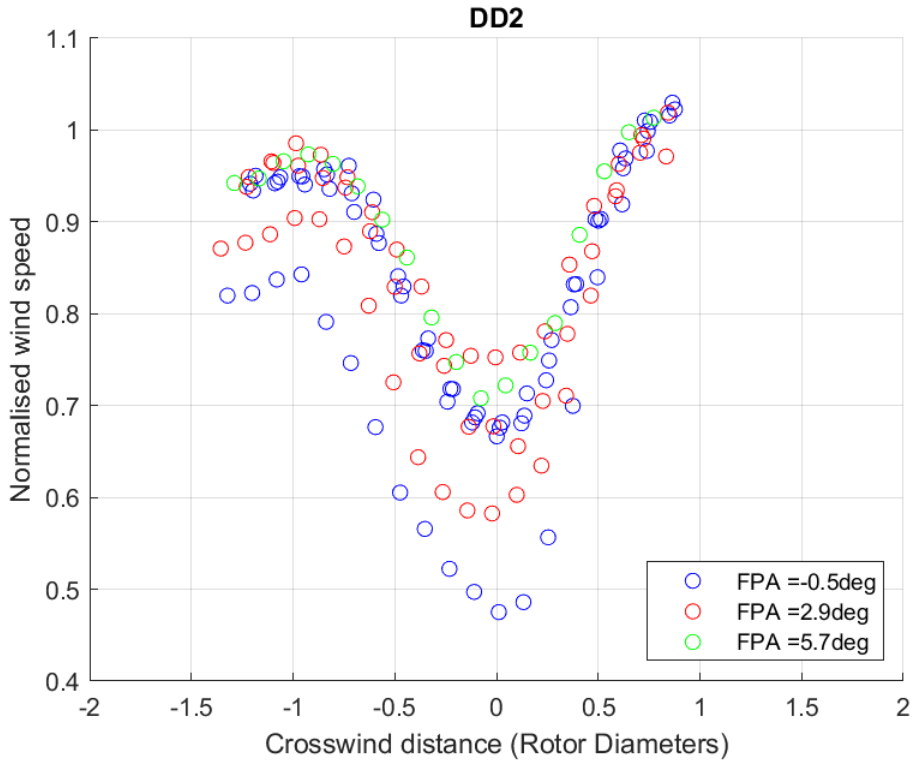

Figure 17 Wake deficit across each fine pitch angle setting for 2 diameters downstream

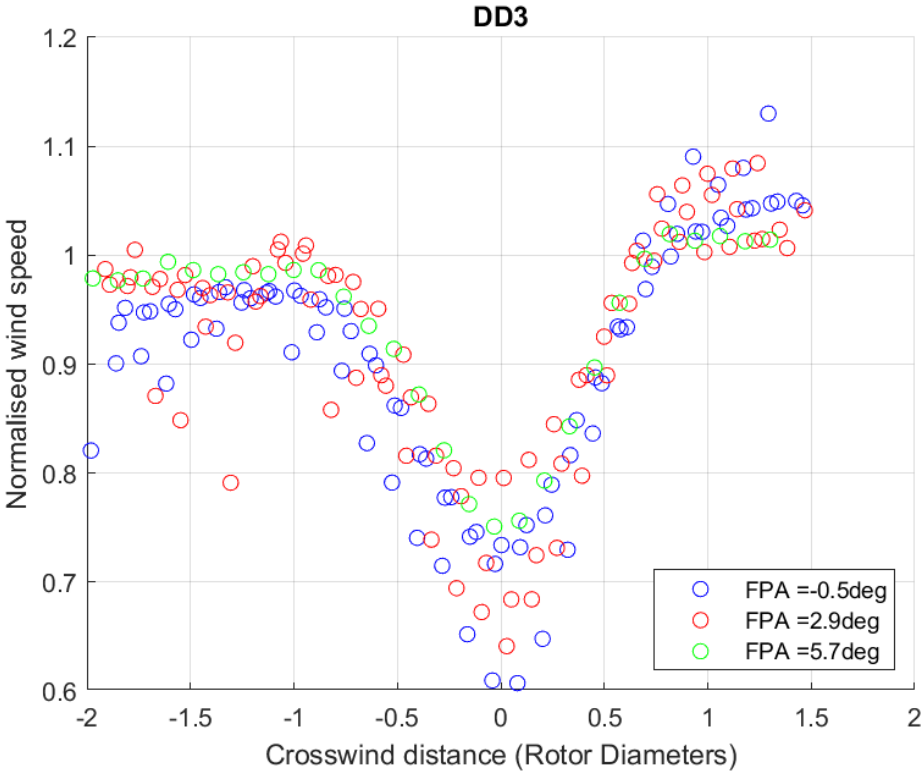

Figure 18 Wake deficit across each fine pitch angle setting for 3 diameters downstream

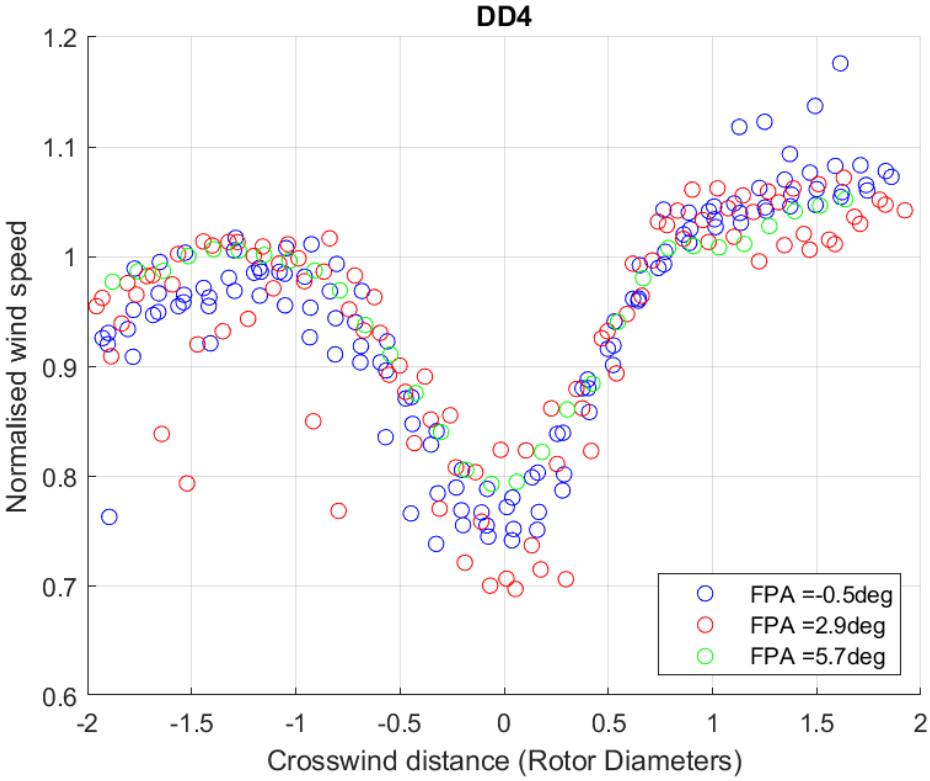

Figure 19 Wake deficit across each fine pitch angle setting for 4 diameters downstream

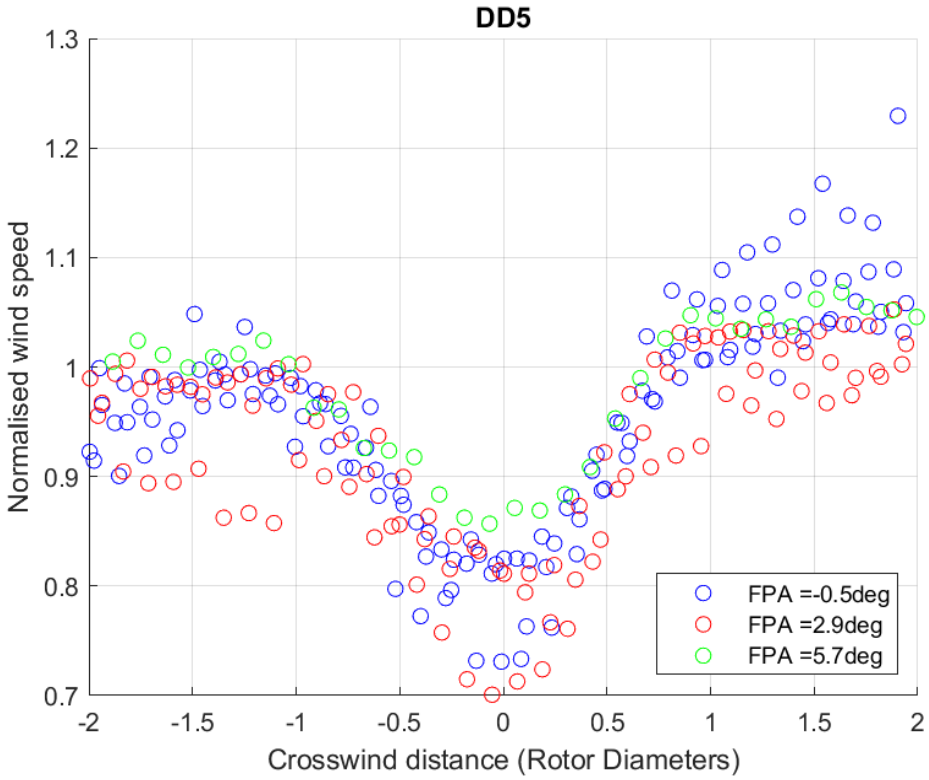

Figure 20 Wake deficit across each fine pitch angle setting for 5 diameters downstream

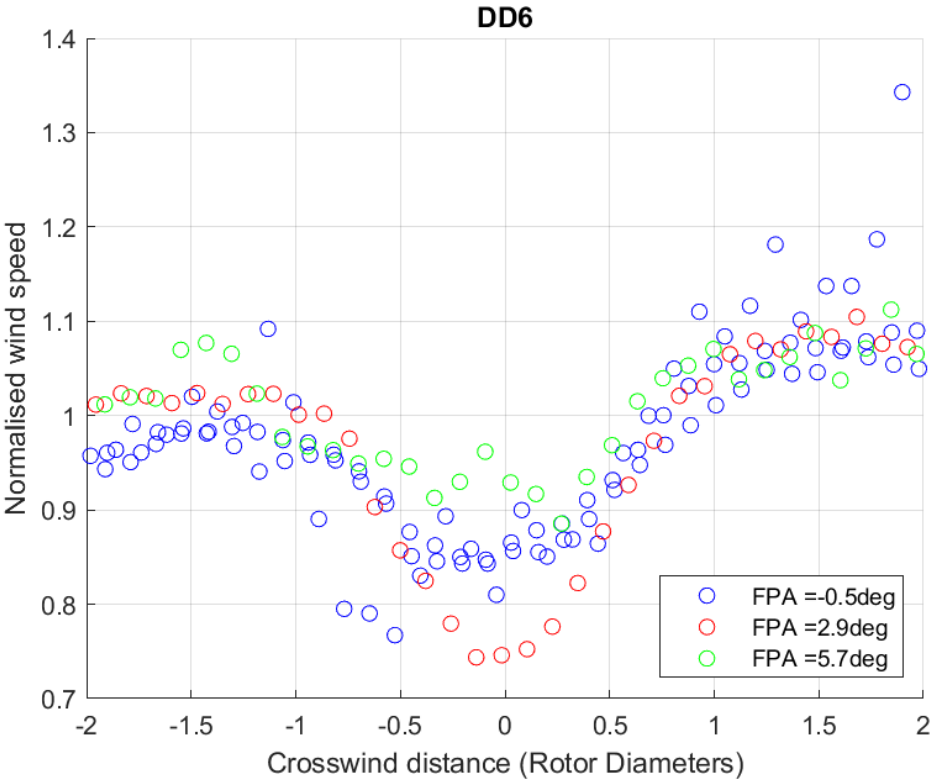

Figure 21 Wake deficit across each fine pitch angle setting for 5 diameters downstream

Figure 17 to Figure 21 show how the wake velocity deficit changes with increasing fine pitch angle settings. While the higher fine pitch settings generally reduce the wake deficit, the deficit is actually a function of thrust coefficient, and the relationship between fine pitch and thrust coefficient is not simple for this turbine because of the speed exclusion zone. In addition, the inflow turbulence intensity influences the rate of wake recovery and therefore the wake deficit at positions downstream from the turbine. A full analysis will take both of these factors into account, so that candidate wake deficit and propagation models can be validated against the measured wake deficits.

4. DERATING TESTS

In the event of the need to curtail wind farm output at above-rated wind speeds, the turbine power can be reduced by reducing the generator torque, the rotor speed, or a combination of both. The choice will affect turbine loads in different ways for the same amount of power reduction. Two different power reduction strategies were investigated by DTU, as described in deliverable D3.2 [2], which also presents the results of test simulations using Bladed.

4.1. DTU Power Reduction Test setup

The DTU power reduction experiment aimed to:

- Implement two derating strategies:
  - 'Constant Rotation' – both speed and torque reduce when power is derated, following Kopt curve
  - 'Maximum Rotation' – only torque reduces when derated, speed remains at rated speed
- Test the following power fraction setpoints, for both derating strategies:
  - 1
  - 0.8
  - 0.6
  - 0.4
- Operate in wind speeds above rated wind speed (11m/s)
- Operate at a range of turbulence intensities (5-15%)

The test schedule for the DTU power reduction tests was owned and defined by the ORE Catapult. Testing was undertaken by WOOD. as per ORE Catapult instruction.

4.1.1. DTU Power Reduction Test Stages

To reduce risk of damage to the turbine the tests were performed in a structured and staged manner. The test stages for both derating strategies for the DTU power reduction tests are outlined in Table 8.

Table 8 DTU Power Reduction Test Stages

Test Stage	Power Fraction	Stage wind speed limits
Constant Rotation Stage 1	1	10 m/s - 21 m/s average
Constant Rotation Stage 2	0.8	10 m/s - 21 m/s average

Constant Rotation Stage 3	0.6	10 m/s - 21 m/s average
Constant Rotation Stage 4	0.4	10 m/s - 21 m/s average
Maximum Rotation Stage 1	1	10 m/s - 21 m/s average
Maximum Rotation Stage 2	0.8	10 m/s - 21 m/s average
Maximum Rotation Stage 3	0.6	10 m/s - 21 m/s average
Maximum Rotation Stage 4	0.4	10 m/s - 21 m/s average

4.1.2. DTU Power Reduction Test Stage Limits

Before advancing to the next test day and test stage, previous test data was analysed to monitor and compare blade loading with test stage limits. Stage gate limits were based on historic loading and turbine design information, these were considered for the following loads:

- Maximum and mean blade flapwise bending
- Equivalent fatigue from flapwise bending
- Maximum and mean blade edgewise bending
- Equivalent fatigue from edgewise bending

If blade load thresholds were exceeded, a full review of the test stage would be performed, and a load analysis done to assess risk of advancing to the next test stage.

4.1.3. DTU Power Reduction Daily Test Procedure

Before daily DTU power reduction tests could proceed, commissioning tests were carried out to ensure the necessary controller updates had been implemented correctly and ran without issue. These tests were carried out successfully.

The daily test process involved -

1. Review forecast and identify suitable test period
2. Confirm target derating strategy and power fraction (PF) for testing with Wood, recorded in DTU power reduction test log
3. Set turbine parameters to adjust the derating strategy and PF to test stage requirement, record both in test log
4. Start-up turbine, record start time in test log
5. Test for 2hrs
6. Review weather forecast, record in log
7. Repeat steps 6 and 7 until end of test period
8. Shutdown turbine, record time in test log
9. Reset turbine parameters to default, checked by operator and 2nd competent person, record value set in the test log and sign and date.
10. Test end

4.2. DTU Power Reduction Data collected

DTU power reduction tests were carried out between February 2022 and April 2022. SCADA and MET data were recorded for all tests. CLOWT data was also recorded during tests when the

system was not experiencing issues. The test schedule was influenced by suitable weather windows and operator availability.

For both derating strategies and each of the power fraction setpoints, the tests aimed to fill the bins of the occurrence matrix presented in Table 9. The occurrence matrix allowed test progress to be monitored and informed the upcoming test schedule. Bins shown in the table are bin centres, each bin was 1 m/s wide. Bin counts were increased when a 10-minute period of data met the bin conditions.

Table 9 DTU Power Reduction test condition occurrence matrix

		Wind Speed bin centre (m/s)																
		4	5	6	7	8	9	10	11	12	13	14	15	16	17	18	19	20
Turbulence intensity bin centre (%)	5																	
	10																	
	15																	

Table 10 summarises the bin count and overall test time for each of the test stages carried out for the DTU power reduction tests. Testing for the maximum rotation test strategy was not carried out for all power fraction setpoints, this was due to unsuitable weather conditions and project timeline considerations.

Table 10 DTU Power Reduction Test Summary

Test Stage	**Derating Strategy**	**Power Fraction**	**Bins of 10 mins data**	**Test time (hours)**
1	Constant Rotation	1	29	8.15
2	Constant Rotation	0.8	48	10.5
3	Constant Rotation	0.6	62	13
4	Constant Rotation	0.4	61	11.55
1	Maximum Rotation	1	14	3.55
2	Maximum Rotation	0.8	20	4.55
All Testing			**234**	**51.3**

Power curves were plotted for each of the power fractions, for both derating strategies. This allowed for comparison with the modelling completed, to ensure the derating strategies were operating as expected and as a check of test progress. Figure 22 shows the power curves plotted using 10-minute averages of the data gathered during the tests for both derating strategies.

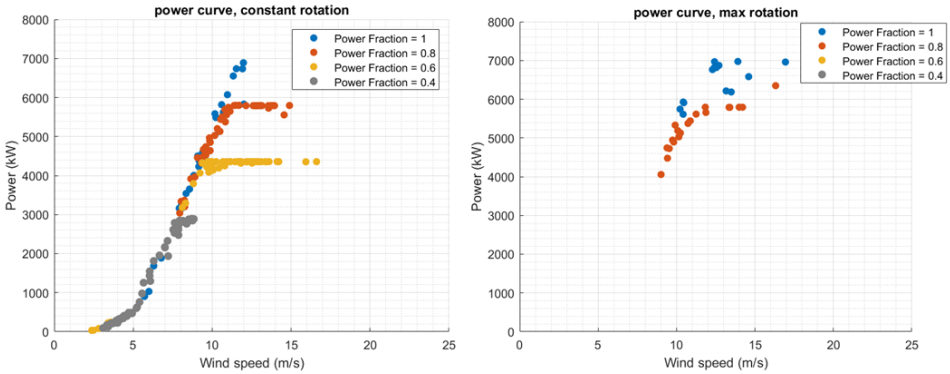

Figure 22 Power vs wind speed data collected for power reduction tests (10-minute average points)

4.3. Results

The following section presents the results of the collected SCADA data following the procedure outlined above. The results include data from both DTU Derating algorithms. The results presented show the rotor speed, measured power, torque and pitch angle across each of the power factors for each DTU derating algorithms. The loading level of each blade root is also presented vs wind speed. The data points shown in each figure represent a mean value over 1 minute data. The line plot in each figure represents the mean value over wind bins of 0.5 m/s increments.

4.3.1. Maximum rotation

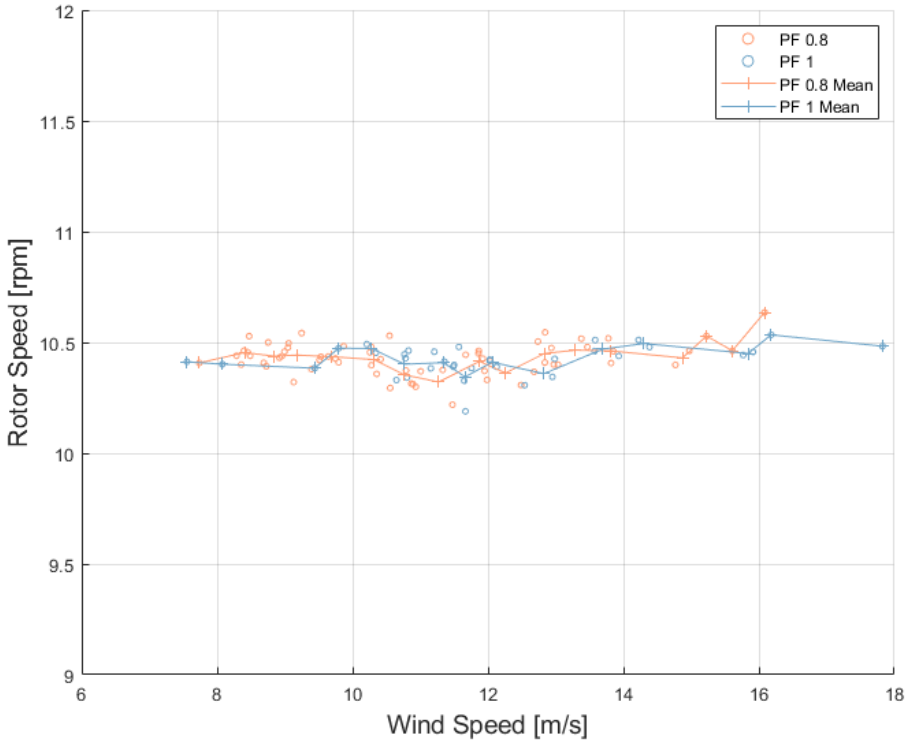

Figure 23 Rotor speed vs wind speed for the maximum rotation derating algorithm across each power fraction setting

Figure 23 shows that with this strategy the rotor speed remains the same for the two setpoints. The slight spread in the results is due to the lack of data collected.

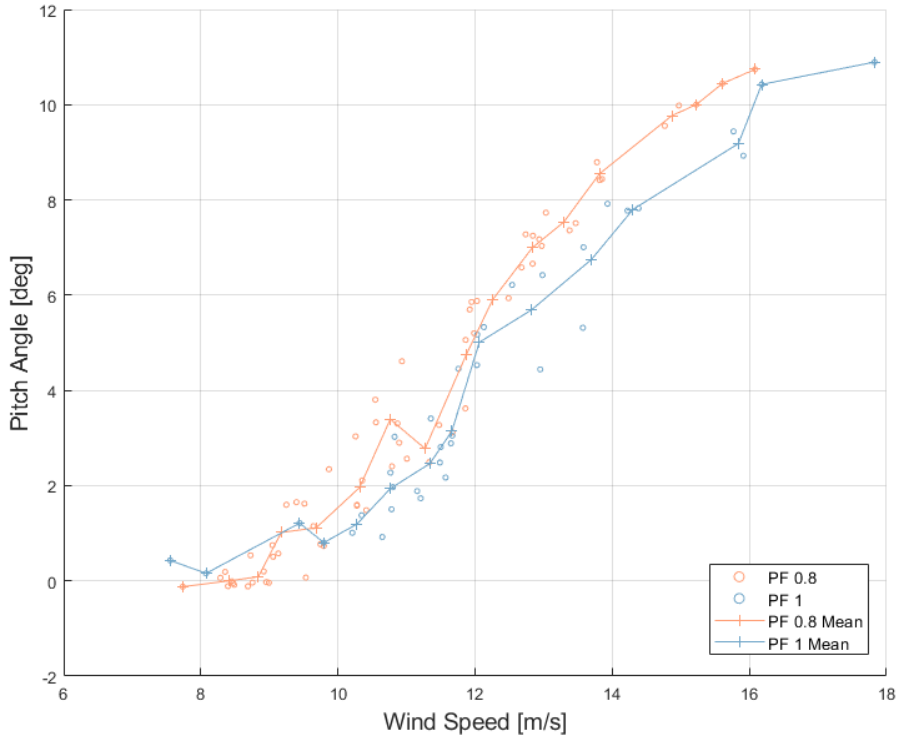

Figure 24 Pitch angle vs wind speed for the maximum rotation derating algorithm across each power fraction setting

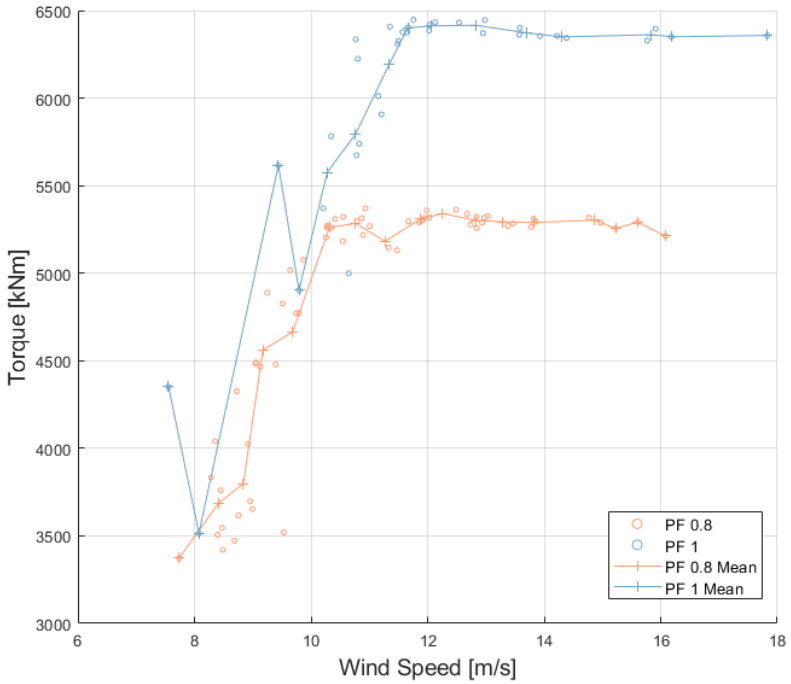

Figure 25 Torque vs wind speed for the maximum rotation derating algorithm across each power fraction setting

Figure 25 shows a drop in torque of approximately 25% from a power fraction of 1 to 0.8 for above rated speed which is consistent with the report in [2].

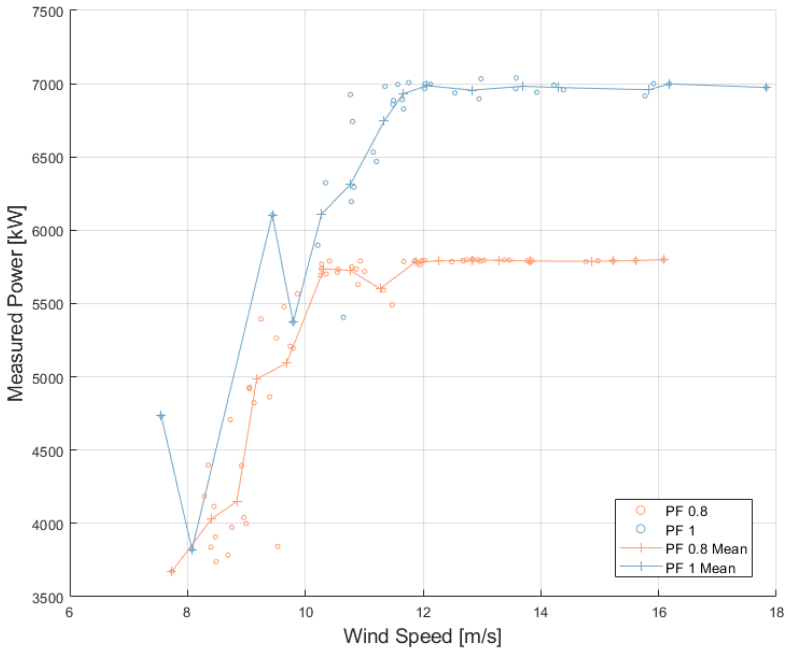

Figure 26 Measured power vs wind speed for the maximum rotation derating algorithm across each power fraction setting

As expected, there is an equivalent drop in power of approximately 25% from a power fraction of 1 to 0.8 for above rated speed which is consistent with the report in [2].

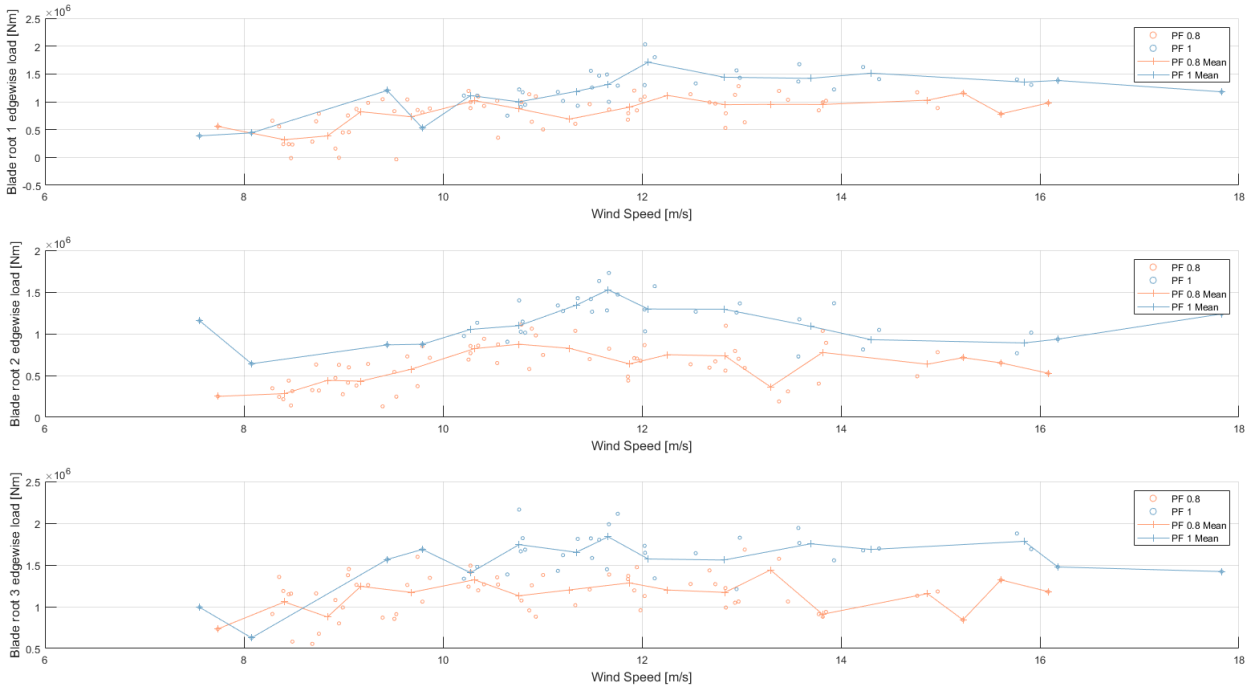

Figure 27 Blade root edgewise load vs wind speed for the maximum rotation derating algorithm across each power fraction setting

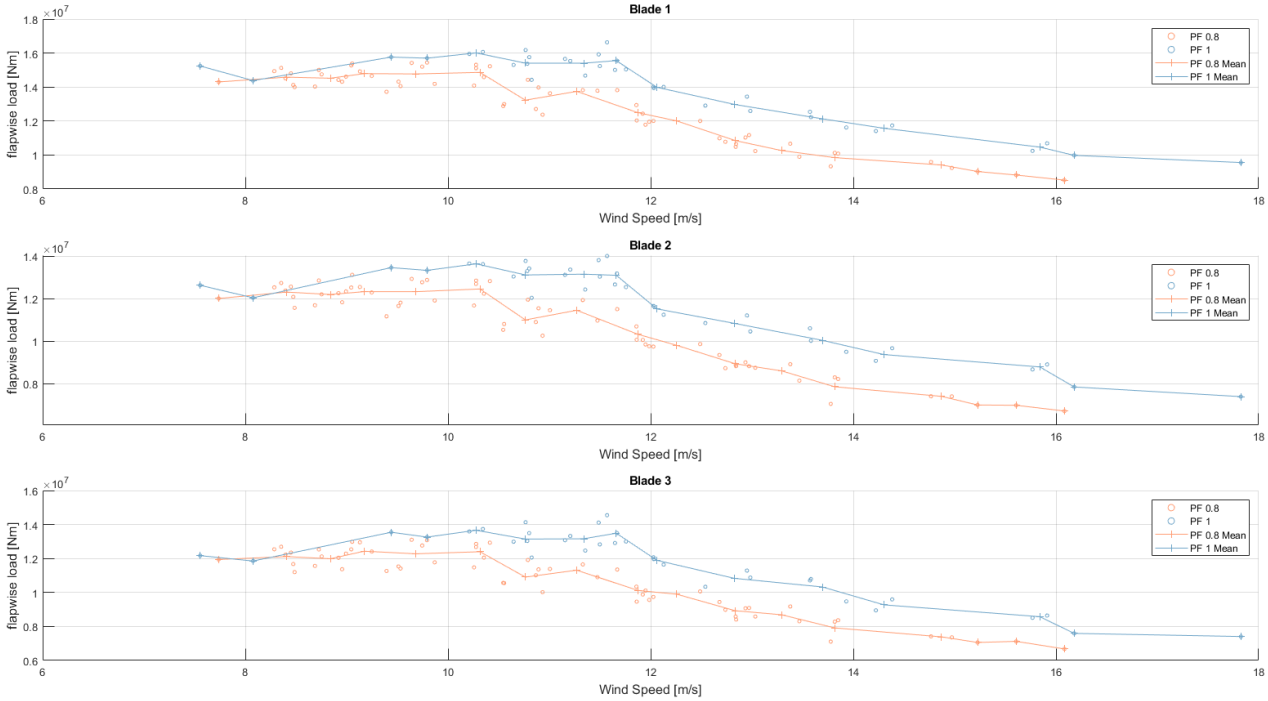

Figure 28 Blade root flapwise vs wind speed for the maximum rotation derating algorithm across each power fraction setting

Figure 27 and Figure 28 show a slight drop in blade root edgewise and flapwise load for each of the three blades from a power fraction of 1 to 0.8 which is consistent with the results in [2].

4.3.2. Constant rotation

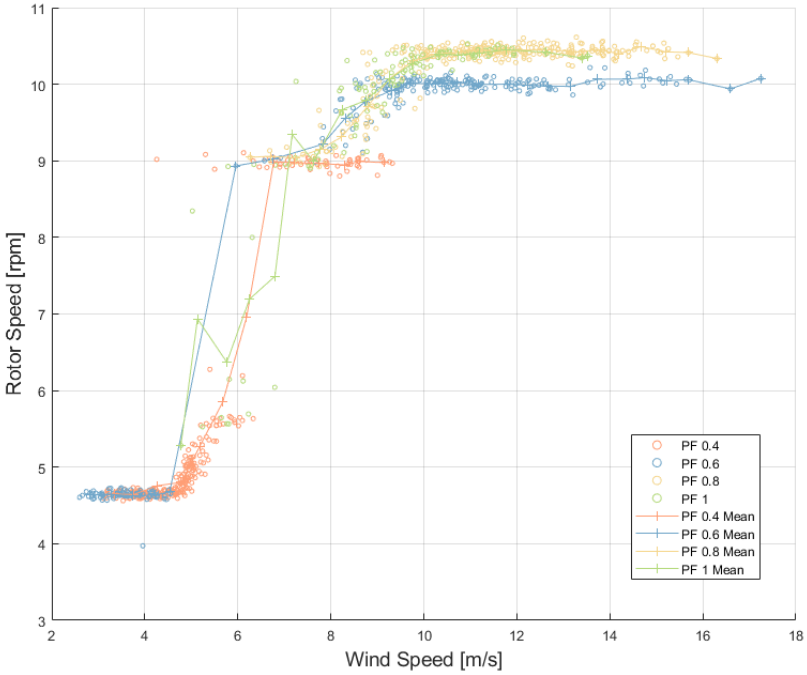

Figure 29 Rotor speed vs wind speed for the constant rotation derating algorithm across each power fraction setting

Figure 29 shows a drop in rotor speed with a reduced power fraction which is consistent with the results in [2].

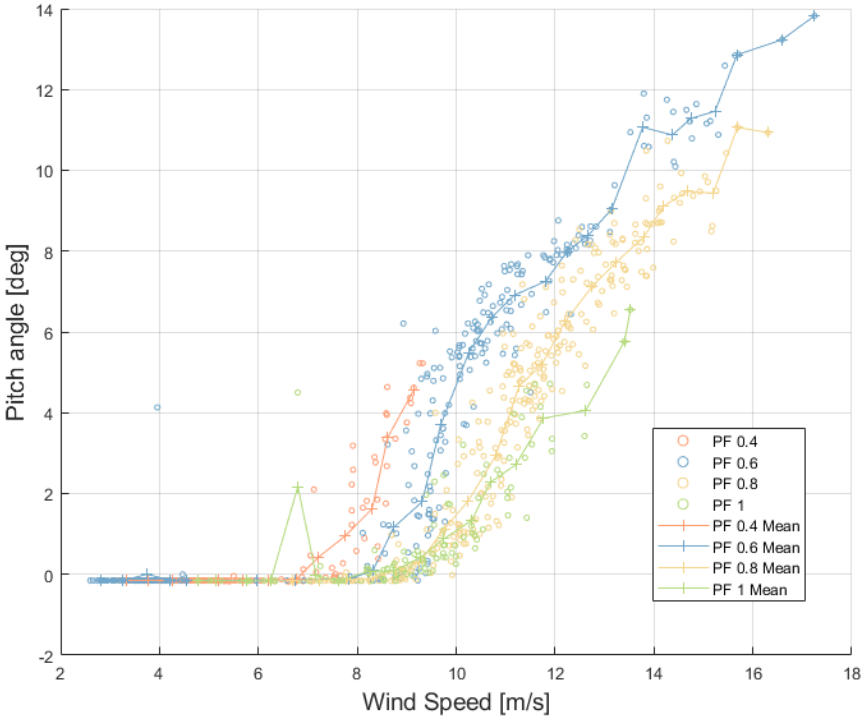

Figure 30 Pitch angle vs wind speed for the constant rotation derating algorithm across each power fraction setting

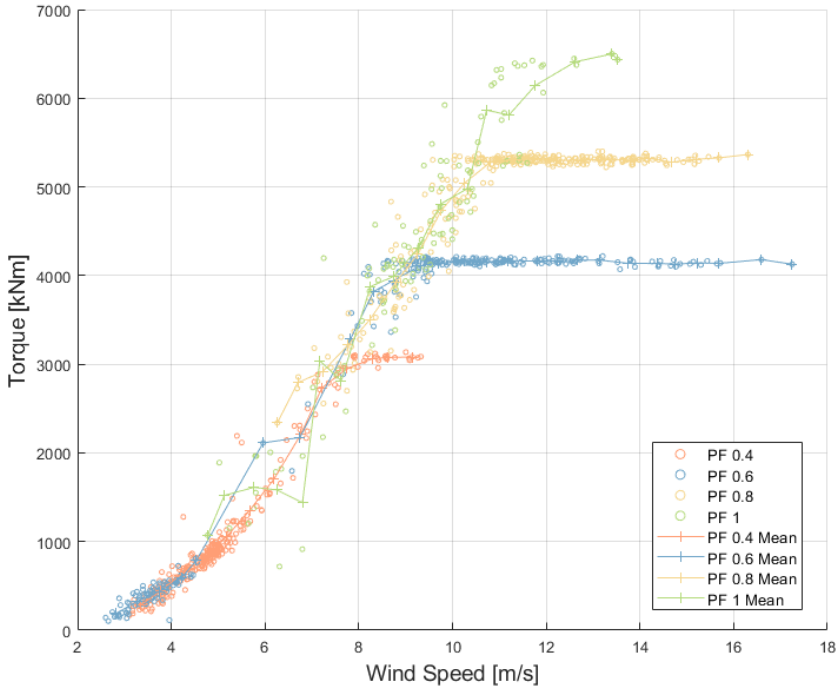

Figure 31 torque vs wind speed for the constant rotation derating algorithm across each power fraction setting

Figure 31 shows a drop of approximately 33% across the power fractions which is approximately consistent with report [2]

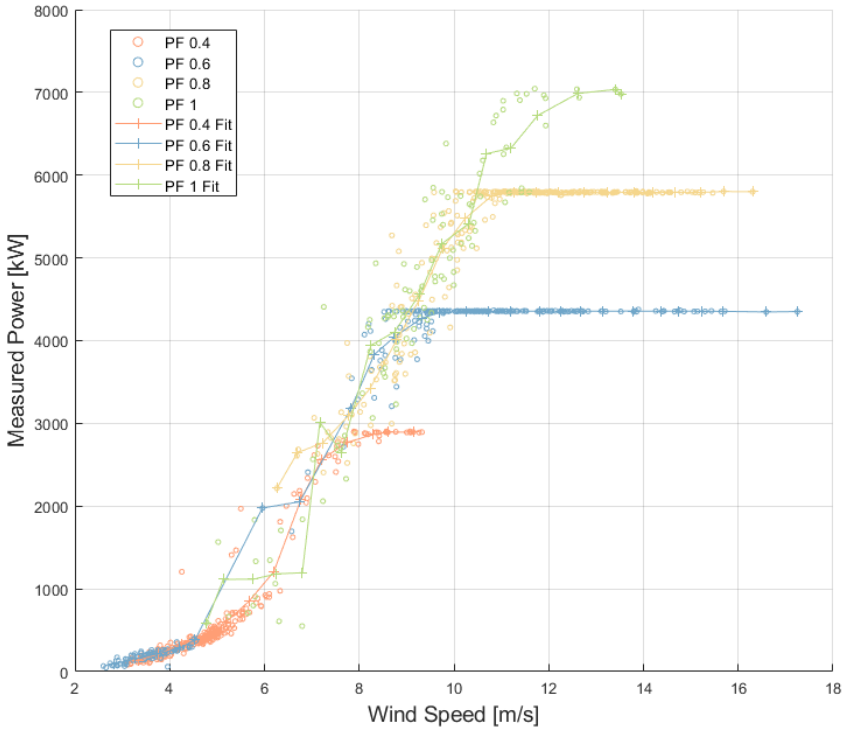

Figure 32 Measured power vs wind speed for the constant rotation derating algorithm across each power fraction setting

As expected, there is a there is a drop in measured power approximately equivalent to the power fraction.

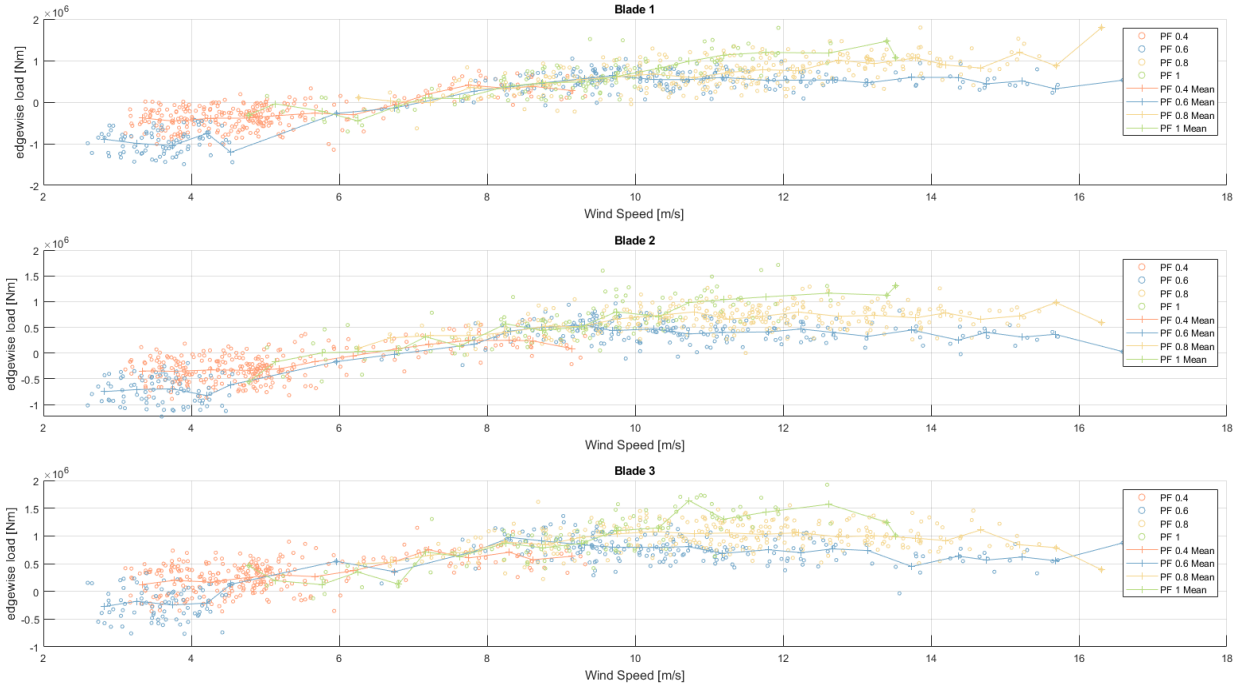

Figure 33 Blade root edgewise moment vs wind speed for the constant rotation derating algorithm across each power fraction setting

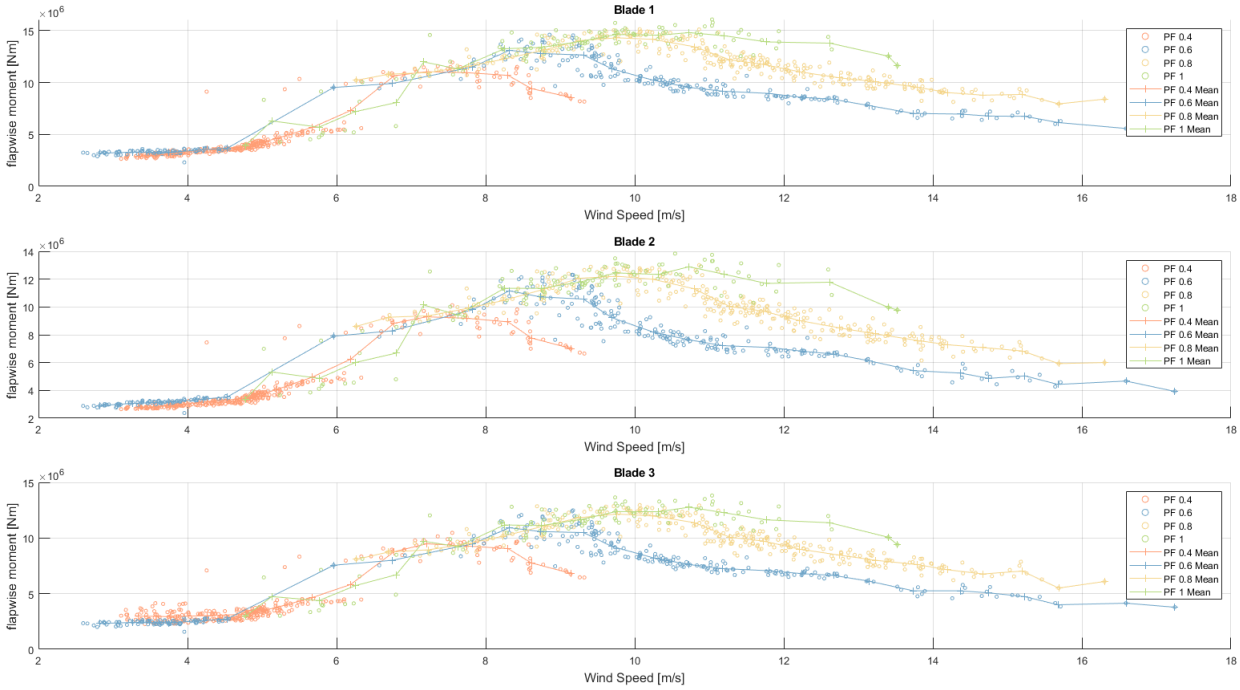

Figure 34 Blade root flapwise moment vs wind speed for the constant rotation derating algorithm across each power fraction setting

Figures 33 and 34 show a drop in blade root edgewise and flapwise load for each of the three blades as the power fraction goes from 1 to 0.4 which is consistent with the results in [2].

5. LiDAR-ASSISTED CONTROL TESTS

Using the forward-facing spinner LiDAR to provide a preview of the approaching wind, a feed-forward term is added to the controller to help reduce pitch duty and tower loading. This is described in D3.5 [5], along with the results of test simulations using Bladed.

5.1. LiDAR Assisted Control Test setup

The LiDAR assisted control tests aimed to:

- Test with the lidar-assisted control enabled
- Operate in wind speeds at and above rated wind speed (11m/s)
- Operate at a range of turbulence intensities (5-15%)

The forward-facing LiDAR was set to measure a partial rosette curve, with a diameter of 120 meters, focused at a distance of 120 meters in front of the turbine rotor. A combination of all available line-of-sight wind speeds within each rosette scan was used to reconstruct a single wind vector 120 meters upstream of the rotor centre position.

The result of the wind field reconstruction (i.e. the 3-component wind vector and a quality flag) were streamed in real-time via UDP packets to a supervisory control PLC which then fed the real-time upstream wind measurements into the turbine controller. Further details on the spinner LiDAR communication and data formats are presented in [6].

The test schedule for the LiDAR assisted control tests was owned and defined by the ORE Catapult. Testing was undertaken by WOOD. as per ORE Catapult instruction.

5.1.1. LiDAR Assisted Control Test Stages

To reduce risk of damage to the turbine the tests were performed in a structured and staged manner. There was only one test stage for the LiDAR assisted control tests, this is outlined in Table 11.

Table 11 LiDAR Assisted Control Test Stage

Test Stage	LAC Mode	Stage wind speed limit
Test Stage 1	LiDAR Assisted Control enabled	>10m/s average

5.1.2. LiDAR Assisted Control Test Stage Limits

Before advancing to the next test day, previous test data was analysed to monitor and compare blade loading with test stage limits. Stage gate limits were based on historic loading and turbine design information; these were considered for the following loads:

- Maximum and mean blade flapwise bending
- Equivalent fatigue from flapwise bending
- Maximum and mean blade edgewise bending
- Equivalent fatigue from edgewise bending

If blade load thresholds were exceeded, a full review of the test stage would be performed, and a load analysis done to assess risk of advancing to the next test day.

5.1.3. LiDAR Assisted Control Daily Test Procedure

Before daily LiDAR assisted control tests could proceed, commissioning tests were carried out to ensure the necessary controller updates had been implemented correctly and ran without issue. Due to time limitations, only some aspects of the LiDAR assisted control were commissioned successfully.

1. Review forecast and identify suitable test period
2. Confirm LiDAR assisted control enabled for testing with Wood, recorded in LAC test log
3. Set turbine parameters to enable LiDAR Assisted Control, record in test log
4. Start-up turbine, record start time in test log
5. Test for 2hrs
6. Review weather forecast, record in log
7. Repeat steps 6 and 7 until end of test period
8. Shutdown turbine, record time in test log
9. Reset turbine parameters to default, checked by operator and 2nd competent person, record value set in the test log and sign and date.
10. Test end

5.2. LiDAR Assisted Control Data collected

The LiDAR assisted control tests were carried out in April 2022. Due to some difficulties establishing the communications between the LiDAR and the turbine PLC, then verifying the data being sent by the LiDAR to the turbine PLC, there was limited time to carry out the LiDAR assisted control tests. For the majority of April, the forecast was unsuitable for the LiDAR Assisted control tests. In the end, only one day of testing LAC was completed, after the commissioning tests had been completed. Table 12 summarises the LiDAR assisted control tests.

Table 12 LiDAR Assisted Control Test Summary

Test Day	Test Time (hours)	Wind Speed Range (m/s)
Day 1	3.5	10 - 14

5.3. Results

The primary objective of Lidar assisted control (LAC) is to reduce tower base My (fore-aft) and blade root My (out of plane) fatigue loading in above rated wind speed conditions. Therefore, to validate the performance of the algorithm, large amount of test data in above rated wind is required so that comparisons between the fatigue loading with the algorithm on and off can be made. Unfortunately, during the LAC testing window, only near rated wind speeds were observed on site, meaning the algorithm performance could not be thoroughly evaluated. In addition, the conversion from tower base strain to tower base bending moment had not yet been calibrated. The raw strain, once transformed to the yaw bearing coordinate system, was used as a proxy for tower base loads. Figure 35 - Figure 37 on the following pages show 10-minute time series results comparing LAC on to LAC off for similar inflow conditions.

The time series plots show that the LAC algorithm is executing on the PLC, as the feed forward pitch increment rate is non-zero in the LAC on data. The difference in the mean tower base My strain between LAC on and LAC off seems to change depending on the difference in the Nacelle heading for the equivalent periods. This indicates that perhaps the transformation of the raw strain values onto the yaw bearing coordinate system could be incorrect. Nevertheless, the algorithm is indeed executing on the PLC which is in part a successful outcome of the tests.

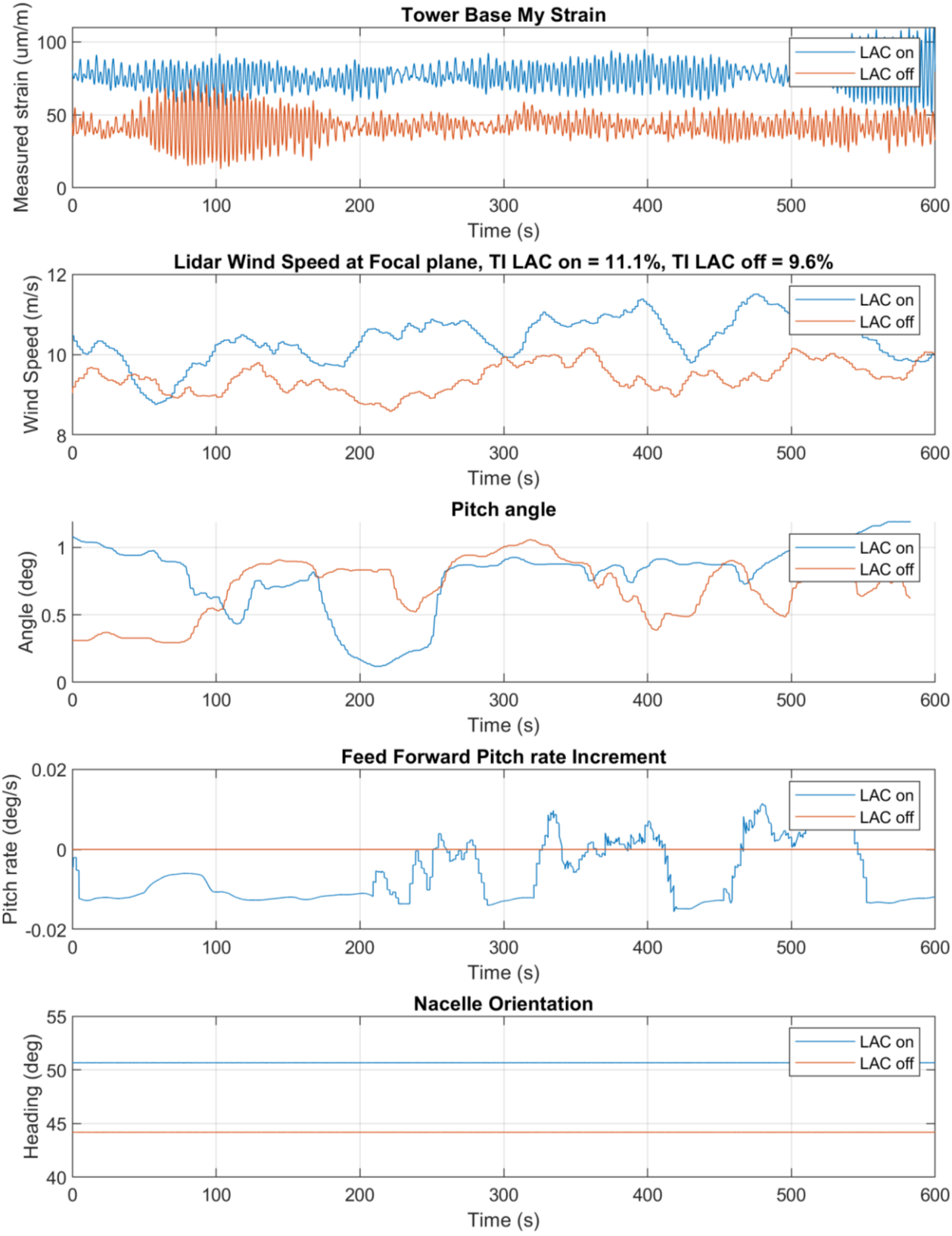

Figure 35 Time series results from LAC testing example 1

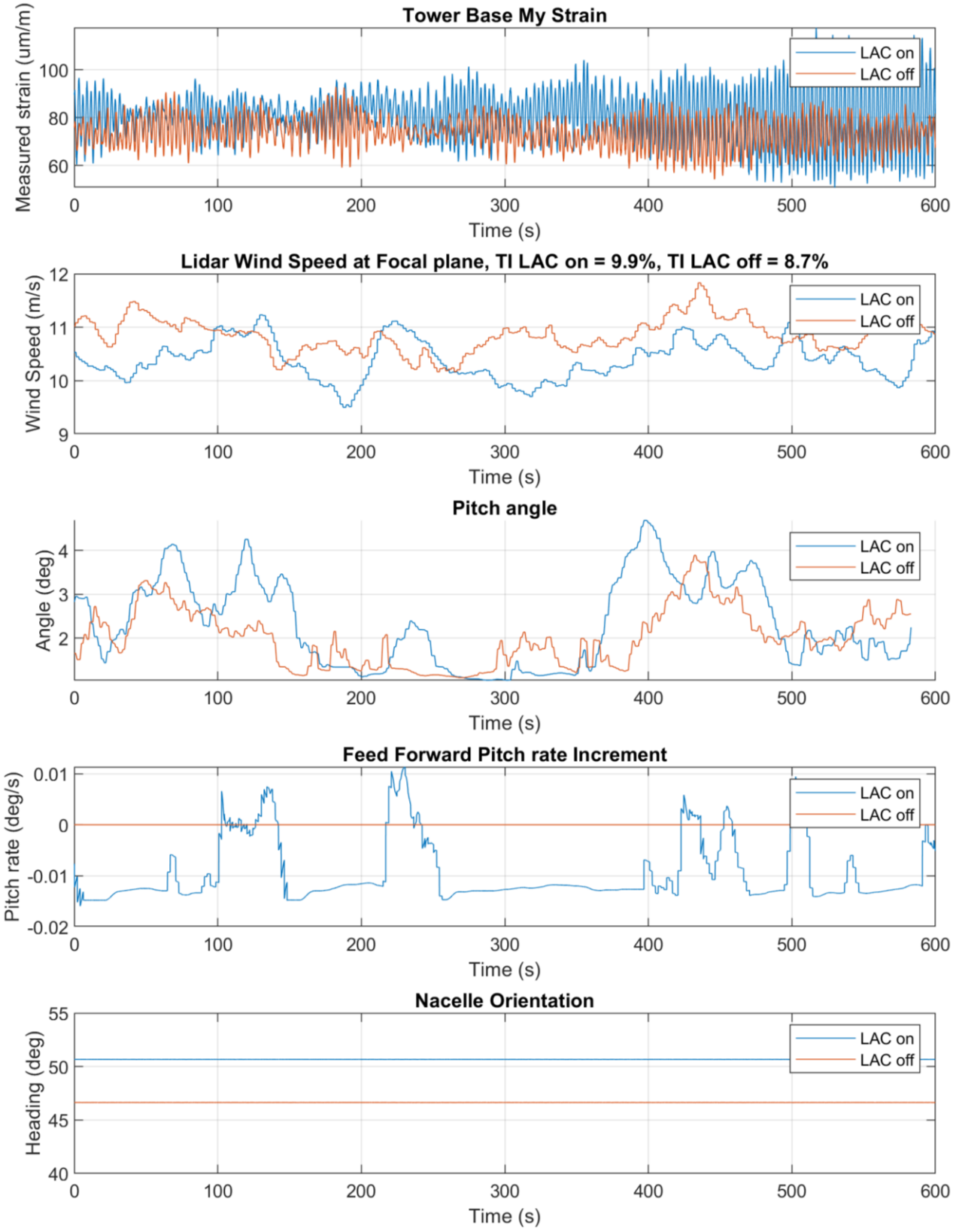

Figure 36 Time series results from LAC testing example 2

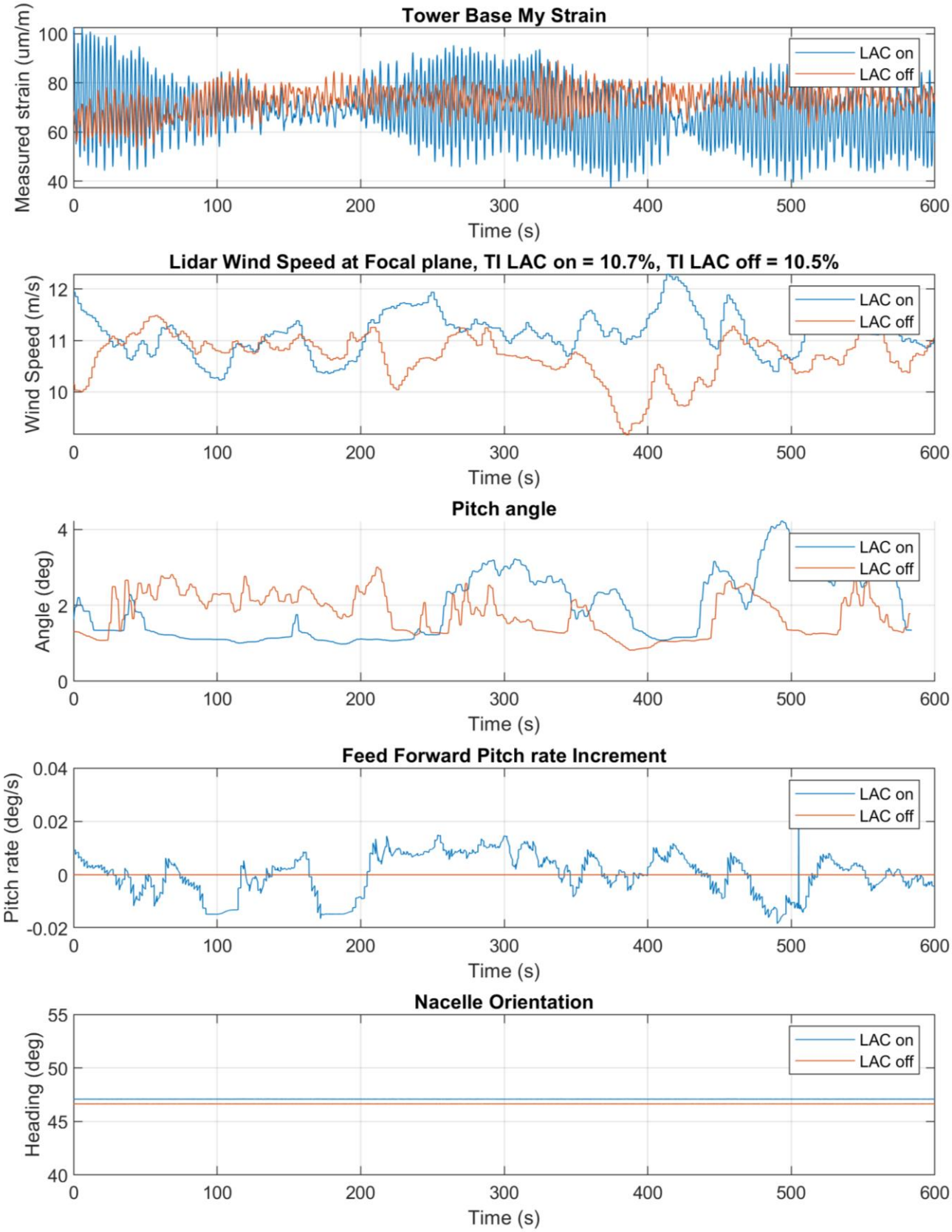

Figure 37 Time series results from LAC testing example 3

For each 10-minute period, the average blade flapwise moment DEL and Tower base My strain DEL were calculated. Figure 38 below shows the DEL results plotted against the mean Lidar wind speed for each 10-min data point.

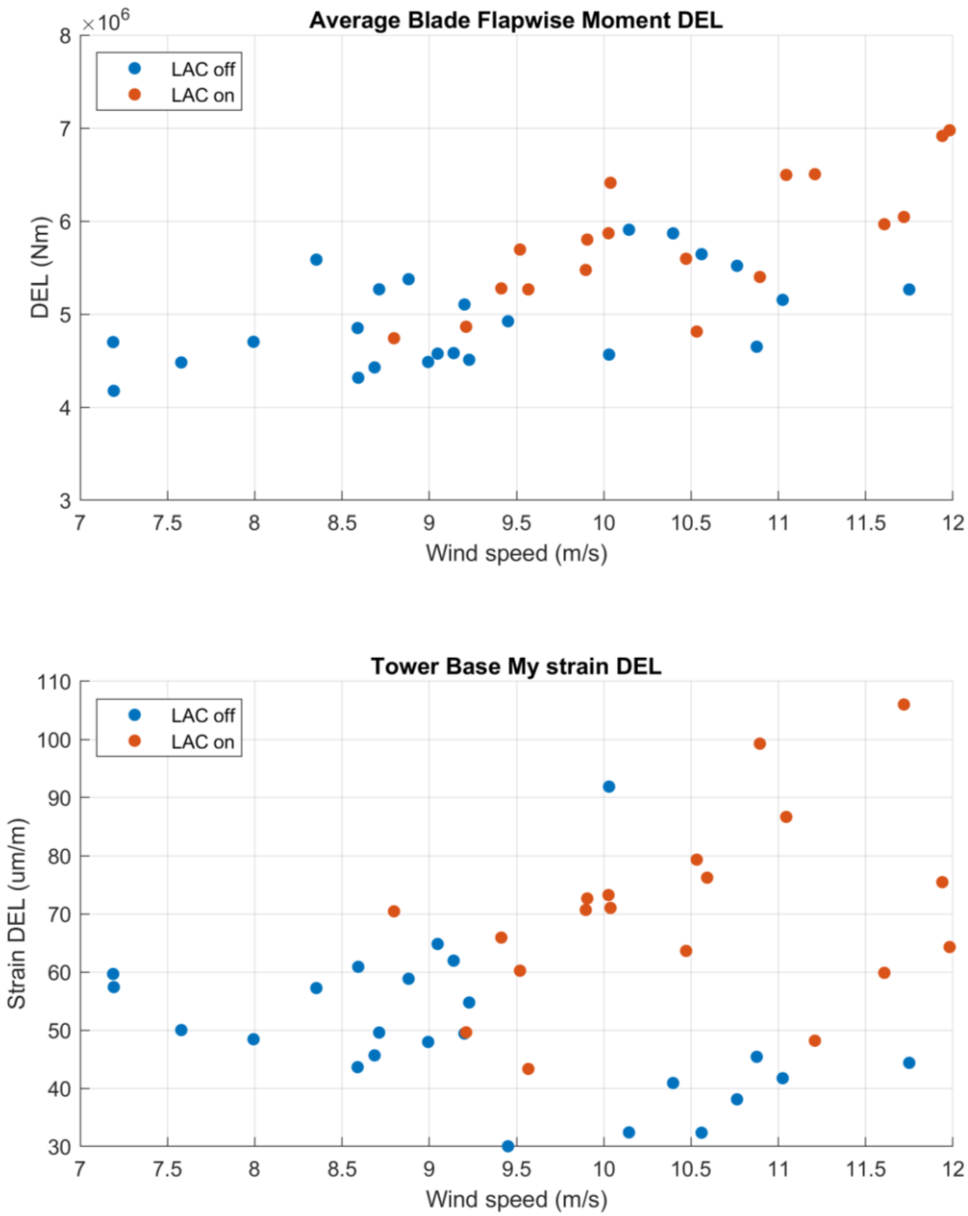

Figure 38 DEL comparison between LAC on and LAC off data

It is difficult to draw any firm conclusions from this limited set of DEL results. As discussed previously, the limited wind speeds mean that almost no data was collected above rated wind speed, which is where the LAC is designed to work. Also, because of the limited time available, the LAC algorithm was simply allowed to run for that short period, without toggling on and off, and the results above are compared against results with LAC off which are for a different period when the turbulence intensity may have been different, and turbulence has a dominant effect on fatigue loading. However, the time series analysis shows that the algorithm has been successfully implemented and commissioned and is indeed working as designed.

6. INDIVIDUAL PITCH CONTROL TESTS

As part of its design, the 7MW turbine already uses 1P-IPC to reduce 1P blade fatigue loads, using blade root load measurements. Two additional features are tested here, as reported in D3.5 [5], namely the use of potentially cheaper and more robust tower-top strain gauges instead of blade root gauges, and the addition of 2P-IPC to reduce the 3P non-rotating fatigue loads. These features are described in D3.5 [5], along with the results of test simulations using Bladed.

6.1. Individual Pitch Control Test setup

The IPC tests aimed to:

- Test the following IPC Modes:
  - IPC Mode 1 – switches between no IPC and 1P IPC, using blade root strain gauges
  - IPC Mode 2 – switches between no IPC and 1P&2P IPC, using blade root strain gauges
  - IPC Mode 3 – switches between blade root and tower top strain gauges, using 1P IPC
  - IPC Mode 4 – switches between blade root and tower top strain gauges, using 1P&2P IPC
- Operate in wind speeds below and above rated wind speed (11m/s)
- Operate at a range of turbulence intensities (5-15%)

The test schedule for the IPC tests was owned and defined by the ORE Catapult. Testing was undertaken by WOOD. as per ORE Catapult instruction.

6.1.1. Individual Pitch Control Test Stages

To reduce risk of damage to the turbine the tests were performed in a structured and staged manner. The test stages for the IPC tests are outlined in Table 13.

Table 13 IPC test Stages

Test Stage	IPC Mode	Stage wind speed limit
Test Stage 1	IPC Mode 1	4m/s – 21m/s average
Test Stage 2	IPC Mode 2	4m/s – 21m/s average
Test Stage 3	IPC Mode 3	4m/s – 21m/s average
Test Stage 4	IPC Mode 4	4m/s – 21m/s average

6.1.2. Individual Pitch Control Test Stage Limits

Before advancing to the next test day and test stage, previous test data was analysed to monitor and compare blade loading with test stage limits. Stage gate limits were based on historic loading and turbine design information, these were considered for the following loads:

- Maximum and mean blade flapwise bending
- Equivalent fatigue from flapwise bending
- Maximum and mean blade edgewise bending
- Equivalent fatigue from edgewise bending

If blade load thresholds were exceeded, a full review of the test stage would be performed, and a load analysis done to assess risk of advancing to the next test stage.

6.1.3. Individual Pitch Control Daily Test Procedure

Before daily IPC tests could proceed, commissioning tests were carried out to ensure the necessary controller updates had been implemented correctly and ran without issue. These tests were carried out successfully for the IPC tests involving the blade root strain gauges.

The daily test process involved -

1. Review forecast and identify suitable test period
2. Confirm target IPC mode for testing with Wood, recorded in IPC test log
3. Set turbine parameters to adjust the IPC mode to the test stage requirement, record IPC mode in test log
4. Start-up turbine, record start time in test log
5. Test for 2hrs
6. Review weather forecast, record in log
7. Repeat steps 6 and 7 until end of test period
8. Shutdown turbine, record time in test log
9. Reset turbine parameters to default, checked by operator and 2nd competent person, record value set in the test log and sign and date.
10. Test end

6.2. Individual Pitch Control Data collected

Individual pitch control tests were carried out between February 2022 and April 2022. SCADA, MET mast and CLOWT sensor data were recorded for all tests. The test schedule was influenced by suitable weather windows and operator availability.

For all IPC modes, the tests aimed to fill the bins of the occurrence matrix presented in Table 14. The occurrence matrix allowed test progress to be monitored and informed the upcoming test schedule. Bins shown in the table are bin centres, each bin was 1 m/s wide. Bin counts were increased when a 10-minute period of data met the bin conditions.

Table 14 IPC test condition occurrence matrix

		Wind Speed bin centre (m/s)																
		4	5	6	7	8	9	10	11	12	13	14	15	16	17	18	19	20
Turbulence intensity bin centre (%)	5																	
	10																	
	15																	

Table 15 summarises the bin count and overall test time for each of the test stages carried out for the IPC tests. Test stages 3 and 4 were not carried out due to project timeline limitations and unresolved technical challenges surrounding the calibration of the tower top strain gauges and the preparation for these tests.

Table 15 IPC Test Summary

Test Stage	IPC Mode	Bins of 10 mins data	Test time (hours)
1	1	99	17.63
2	2	110	18.83
3	3	0	0
4	4	0	0
All Testing		**209**	**39.5**

6.3. Results

In this section the power spectral density of the blade root flapwise load is presented when 1P IPC is activated and deactivated shown in Figure 39. Unfortunately, due to a persistent issue with the pitch motor saturation limitations which caused the 2P IPC to be phased out, no data for 2P IPC was successfully collected in the time available.

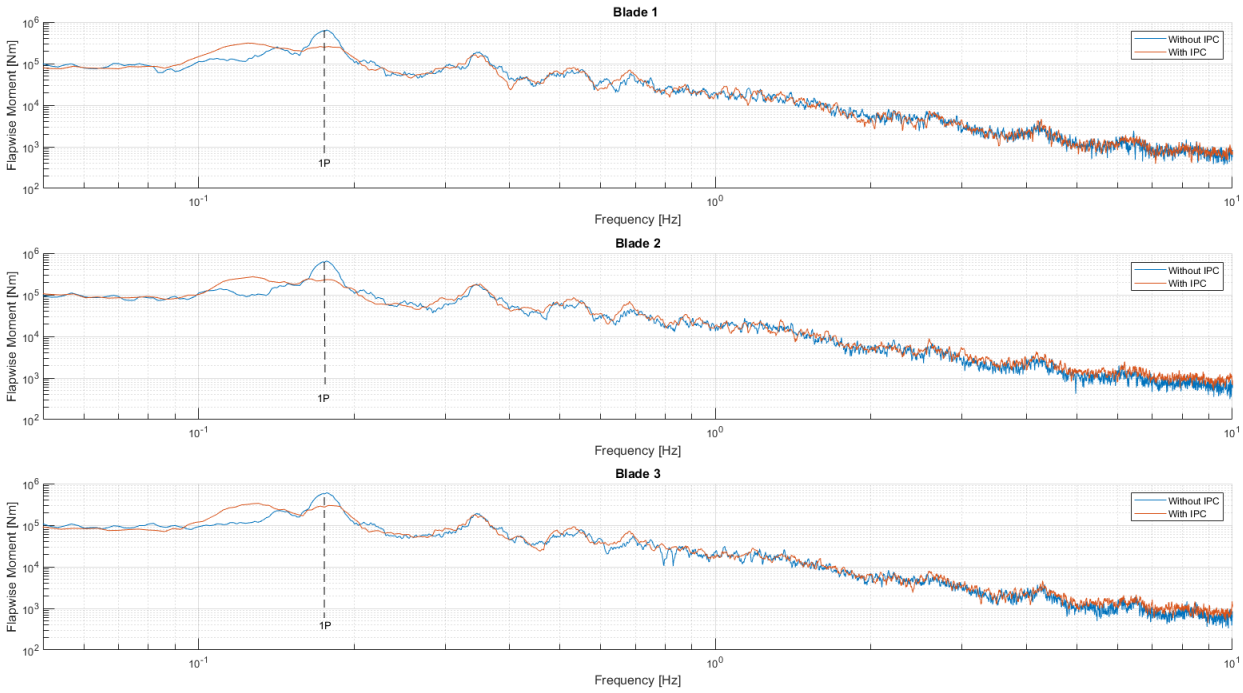

Figure 39 Power spectral density of blade root flapwise moment for 1P IPC on vs off

Figure 39 indicates a clear reduction in the dominant blade flapwise loading peak in the rotor 1P frequency range, indicating that the 1P IPC is working correctly. No analysis of damage equivalent loads is presented because of the small amount of useful data.

The technical problems with the tower top strain gauges have since been resolved, so further testing including modes 3 and 4 may be possible if a suitable opportunity arises in future.

7. FAST FREQUENCY RESPONSE TESTS

As an ancillary service to enhance grid stability in the presence of a high penetration of renewables, the wind turbine controller can transiently alter the active power produced in response to variations in grid frequency. Since this response is programmed in the controller, it can be designed to act in various ways. The algorithm tested includes three different responses: synthetic inertia, where the change in power is proportional the rate of change of frequency to mimic a conventional (e.g. steam turbine) generator; droop response, where the change in power is proportional to the frequency deviation, and a power boost where the power increases by a pre-defined amount for a short time when the frequency drops below some critical threshold. Details are given in Appendix 2.

7.1. Fast Frequency Response Test setup

The fast frequency response (FFR) tests aimed to:

- Test the fast frequency response strategy with the grid disturbances enabled
- Operate in wind speeds below rated wind speed (11m/s)
- Operate at a range of turbulence intensities (5-15%)

The test schedule for the fast frequency response tests was owned and defined by the ORE Catapult. Testing was undertaken by WOOD. as per ORE Catapult instruction.

7.1.1. Fast Frequency Response Test Stages

To reduce risk of damage to the turbine the tests were performed in a structured and staged manner. There was only one test stage for the FFR tests, this is outlined in Table 16.

Table 16 FFR Test Stages

Test Stage	FFR Mode	Stage wind speed limit
Test Stage 1	Grid disturbance enabled	<11m/s average

7.1.2. Fast Frequency Response Test Stage Limits

Before advancing to the next test day, previous test data was analysed to monitor and compare blade loading with test stage limits. Stage gate limits were based on historic loading and turbine design information, these were considered for the following loads:

- Maximum and mean blade flapwise bending
- Equivalent fatigue from flapwise bending
- Maximum and mean blade edgewise bending
- Equivalent fatigue from edgewise bending

If blade load thresholds were exceeded, a full review of the test stage would be performed, and a load analysis done to assess risk of advancing to the next test day.

7.1.3. Fast Frequency Response Daily Test Procedure

Before daily fast frequency response tests could proceed, commissioning tests were carried out to ensure the necessary controller updates had been implemented correctly and ran without issue. These tests were carried out successfully.

The daily test process involved -

1. Review forecast and identify suitable test period
2. Confirm FFR grid disturbances for testing with Wood, recorded in FFR test log
3. Set turbine parameters to enable grid disturbances, record in test log
4. Start-up turbine, record start time in test log
5. Test for 2hrs
6. Review weather forecast, record in log
7. Repeat steps 6 and 7 until end of test period
8. Shutdown turbine, record time in test log
9. Reset turbine parameters to default, checked by operator and 2nd competent person, record value set in the test log and sign and date.
10. Test end

7.2. Fast Frequency Response Data collected

Fast frequency response tests were carried out in April 2022 over five days. SCADA, MET mast and CLOWT sensor data were recorded for all tests. The test schedule was influenced by suitable weather windows and operator availability.

The FFR tests aimed to gather data over a range of wind speeds. Due to the nature of the emulated grid disturbances, and therefore the fast frequency response, 10-minute bins were not a suitable measure of test progress. Instead, total test time was monitored, and the wind speed range covered by testing each day. Table 17 summarises fast frequency response tests.

Table 17 Fast Frequency Response Test Summary

Test Day	Test Time (hours)	Wind Speed Range (m/s)
Day 1	4.5	2 - 6
Day 2	1.5	6 - 14
Day 3	4	4 - 10
Day 4	3.75	3 - 7.5
Day 5	4.25	4 - 10
All testing	**18**	

7.3. Results

As per the algorithm description in Appendix 2, FFR was tested by emulating a grid disturbance through pre-determined look up tables, stored as state variables onboard the turbine PLC. In response to each grid disturbance a power increment is calculated based on three components. The Boost component is activated if the grid disturbance exceeds a certain threshold, the Droop component is proportional to the level of the grid disturbance, and the Synthetic Inertia

component is proportional to the rate of change of the grid disturbance. The sum of the three components is taken as the required power increment in response to the grid disturbance. The control algorithm then limits the required increment to prevent the rotor from stalling and to limit the total power so that it doesn't exceed rated power.

Figure 40 below shows a zoomed-in plot of the time series results for Day 3's tests. The plot shows the emulated grid disturbance, consisting of three different frequency dips and one period of 'typical' dynamic frequency variations, and the resultant FFR power increments. Figure 41 shows the resulting impact on the generator output power, generator speed and the mean of the three blade root edgewise bending moments (used as a proxy for rotational hub Mx loading).

As can be seen, the FFR algorithm has successfully calculated a power increment in response to a grid disturbance, limited the power increment accordingly and implemented the increment resulting in a short-term increase in the generator output power. The FFR algorithm has avoided rotor stall, shown by the maintained generator speed, and the increase in edgewise blade loading is not significant. It must be noted that the Boost contribution seems to have not been calculated or logged during the experiment. However, the allowed increment has already been exceeded by the required increment, therefore the missing boost contribution has no effect on the resultant increment applied by the FFE algorithm.

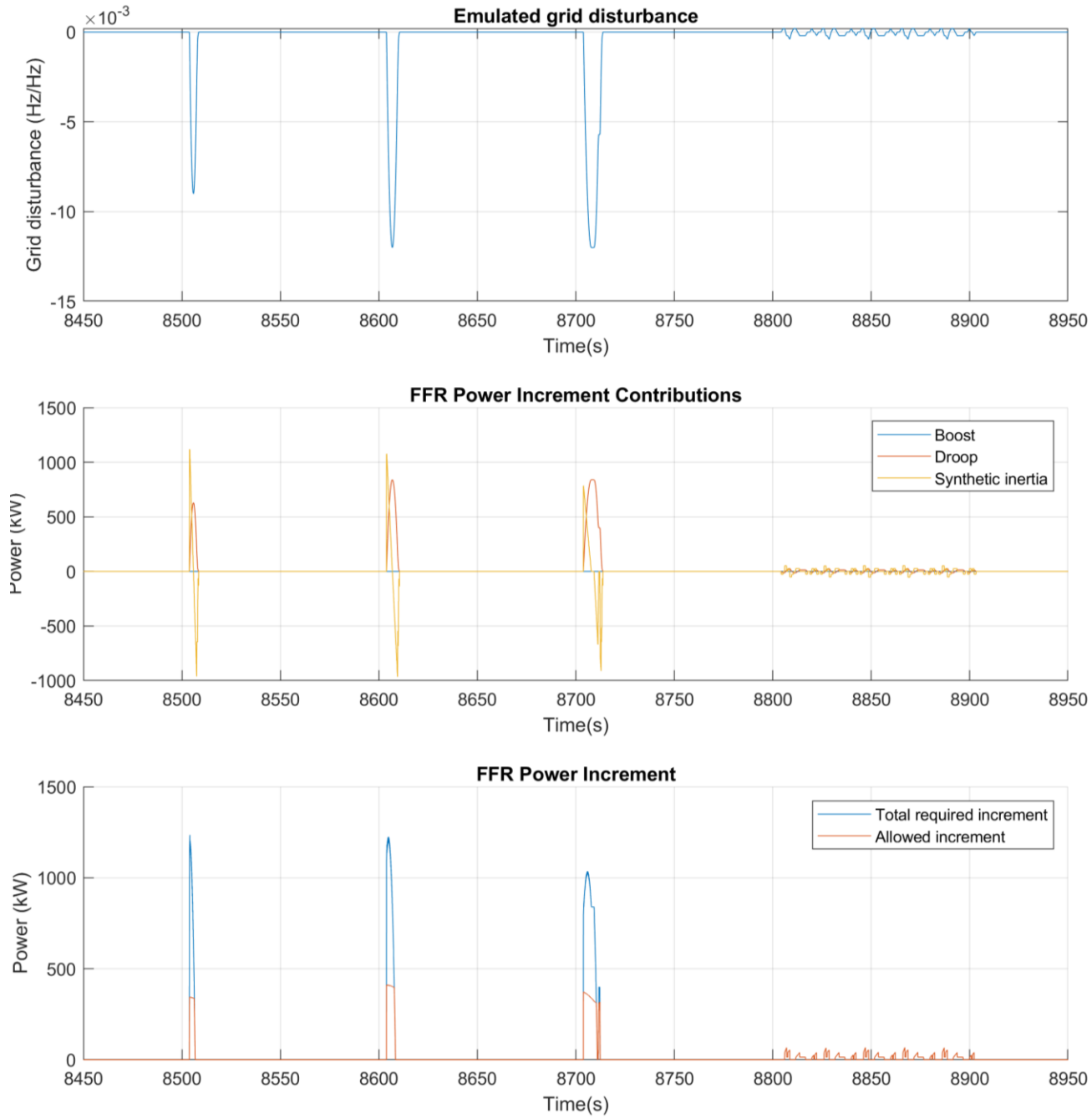

Figure 40 Zoomed in field test time series of emulated grid disturbance and resultant power increments

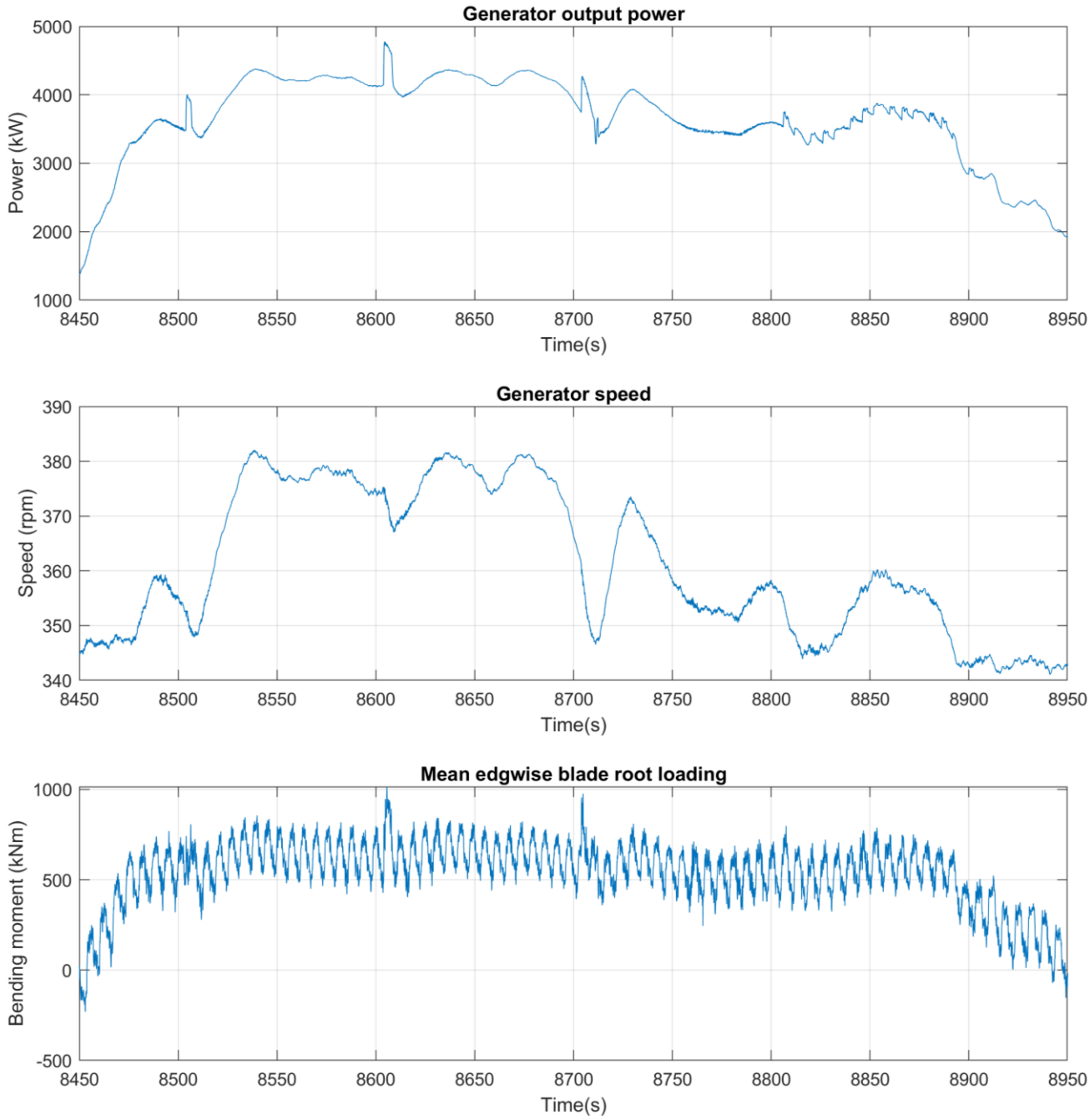

Figure 41 Zoomed in field test time series of key turbine operational and loads signals in response to applied FFR power increments

Figure 42 and Figure 43 show zoomed out plots of the FFR results capturing the entire day 3 test period.

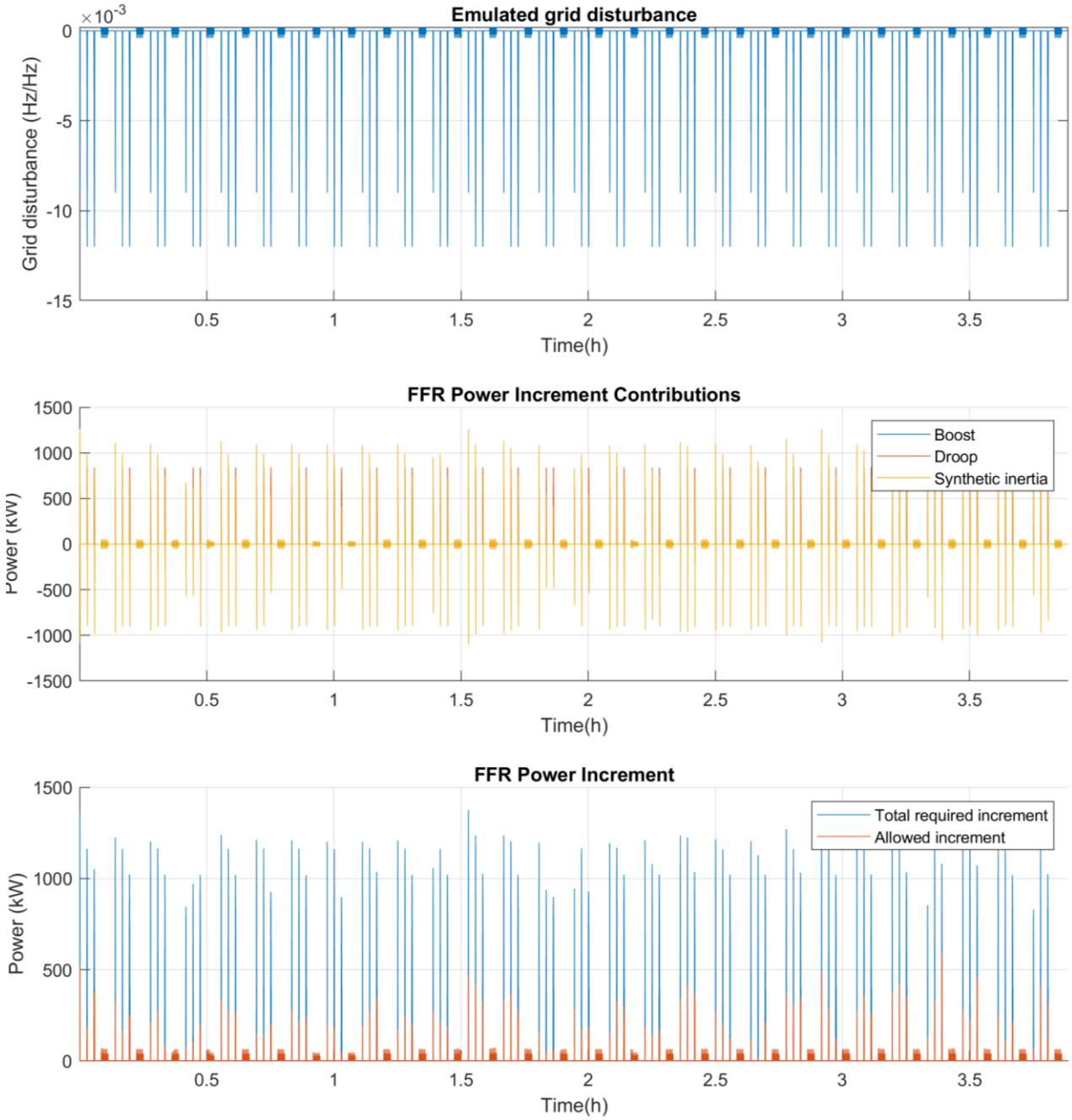

Figure 42 Zoomed out field test time series of emulated grid disturbance and resultant power increments

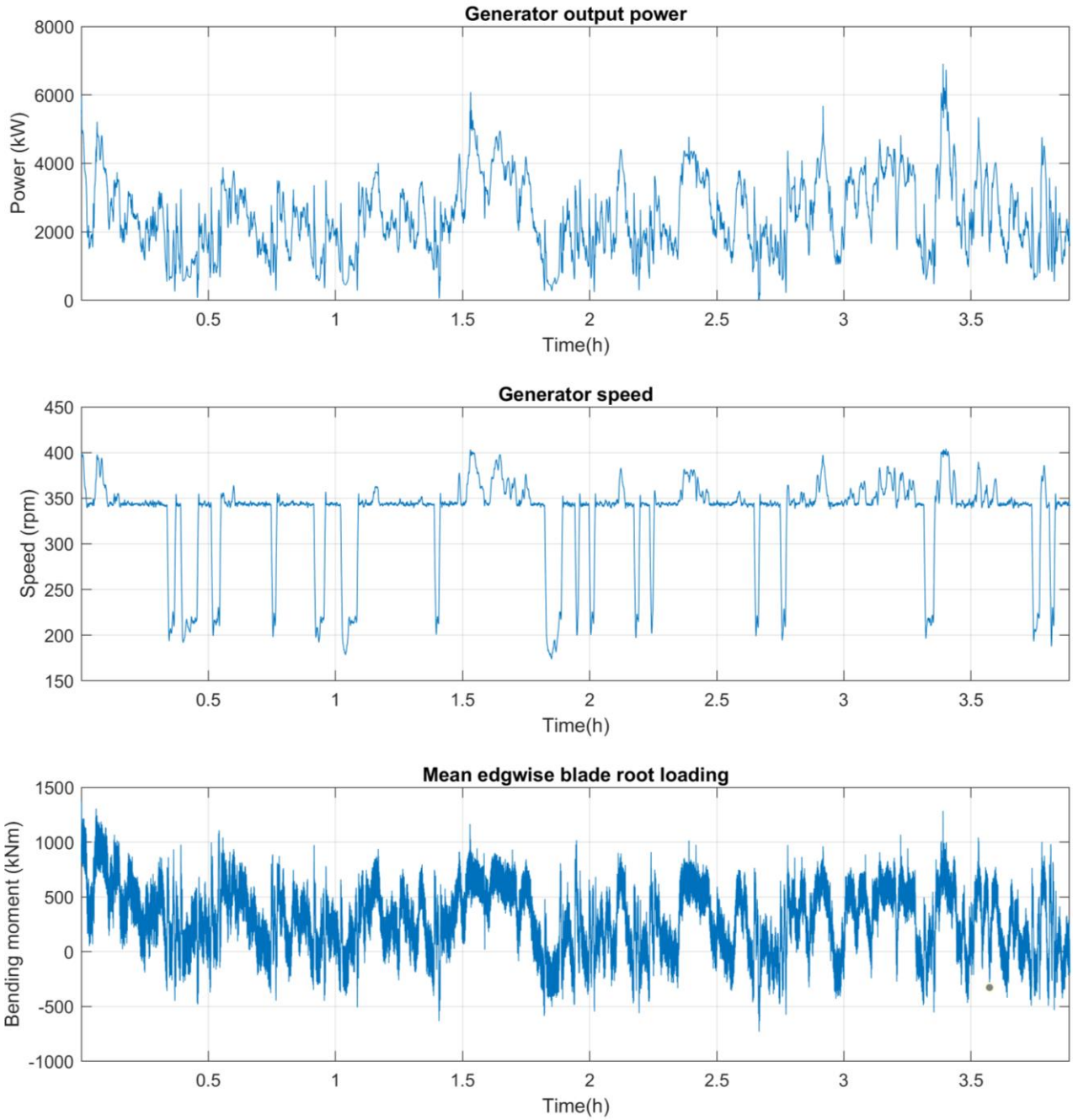

Figure 43 Zoomed out field test time series of key turbine operational and loads signals in response to applied FFR power incrments

As can be seen from Figure 42 and Figure 43, throughout the test period, the FFR algorithm has negligible effect on the generator speed and blade edgewise loading. All test days were analysed and showed similar results. It can therefore be concluded that the FFR algorithm has been implemented correctly and is able to output increased power for short periods of time in response to a grid disturbance without stalling the rotor or increasing rotational hub Mx loads significantly. An interesting next step, if feasible, might be to test the FFR algorithm on a small wind farm within a micro-grid, to observe the improved grid frequency stability that can be achieved.

8. CONCLUSIONS

This report describes the various controller field tests which were carried out on the 7MW Levenmouth Demonstration Turbine as part of Task 3.2 of the TotalControl project and the data which has been collected. Preliminary analyses of the results for each of the tests are also presented. The experiments have yielded a large amount of valuable data, which will continue to be analysed well beyond the end of the TotalControl project, and further results will be published in due course.

The yaw misalignment tests have produced convincing wake deflection results from the rear-facing scanning LiDAR, which will be particularly valuable for validating and increasing confidence in the engineering models currently used to predict wake deflection, while the measured turbine power and loading results will increase confidence in the use of aeroelastic models for yawed turbines.

The delta control tests have demonstrated how large reductions in rotor thrust can be achieved by means of smaller reductions in output power. Concurrent scanning LiDAR measurements clearly show the wake velocity deficits which are expected to be reduced, giving the potential for reducing the wake losses in a wind farm context.

Derating tests have successfully demonstrated two alternative algorithms for power reduction with different consequences for turbine loads.

Successful operation of the LiDAR-assisted control feature has been demonstrated, although this test eventually only ran for a few hours because of a long period of insufficient wind speeds in the period before the LiDAR system had to be decommissioned.

Some data has been collected with different modes of individual pitch control operation, although the amount of useful data was found to be small because of limitations on the allowable pitch demands and technical issues with the tower top strain gauges which still needed to be resolved.

The performance of the fast frequency response algorithm was successfully demonstrated, with data for different simulated grid frequency disturbances collected over a good range of wind conditions.

The project has clearly demonstrated how a large wind turbine controller can be adapted for testing significant controller modifications while maintaining safety and integrity of the turbine at all times. Thanks to careful testing prior to implementation, every test ran successfully from its first commissioning. Overall, a large amount of useful data has been collected despite many challenges, which included limited site access during the Covid-19 pandemic, significant turbine downtime at critical periods, equipment problems, and lack of suitable wind conditions at other critical times.

8.1. Measure of success according to DoA

Where appropriate, the measured results have been compared against computer simulation results from tasks 3.1.2, 3.1.3 and 3.1.4, as specified in the DoA. The delta control, derating and fast frequency response tests satisfy this criterion for task 3.1.2 (Controller adaptability and operational flexibility) and Task 3.1.3 (Ancillary services active power control), and the LiDAR-assisted control for Task 3.1.4 (Load reduction and damping).

9. REFERENCES

[1] TotalControl deliverable D3.1: 7 MW turbine model and reference loadset (Confidential, only for members of the consortium)

[2] TotalControl deliverable D3.2: Controller adaptation for varying conditions and ancillary services, https://ec.europa.eu/research/participants/documents/downloadPublic?documentIds=080166e5c8dea85c&appId=PPGMS

[3] TotalControl deliverable D3.3: Tower load reduction using active damping, https://www.totalcontrolproject.eu/-/media/sites/totalcontrol/publications/public-deliverables/d3-3_tower-load-reduction-using-active-damping.pdf?la=da&hash=9045A99E843CE62DA75CB55667ACD2BF248B89DE

[4] TotalControl deliverable D3.4: Model predictive turbine control, https://ec.europa.eu/research/participants/documents/downloadPublic?documentIds=080166e5c533e798&appId=PPGMS

[5] TotalControl deliverable D3.5: Tower load reduction with LiDAR-assisted control, https://ec.europa.eu/research/participants/documents/downloadPublic?documentIds=080166e5cabc44d7&appId=PPGMS

[6] TotalControl deliverable D3.6: Wind field measurements using LiDAR, https://www.totalcontrolproject.eu/-/media/sites/totalcontrol/publications/public-deliverables/deliverable_3_6_totalcontrol_final.pdf?la=da&hash=668DA615A411448F98A48C4C82B482D6D83B1C73

[7] TotalControl deliverable D3.8: MPC Validation, https://www.totalcontrolproject.eu/-/media/sites/totalcontrol/publications/public-deliverables/d3-8_model-predictive-control-theory-and-implementation-for-wind-turbines.pdf?la=da&hash=BB41B59930B25169EE41CDE9AF636B66ECD30BCA

[8] TotalControl deliverable D3.9: Predictive wind field model, https://www.totalcontrolproject.eu/-/media/sites/totalcontrol/publications/public-deliverables/d3-9_predictive-wind-field-model.pdf?la=da&hash=1436422FF974A2847E47A9E5538D9714931399E5

[9] TotalControl deliverable D2.3: Optimization of WPP set-points, https://www.totalcontrolproject.eu/-/media/sites/totalcontrol/publications/public-deliverables/d2-3-optimization-of-wpp-set-points.pdf?la=da&hash=46AA2A378049E2BCD4C9A0C671CA8C3A4CF09315

APPENDIX 1: DELTA CONTROL ALGORITHM DESCRIPTION AND TESTING IN BLADED

INTRODUCTION

DNV GL have proposed several controller adaptations to be tested on the Samsung 7MW test turbine located in Levonmouth, Scotland, as part of Task 3.2 in the ongoing EU funded research project TotalControl. One of the proposed controller adaptations is a delta control algorithm which allows the turbine power to be decreased at any wind speed in the operational range. This has potential applications both for responding to curtailment demands from the grid and for axial induction control of a wind farm, where power reductions on some turbines can increase overall wind farm production due to reduction of wake losses.

DNV GL have recently developed an improved delta control algorithm which is optimised for wind farm control applications. The algorithm aims to maximise power production for a given thrust reduction, and is also more straightforward to implement within the controller architecture. DNV GL therefore propose to use this algorithm for the field testing. This document gives an overview of the algorithm developed and summarises the Bladed simulation test results. The results demonstrate the correct operation of the algorithm and indicate that the loading implications of the new algorithm should be benign.

BACKGROUND

Axial induction control is a wake control method used in wind farm control. The fundamental principle is to reduce the thrust of some upstream turbines in such a way as to decrease the wake effects on downstream turbines so that the resultant power production of the whole wind farm is greater due to the control action. Delta control is a means of reducing the turbine power for this purpose, and also for implementing any power curtailments that might be desired or mandated for assisting the operation of the grid system.

Thrust reduction on the upstream turbine can be achieved in many ways. Previous methods employed by DNV GL involved using a power reduction setpoint as a proxy for controlling the thrust on the turbine. In order to maintain a constant power delta in varying wind conditions, this algorithm relied on a wind speed estimator and a simplified turbine model within the controller to predict what the power would have been if the turbine was operating normally. It then calculated the target power by subtracting the power delta from the expected power. A new fine pitch angle and torque demand were calculated online in order to achieve the target power while maintaining the rotor speed. This method resulted in excellent active power control as the power delta was maintained through turbulent wind conditions. The power delta resulted in a corresponding thrust reduction, enabling the delta control to be used for wind farm control applications.

Although effective, this method requires significant modifications to the turbine's normal control algorithm. The new approach maintains the normal control algorithm and achieves the desired performance by dynamically adjusting three of the algorithm setpoints which are normally fixed. The fine pitch angle is used as for the basic thrust control setpoint. The optimal mode gain and the maximum torque setting are then also changed as a function of the fine pitch setting using pre-defined look-up tables. Changing the optimal mode gain causes rotor speed changes which maximise the power produced for each fine pitch setting, while reducing the maximum torque setpoint allows the power reduction to continue smoothly into the above-rated region.

An overview of the algorithm is described next, followed by a review of Bladed test results.

ALGORITHM OVERVIEW

The aerodynamic behaviour of the turbine changes as a function of the turbine's fine pitch angle. The maximum power coefficient changes and the corresponding optimal tip speed ratio changes. In order to maximise power production for the given fine pitch angle, the optimal mode gain must be adjusted with respect to the new optimal tip speed ratio. By doing this, the torque will be controlled optimally so that maximum power is produced for the given thrust reduction. The optimal mode gain for each fine pitch setting is calculated offline using Bladed.

Adjusting the fine pitch only influences the turbine's operation below rated generator speed. In order to maintain thrust reduction above rated, the maximum torque setting for the turbine needs to be adjusted as well. This torque setting is somewhat arbitrary as the current algorithm is based on a fine pitch setting and not a power reduction setpoint. The maximum torque is calculated based on a set of steady power curves for the range of fine pitch angle and optimal mode gain settings. The power delta observed at rated generator speed for the given fine pitch angle compared to the baseline fine pitch angle was used to calculate the maximum torque setting to maintain this power delta above rated generator speed. Thus, the achieved power delta changes with wind speed until the maximum rotor speed is reached and is kept constant thereafter. The appropriate torque limit was calculated offline and added to the look up table, which now gives an optimal mode gain and maximum torque setting for each fine pitch angle setting.

This is simply implemented in the controller by filtering the fine pitch angle input and interpolating the respective parameters from the look up table to be used in the existing power production algorithm.

The turbine has a large speed exclusion zone, and it is important to check that the turbine is able to transition through this zone with the changes in fine pitch angle. After some initial testing it was found that some of the tower exclusion parameters would need to be adjusted as a function of the pitch angle as well, to prevent oscillations back and forth through the speed exclusion zone. The speed exclusion zone torque limits were changed based on the changes in the slope of the aerodynamic torque speed curve. The wait time before an exclusion zone transition was increased as a function of the fine pitch angle to minimise transitions through the speed exclusion zones at higher fine pitch settings.

The resultant operating curve for the turbine at a range of fine pitch angles and the corresponding optimal mode gain and max torque settings is shown in Figure 0-1 and Figure 0-2 on the following pages. The coloured lines represent the aerodynamic torque speed curves for the turbine at each wind speed, with the bold lines representing the operating torque speed behaviour of the turbine accounting for the speed exclusion zone. For large fine pitch angles, it was found that the corresponding optimal model gain increased substantially relative to the baseline value. This resulted in the optimal torque (Kopt x gen speed2) being greater than the torque limit below rated gen speed. In order to maximise power production in these cases, the

torque limit was calculated as function of the generator speed to ensure a constant power delta. This is seen by the quadratic downward ramp of the torque as it approaches rated generator speed for the higher fine pitch settings in Figure 0-2.

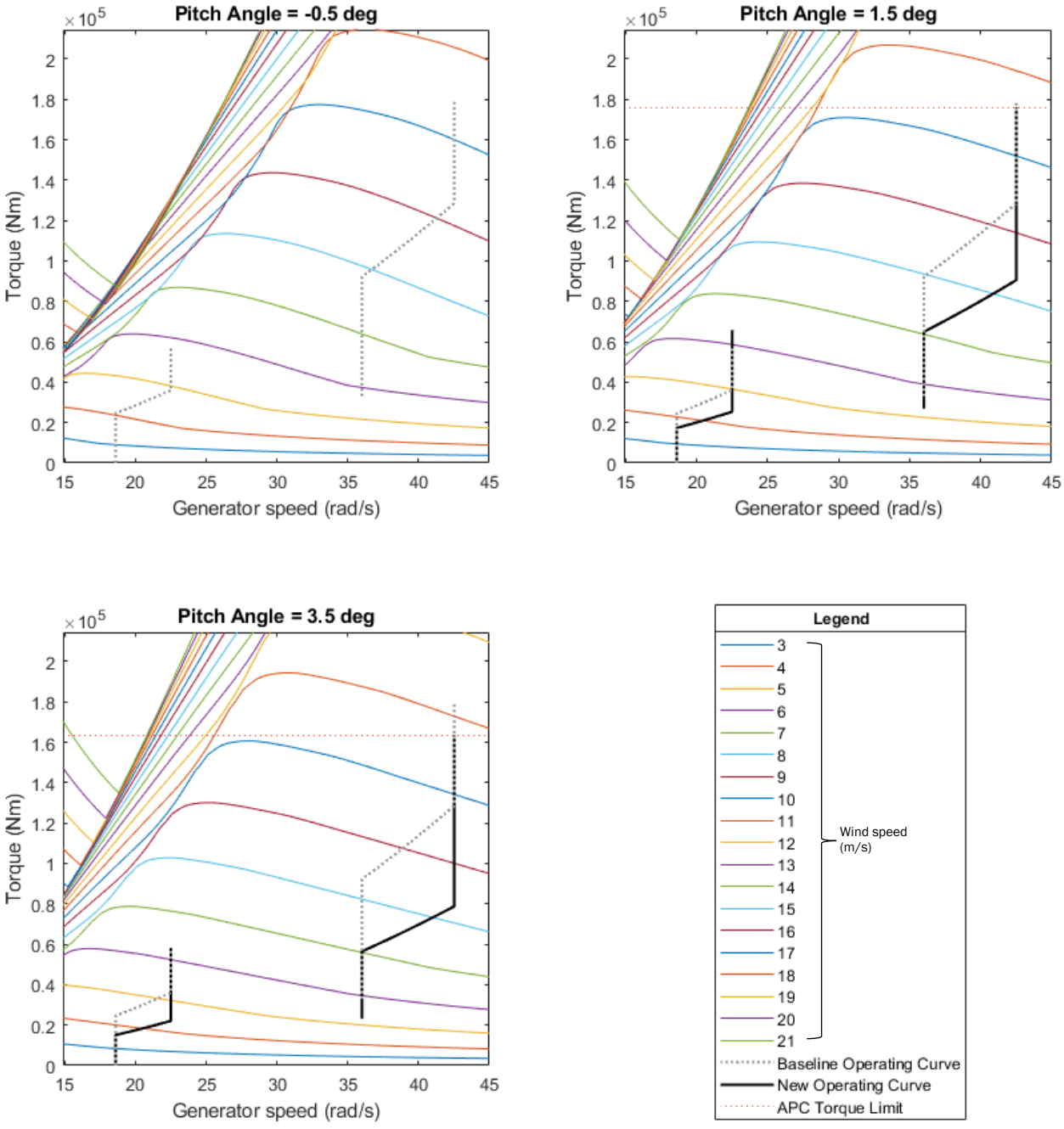

FIGURE 0-1 AERODYNAMIC AND OPERATIONAL TORQUE SPEED CURVES FOR FINE PITCH ANGLES -0,5° TO 3.5°

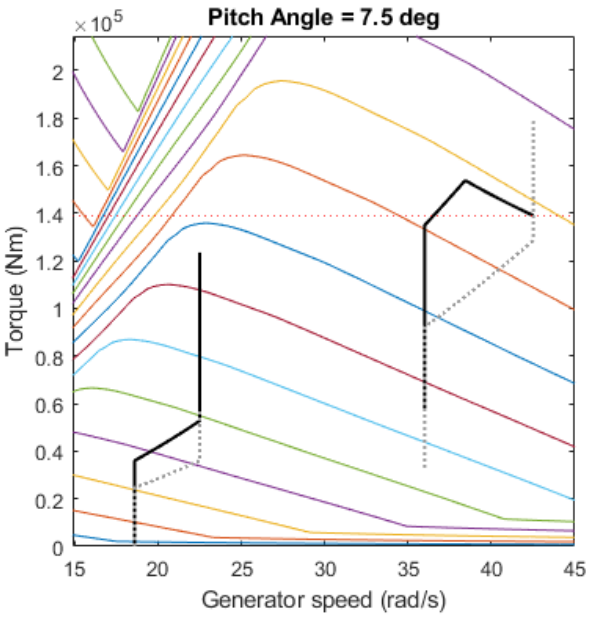
Pitch Angle = 7.5 deg
×10^5
Torque (Nm)
Generator speed (rad/s)

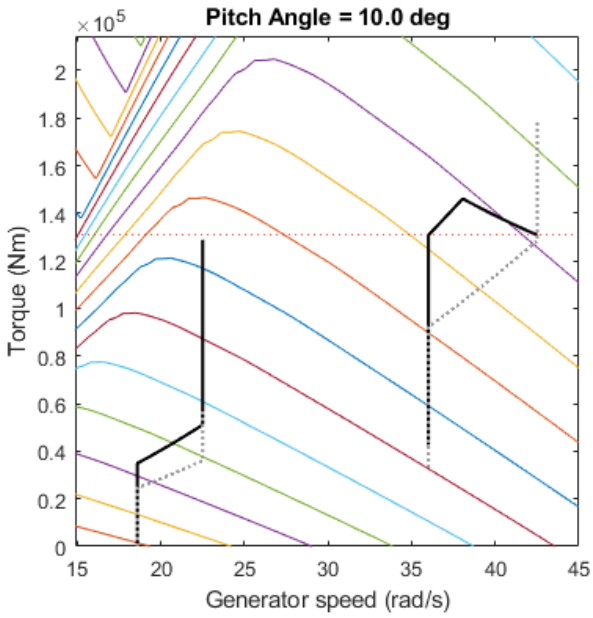
Pitch Angle = 10.0 deg
×10^5
Torque (Nm)
Generator speed (rad/s)

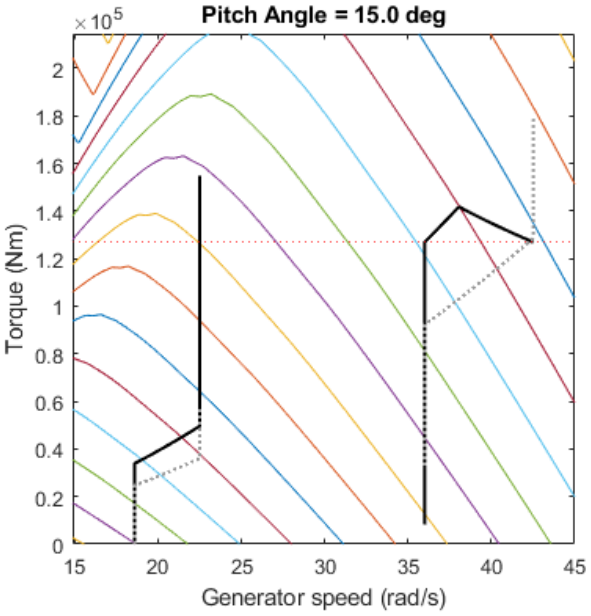
Pitch Angle = 15.0 deg
×10^5
Torque (Nm)
Generator speed (rad/s)

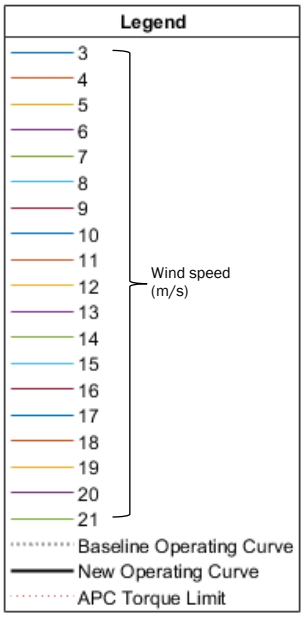
Legend
3
4
5
6
7
8
9
10
11
12
13
14
15
16
17
18
19
20
21
Wind speed (m/s)
Baseline Operating Curve
New Operating Curve
APC Torque Limit

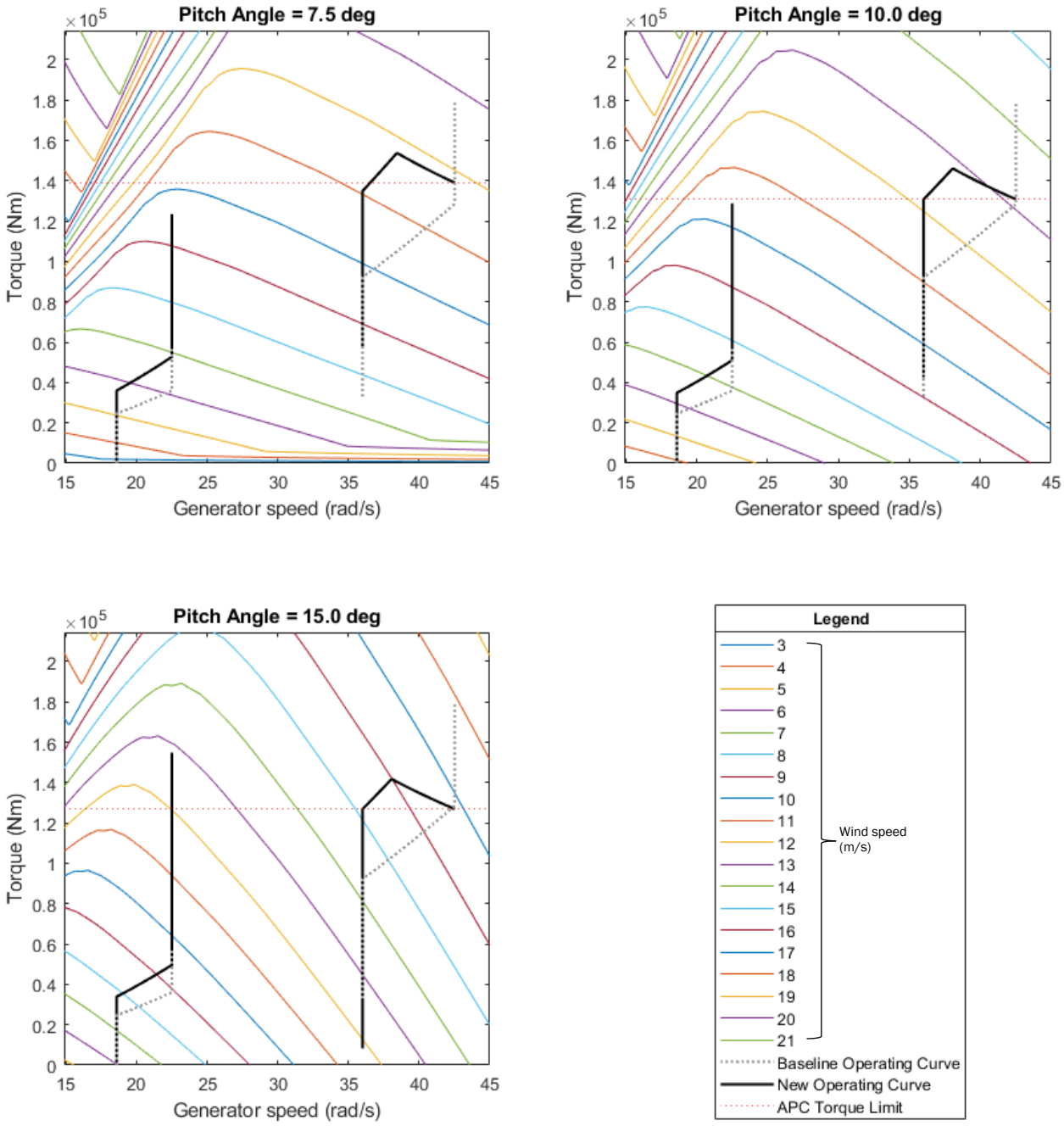

FIGURE 0-2 AERODYNAMIC AND OPERATIONAL TORQUE SPEED CURVES FOR FINE PITCH ANGLES -7.5° TO 15.0°

BLADED TESTING

The algorithm was compiled in the controller source code and tested in Bladed through a range of wind speeds and fine pitch angles. The turbine has a cut in wind speed of ~3.5m/s and rated wind speed of ~10.5m/s. The following wind speeds were chosen to cover the operating range of the turbine.

3, 6, 8, 10, 12 and 16 m/s.

The turbulence intensity for each of the wind speeds matched that used for the power production load cases (DLC 1.2) for the turbine's design class. Two different turbulence seeds for each wind speed were used so that the sensitivity to turbulence seed could be observed. The following fine pitch angles for each of the wind speeds were tested to cover the range of expected fine pitch angles during operation.

-0.5º (default), 1.5º, 3.5º, 7.5º, 10º and 15º.

This results in a total of 72, 10-minute, Bladed simulations.

DEL analysis

The resultant damage equivalent load (DEL) for the key loads in each of the simulations was calculated and used to gauge the change in loading due to change in fine pitch angle across the operating wind speeds of the turbine. Although the DEL can be used to indicate changes in loading, due to the turbine having a speed exclusion zone, any transitions through this zone have large loading implications and skew the resultant DEL for that run. For these runs, the time series information was investigated to check that the turbine was able to successfully transition through the exclusion zone with the change in fine pitch angle and exclusion zone parameters. The histograms on the following pages summarise the DELs for each load across all 72 simulations. The subscript a and b represent the different turbulence seeds for that run. Each colour bar represents a different fine pitch angle as per the legend.

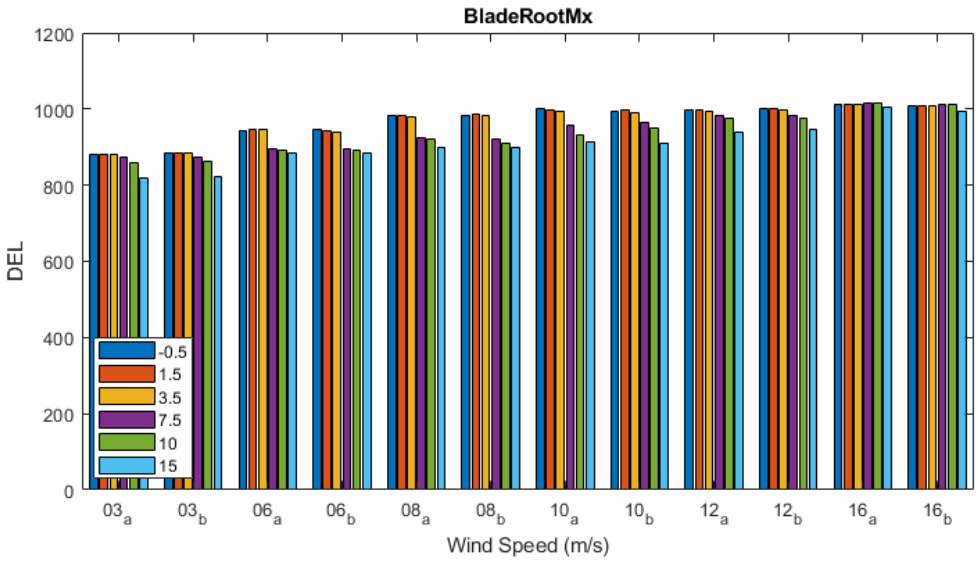

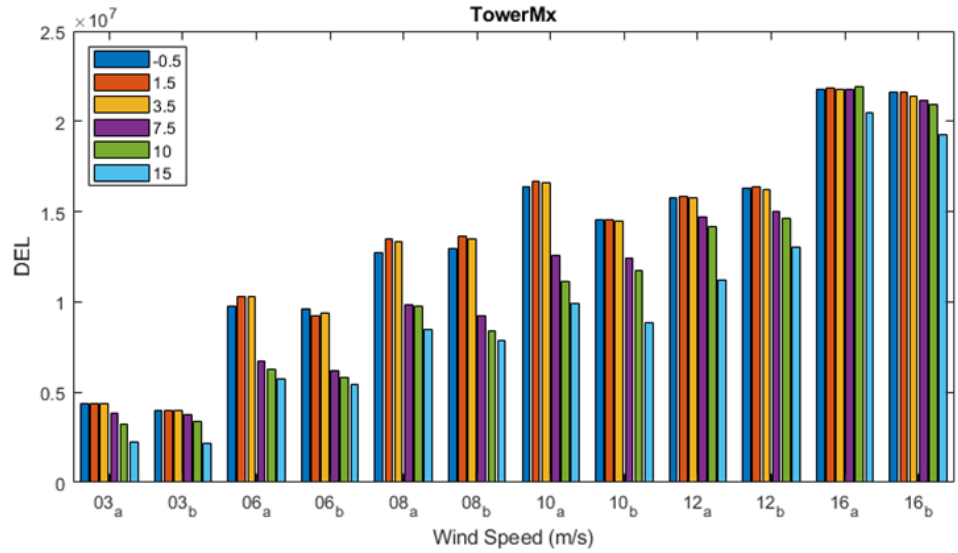
TowerMx
×10^7
2.5
2
1.5
1
0.5
0
DEL
-0.5
1.5
3.5
7.5
10
15
03a
03b
06a
06b
08a
08b
10a
10b
12a
12b
16a
16b
Wind Speed (m/s)

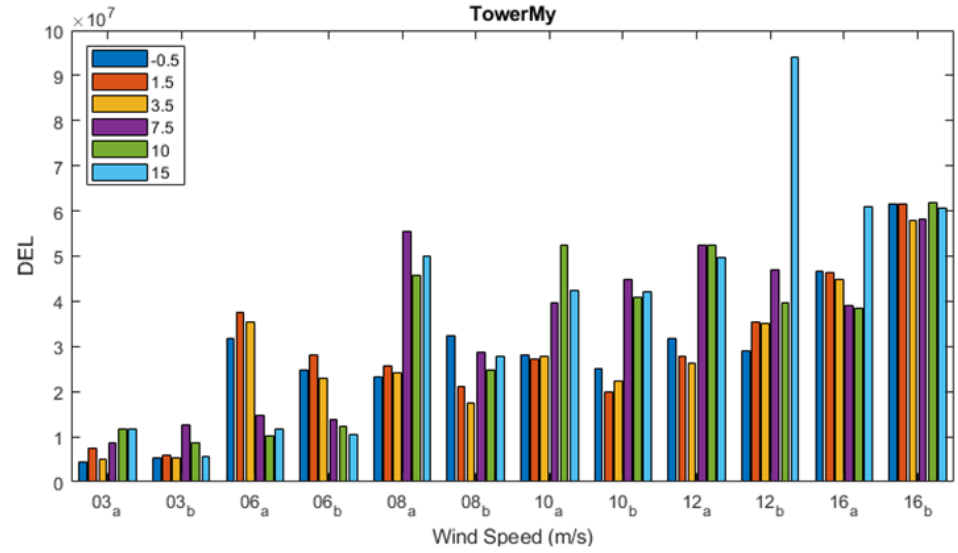
TowerMy
×10^7
10
9
8
7
6
5
4
3
2
1
0
DEL
-0.5
1.5
3.5
7.5
10
15
03a
03b
06a
06b
08a
08b
10a
10b
12a
12b
16a
16b
Wind Speed (m/s)

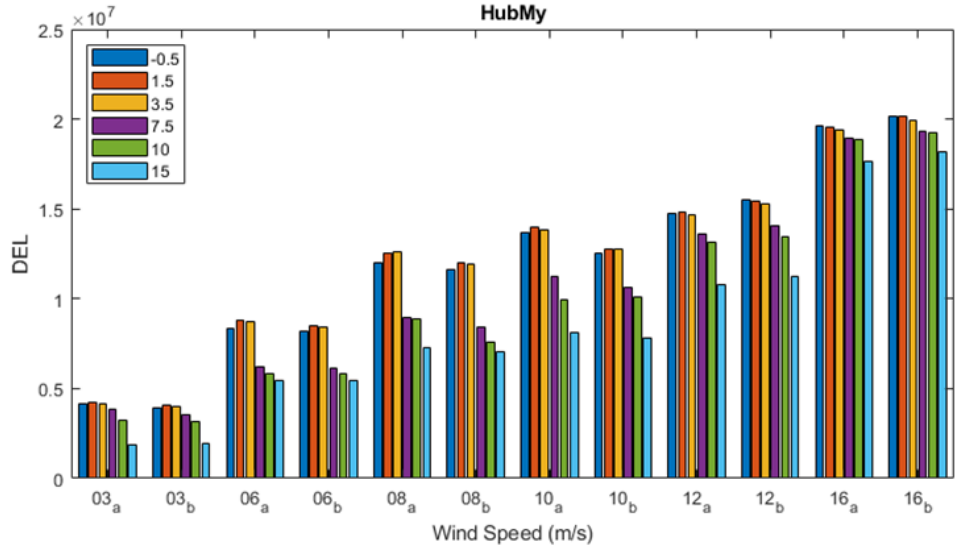
HubMy
×10^7
2.5
2
1.5
1
0.5
0
DEL
-0.5
1.5
3.5
7.5
10
15
03a
03b
06a
06b
08a
08b
10a
10b
12a
12b
16a
16b
Wind Speed (m/s)

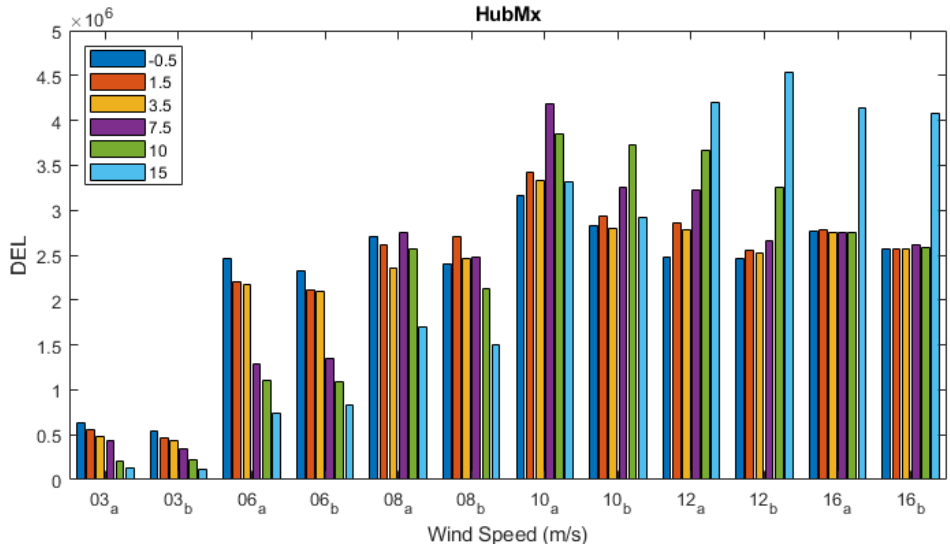
HubMx
×10^6
DEL
-0.5
1.5
3.5
7.5
10
15
03a 03b 06a 06b 08a 08b 10a 10b 12a 12b 16a 16b
Wind Speed (m/s)

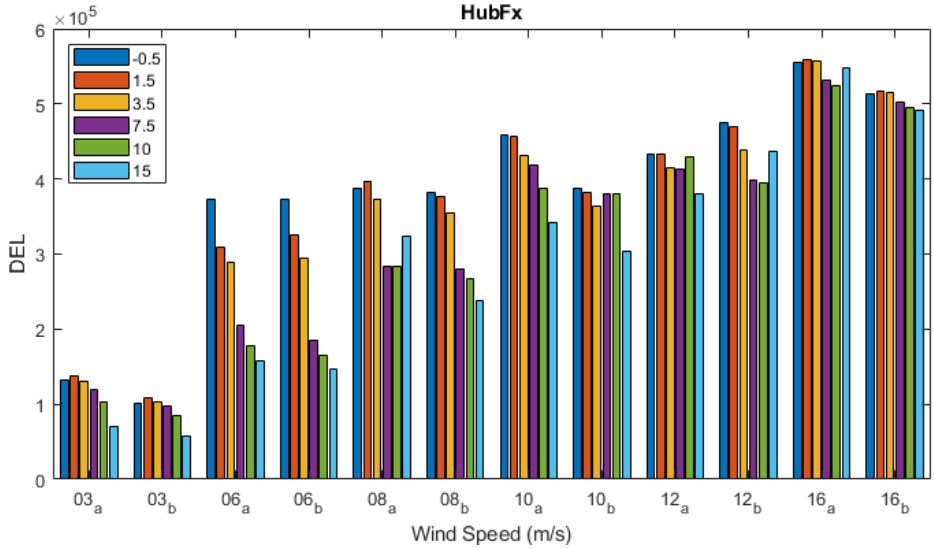
HubFx
×10^5
DEL
-0.5
1.5
3.5
7.5
10
15
03a 03b 06a 06b 08a 08b 10a 10b 12a 12b 16a 16b
Wind Speed (m/s)

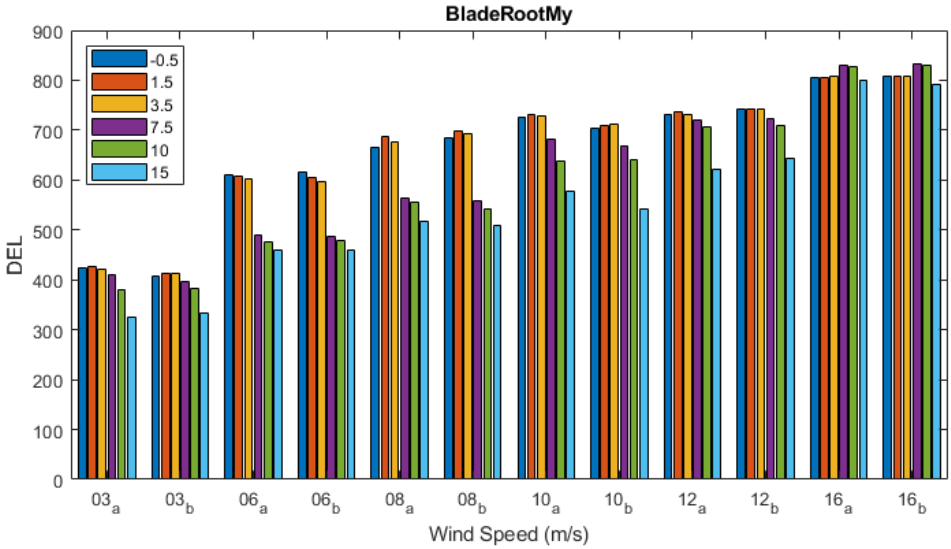
BladeRootMy
DEL
-0.5
1.5
3.5
7.5
10
15
03a 03b 06a 06b 08a 08b 10a 10b 12a 12b 16a 16b
Wind Speed (m/s)

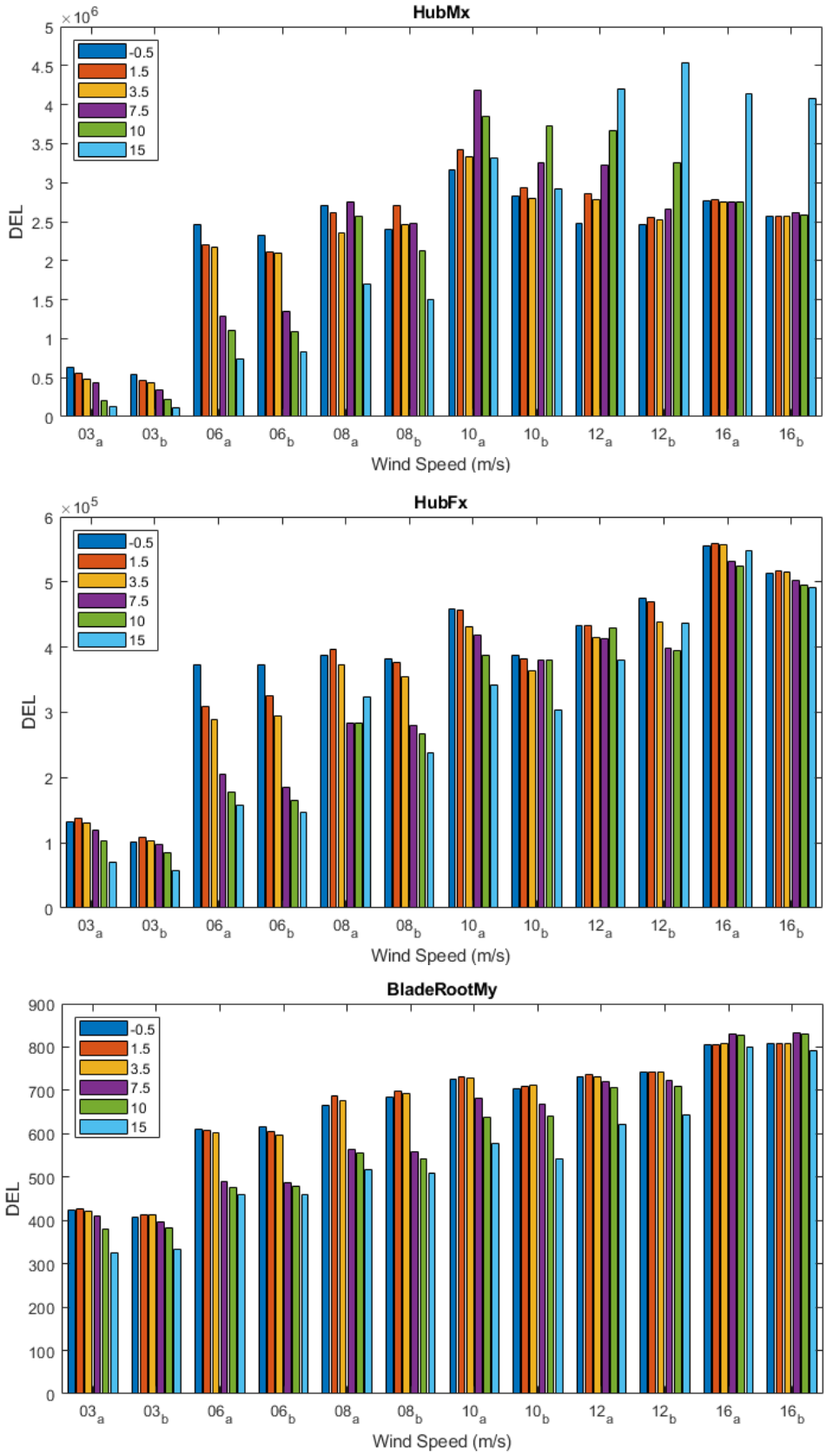

FIGURE 0-1: DEL HISTOGRAMS FOR A RANGE OF LOAD COMPONENTS

From the DEL analysis it can be seen that the only loads which experience an increase in fatigue loading as a result in the fine pitch setting changes are tower base My and hub Mx. For tower base My, there is large variation in loading between turbulence seeds for the same mean wind speed, for example, run 08a and 08b. In 08a, the fine pitch angle setting of 7.5° has the largest DEL, and in 08b, the nominal fine pitch setting of -0.5° has the largest DEL. This is due to sensitivity of the DEL to the speed exclusion zone transitions that occur in the run. Depending on the wind speed time series, the torque ramp required to cross the speed exclusion zone varies. Thus, the damage caused by a speed exclusion zone is not consistent between runs. Over the lifetime of the turbine, the change in accumulated damage due to a single transition is insignificant, however, for a 10-minute simulation, the transition has a significant contribution to the loading over the shorter period, which skews the DEL result. For tower base My, apart from the 15° fine pitch setting, the DELs are all lower than the DEL at 16m/s for the nominal pitch angle in seed B. This shows that the changes in loading due to the changes in fine pitch setting across the operating speeds of the turbine are all within an acceptable range of values. The only other load component which sees an increase in DEL for some fine pitch angle settings is the hub Mx load. The change is loading is acceptable apart from the 15° fine pitch settings at the higher wind speeds. The remaining loads, tower Mx, hub Fx, hub My, blade root My and blade root Mx all see a decrease in DEL with increase in fine pitch setting.

Time series analysis

Run 08a at 7.5° fine pitch angle settings and run 12b at 15° fine pitch settings were analysed in more detail due to their large tower base My DELs. If the delta control algorithm causes the turbine to become trapped in the speed exclusion zone due to the parameter changes it could cause a large increase in the tower base My DEL. To check if this was the case, the speed-torque plots for the two runs was analysed in Figure 0-2 and Figure 0-3 below.

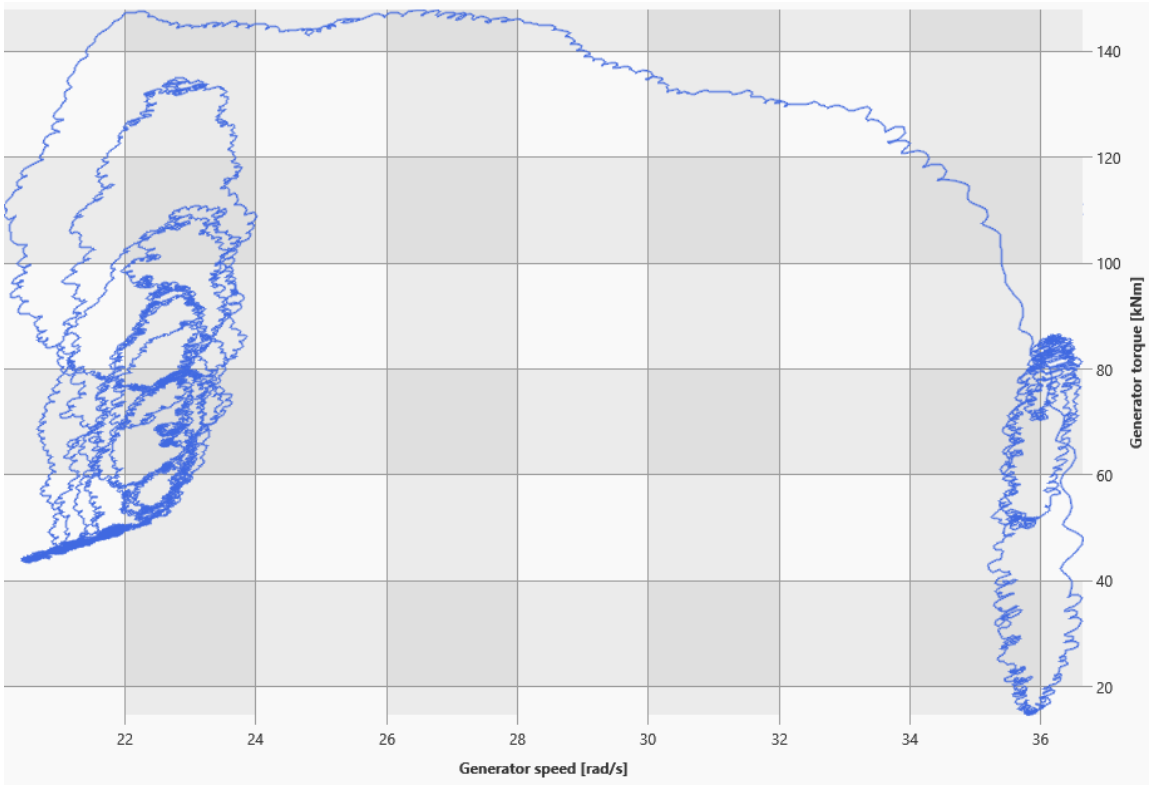

FIGURE 0-2: TORQUE-SPEED PLOT FOR RUN 08A AT 7.5° FINE PITCH SETTINGS

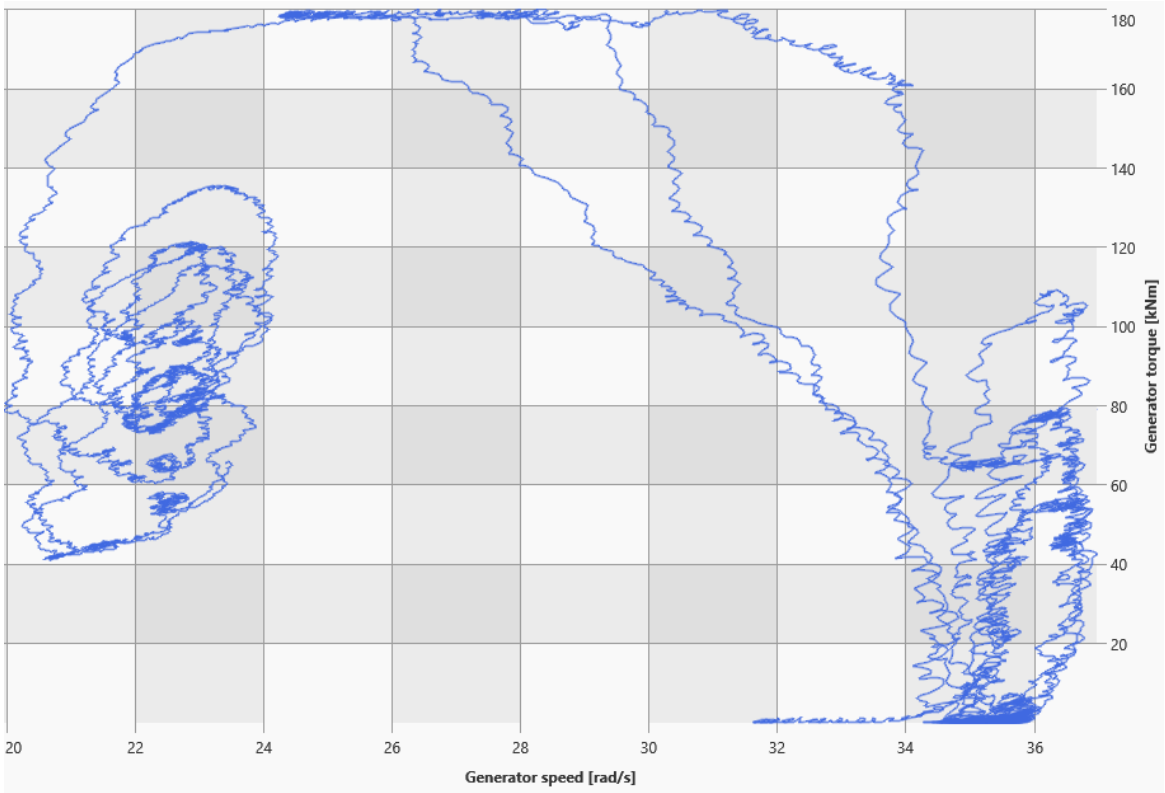

FIGURE 0-3: TORQUE-SPEED PLOT FOR RUN 12B AT 15° FINE PITCH SETTING

From Figure 0-2, it can be seen that turbine obeys the speed exclusion zone boundaries and successfully transitions once through the zone. Therefore, the higher tower base My DEL for this run is due to the specific wind seed based variation and not a fault in the parameter changes from the delta control algorithm. Contrastingly, Figure 0-3 shows that the turbine transitions three times through the zone, each time experiencing large torque variations over much of the range from 0 to rated. This can be attributed to the steep aerodynamic torque-speed curves for the wind speeds around the speed exclusion zone for a 15º fine pitch angle, as shown in Figure 0-2. This suggests that the 15º fine pitch settings are not suitable for deployment as they may result in excessive torque and thrust cycles due to harsh and frequent crossings of the speed exclusion zone. For safe operation of the turbine throughout the testing campaign, we propose that the fine pitch angle should be limited to a maximum of 10º. This will avoid the DEL increases seen in HubMx and TowerMy, and is in any case likely to be sufficient for axial induction control application in most situations.

Conclusion

DNV GL have developed a delta control algorithm that uses fine pitch angle as a proxy for thrust control. To optimise power production the optimal mode gain is also varied as a function of fine pitch. To maintain the thrust delta above rated, the maximum torque is limited accordingly. The speed exclusion zone torque limits and wait times are also varied as a function of fine pitch to compensate for the changes in aerodynamic behaviour of the turbine. The algorithm is simply implemented in the turbine controller by pre-calculating the parameters that vary with fine pitch angle and storing them in a look up table. The look up table is then interpolated from by the controller at run time based on a filtered fine pitch setting input. It was found that the algorithm doesn't significantly impact the loads on the turbine apart from the very high fine pitch setting of 15º. For the test campaign, the fine pitch setting will be limited to 10º to ensure that the turbine is operated safely.

APPENDIX 2: FAST FREQUENCY RESPONSE ALGORITHM DESCRIPTION AND TESTING IN BLADED

1 INTRODUCTION

DNV have proposed several controller adaptations to be tested on the Samsung 7MW test turbine located in Levonmouth, Scotland, as part of Task 3.2 in the ongoing EU funded research project TotalControl. One of the proposed controller adaptations is a fast frequency response (FFR) algorithm which allows the turbine power to be increased for a short period of time in response to a drop in the gird frequency. This has potential applications for grid ancillary services, where wind farms are able to provide grid frequency stabilisation over time periods in the range of 0-10 seconds. For TotalControl, the objective is to demonstrate the algorithm on the test turbine. The grid disturbance is emulated with internal state variables that vary according to a predefined schedule.

2 BACKGROUND

The frequency of an AC grid undergoes small variations which are important in ensuring a constant match between power supply and demand. Conventional power stations use directly-connected synchronous generators whose speed of rotation is tied to the grid frequency. This provides a natural regulation mechanism to help match supply and demand known as inertial response: if more power is being consumed than generated, the extra current drawn increases the generator torque, causing it to slow down; so some of its kinetic energy is used to supply the excess demand, and the grid frequency decreases; and vice-versa if there is excess supply. All such generators are locked together through the grid frequency, so they act together like a single giant flywheel stabilising the system and providing frequency containment. The resulting change in system frequency is linked to governors which adjust the energy input to the turbines, e.g. by controlling steam flow valves, providing closed-loop feedback known as primary frequency response or frequency restoration which ensures that the nominal frequency is maintained on average, and supply and demand are matched over time.

To maximise efficiency in varying winds, most commercial wind turbines use variable rotor speed: the generator is connected indirectly to the grid through a power converter, decoupling the rotor speed from the grid frequency and breaking the inertial response feedback mechanism. Thus the wind turbines do not contribute to frequency regulation, and as wind power (and other renewable sources such as solar PV) penetration increases this regulation duty must be performed by the ever smaller proportion of conventional synchronous plants, resulting in larger frequency variations, and potential system instability if plant starts to trip out. Figure 2-1 below illustrates a typical grid frequency response to a loss of generation event.

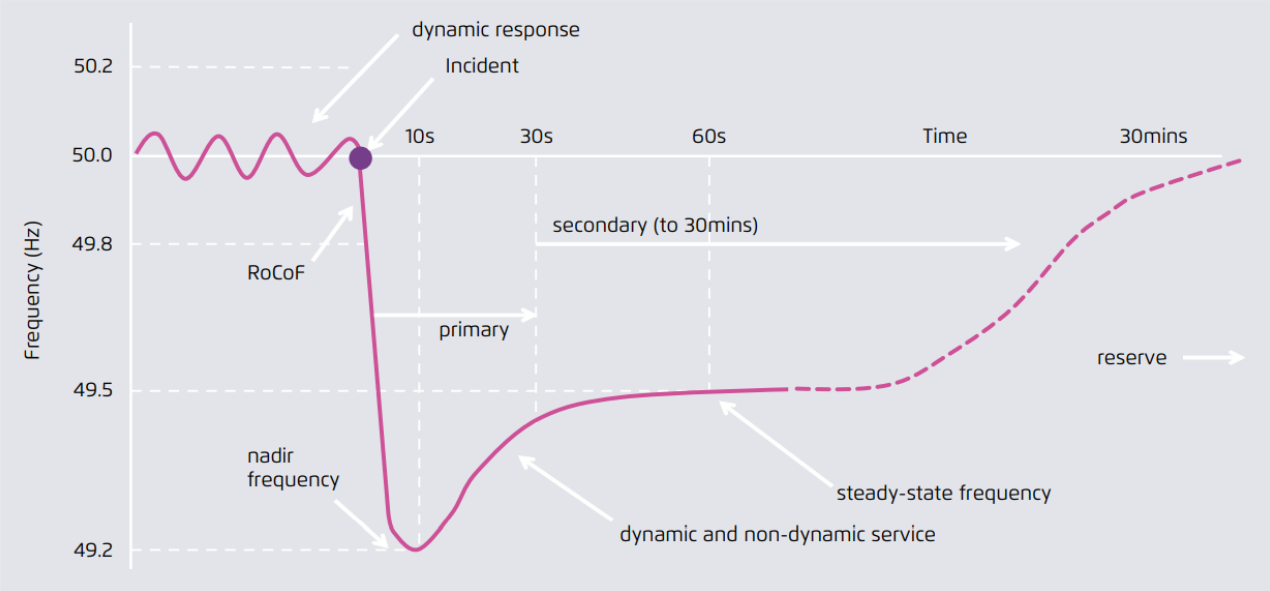

FIGURE 2-1 TYPICAL FREQUENCY RESPONSE BEHAVIOUR IN THE EVENT OF A LOSS OF GENERATION /1/

The primary response to the drop in grid frequency is generally supplied by the inertial contribution of conventional generation units as well as utility scale battery storage technology. The secondary response comprises backup power generation units which take some time to come on line. With less "inertia" on the grid due to renewable sources, the capacity of the primary response decreases and the initial drop in frequency due to a loss of generation event increases. If the drop in frequency goes outside the defined grid regulator's parameters, as it did for the UK in August 2019 /2/, the distribution network operators implement "load shedding" whereby consumers are disconnected from the grid in order to balance supply and demand to restore the grid frequency.

Wind turbines have a large rotational inertia. If an entire wind farm is considered, there is a significant amount of stored potential energy within the rotors across the farm. This stored energy can be used through an FFR algorithm to improve the primary response to frequency drops within the grid. DNV has been involved in the development of FFR algorithms for wind turbines since 2015, publishing a range of papers describing the proposed FFR algorithm tested in various simulations /3//4//5/. The DNV FFR algorithm has been tuned, implemented, and tested through Bladed simulations for the Samsung 7MW turbine. DNV believe that it is safe to proceed to field testing of the algorithm.

3 ALGORITHM OVERVIEW

The FFR algorithm has three main components, namely, calculation of the desired power increment based on the amount of grid disturbance, limitation of the power increment based on the rated power of the machine, current kinetic energy and stall margin of the rotor, and implementation of and recovery from the power increment.

3.1 Calculation of the required power increment

The FFR algorithm calculates the required change in power output as a function of the grid frequency. The power increment comprises three components, each defined to respond to different characteristics of the grid disturbance.

Droop control

Droop control is a proportional action, where the power is changed according to the frequency deviation, beyond a certain dead band. This is implemented as a lookup table of power change versus frequency deviation.

Synthetic inertia

For synthetic inertial response, the change in power is proportional to the rate of change of frequency (RoCoF). An arbitrary value is selected for the proportionality constant. The constant can be interpreted as the speed of a directly-connected synchronous generator, such that the emulated inertial response is the same as that of the synchronous generator with the same inertia as the turbine rotor.

Boost

The boost is a pre-determined increase in power maintained for a pre-determined length of time following the detection of a frequency drop below some threshold value.

3.2 Limitation of the power increment

The calculated power increment is limited such that the output power does not exceed the rated power of the machine. In practice, the rated power can be exceeded for short periods of time, however, to limit the risk for this project, a strict limitation is applied to the power increment to prevent the output power going above rated.

The power increment is achieved by increasing the generator torque rapidly, which in turn extracts the kinetic energy from the rotor, slowing it down. If the rotor is slowed down too much there is a risk that the rotor could stall resulting in a rapid loss of aerodynamic torque and the rotor speed dropping to zero. To prevent stall, DNV have derived from the Bladed model of the Samsung 7MW, the critical tip speed ratio (TSR) as a function of blade pitch angle, beyond which, stall would likely occur. Figure 3-1 below, shows the critical TSR and steady operational TSR versus blade pitch angle.

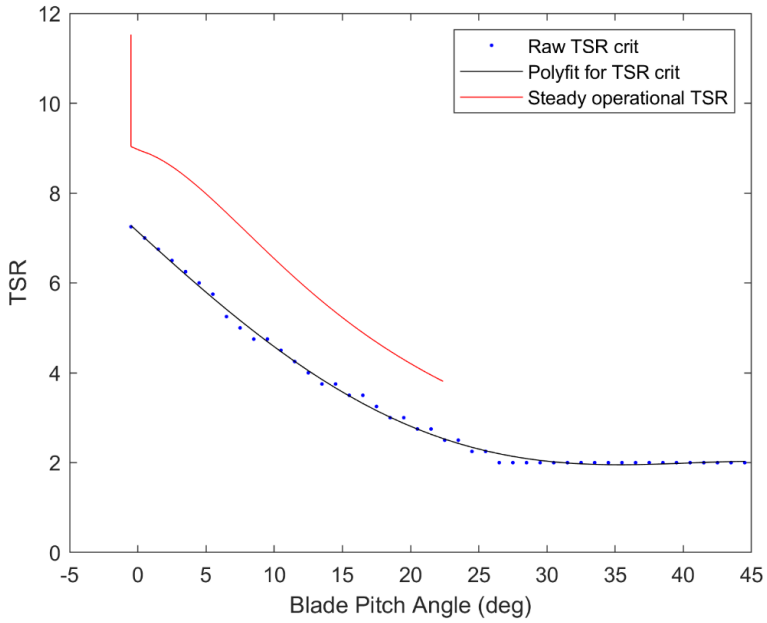

FIGURE 3-1 CRITICAL TIP SPEED RATIO BEFORE STALL AS A FUNCTION OF BLADE PITCH ANGLE

The available kinetic energy in the rotor before stall is induced is calculated using the following equations:

$$\omega_{min} = TSR_{crit}(\theta) \times \frac{U_{est}}{R} \quad or \quad \omega_{min} = minimum\ operational\ speed, whichever\ is\ greater$$

$$E_k = \frac{1}{2} \times I \times ({\omega_R}^2 - {\omega_{min}}^2)$$

Where,

ω_{min}	Minimum allowable rotor speed
$TSR_{crit}(\theta)$	Precalculated critical TSR before stall as a function of blade pitch angle, θ, shown in Figure 3-1.
U_{est}	Estimated rotor averaged wind speed from onboard wind speed estimator algorithm.
R	Rotor radius
E_k	Estimated available kinetic energy
I	Rotor inertia
ω_R	Measured rotor speed (generator speed divided by the gear box ratio)

The allowable power increment is calculated based on the available kinetic energy, described above, and a defined rotor inertia time constant. The inertia time constant can be interpreted as the time for which the stored kinetic energy could, in principle, supply the power output of the machine. It is calculated by dividing the kinetic energy of the rotor at rated rotor speed by the rated shaft mechanical output power. For the

Samsung 7MW, the kinetic energy time constant was calculated as 9.2 seconds (implemented as 9 seconds) which is in line with kinetic energy time constants calculated for other turbine rotors shown in Figure 3-2 below.

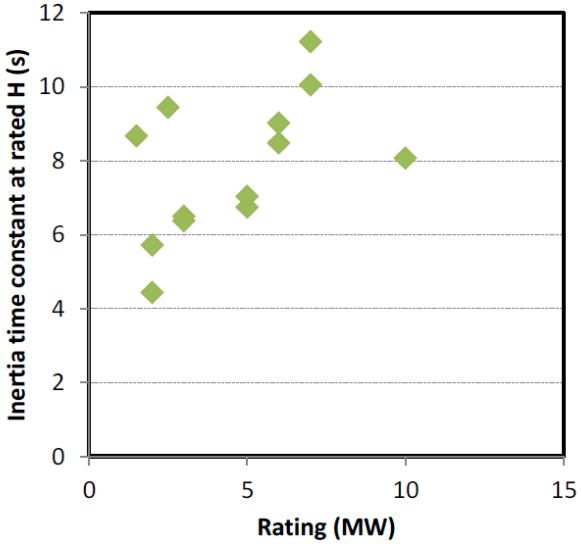

FIGURE 3-2 INERTIA TIME CONSTANTS OF SOME TYPICAL WIND TURBINE DESIGNS OF VARIOUS SIZES, BASED ON POWER AND ROTOR SPEED AT RATED WIND SPEED /3/.

Using the inertial time constant, T_i ,and the available kinetic energy before stall, E_k, the available power increment is then calculated as follows;

$$\Delta P_{available} = \frac{E_k}{T_i}$$

The required increment, calculated using the methodologies described in section 3.1, is then limited according to the available increment described above.

3.3 Implementation of the power increment

The resultant power increment is implemented in the controller by overriding the closed loop VSPR torque demand with a new torque demand, calculated with respect to the target output power. A simplified model of the turbine is implemented in the turbine controller to estimate the expected power of the machine with no FFR disturbances, to provide a baseline to which the power increment is added to so that the target power can be determined.

The expected power is based on the current wind speed estimate and characteristics of the turbine taken from the Bladed model such as the Cp table, rotor inertia, PID controller gains, drive train efficiency and generator efficiency. A low pass filter is then applied to the expected power estimate. The normal VSPR power demand is high pass filtered and added to the expected power to ensure the new torque demand contains the necessary high frequency drive train damping components.

To transition the FFR power demand back to the normal VSPR power demand smoothly, a "fade" fraction is defined which biases the low frequency target power either towards the expected power, or the current

VSPR power demand from the closed loop controller. The fade fraction is determined based on a few factors listed below:

- If the FFR power increment drops to zero, either due to the frequency recovering naturally or the limitations on the power increment to prevent stall or rated power exceedance, then the fraction decays according to a defined FFR decay time to smoothly transition the power demand back to the normal VSPR power demand.
- If the current generator speed begins to approach the minimum operational speed of the machine, the fraction decays according to a defined speed buffer such that the standard VSPR power demand is used at sync speed.

4 BLADED TESTING

The grid disturbance is emulated with state variables that vary according to a predefined schedule as shown in Figure 4-1 below. Note that the actual grid frequency will not be used to trigger any FFR events during the actual field tests of the algorithm.

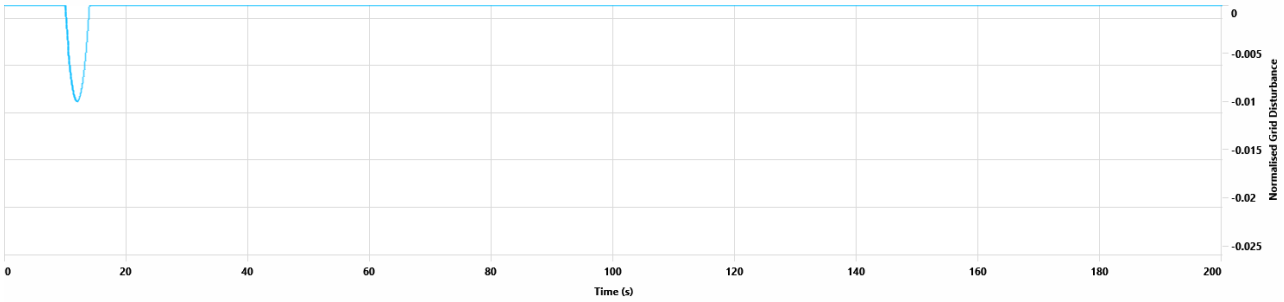

FIGURE 4-1 EMULATED GRID DISTURBANCE USED TO TRIGGER FFR ALGORITHM DURING TESTING

The main objective of the testing to show that the algorithm is doing the following:

1. Calculating the desired power increment based on the grid disturbance
2. Limiting the power increment based on the rated power of the machine and the available kinetic energy before stall
3. Implementing the power increment through a change in the generator torque demand
4. Recovering the loss in rotor speed after the power increment has been implemented
5. Returning back to normal operation

The FFR algorithm was tested in below rated, near rated and above rated conditions. As the FFR algorithm is only implemented over short periods of time, the change in fatigue loads were not analysed, only the ultimate loading on the rotating hub Mx was checked as this is most influenced by the rapid increase in torque demand due to the FFR power demand. Figure 4-2, Figure 4-3, and Figure 4-4 on the following pages show the simulation results.

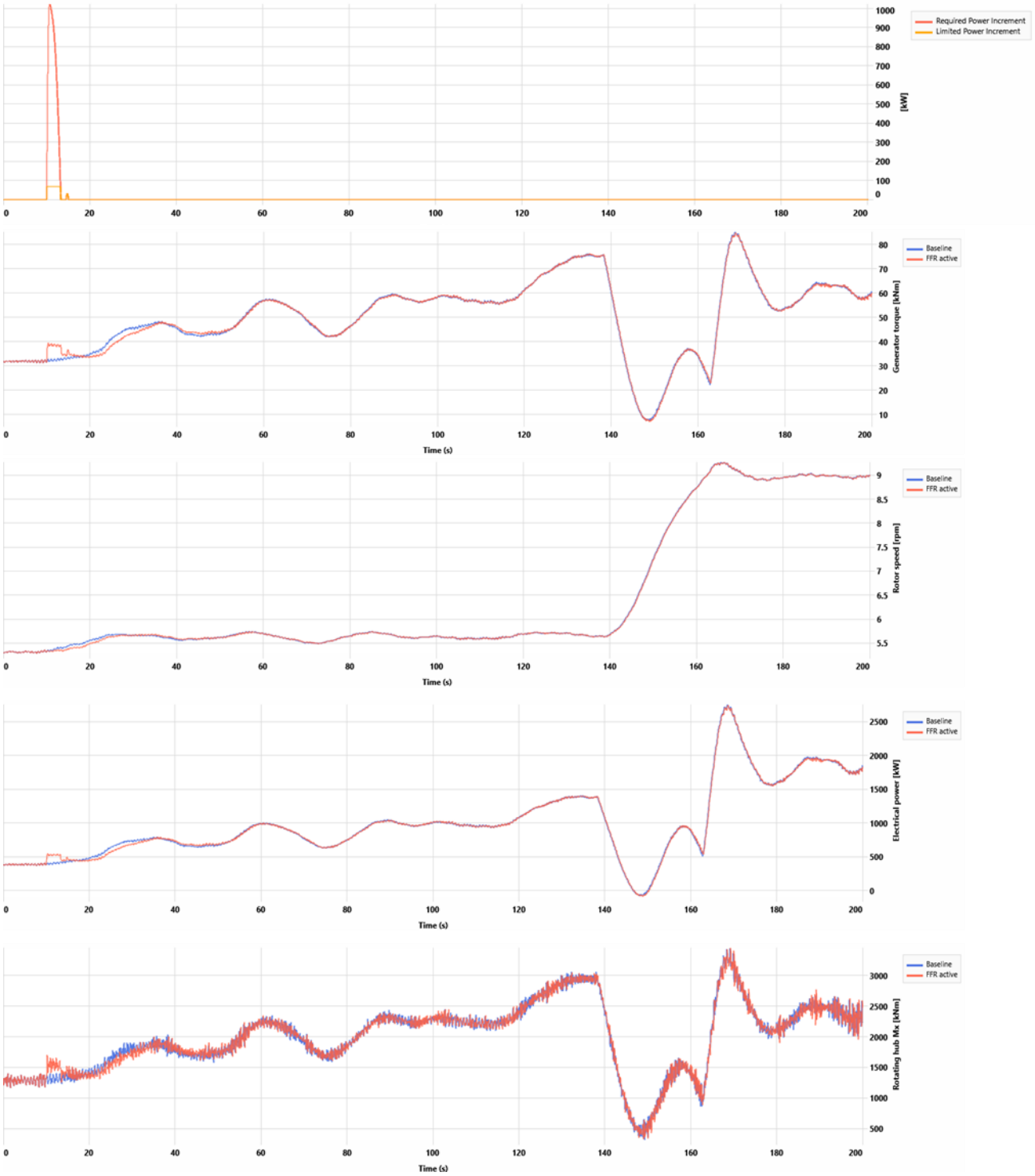

FIGURE 4-2 BLADED SIMULATION RESULTS AT 6M/S (BELOW RATED). FIRST PLOT SHOWS THE POWER INCREMENT, SECOND PLOT SHOWS THE GENERATOR TORQUE DEMAND, THIRD PLOT SHOWS THE ROTOR SPEED, FOURTH PLOT SHOWS THE OUTPUT POWER, AND FIFTH PLOT SHOWS THE ROTATING HUB MX LOADING

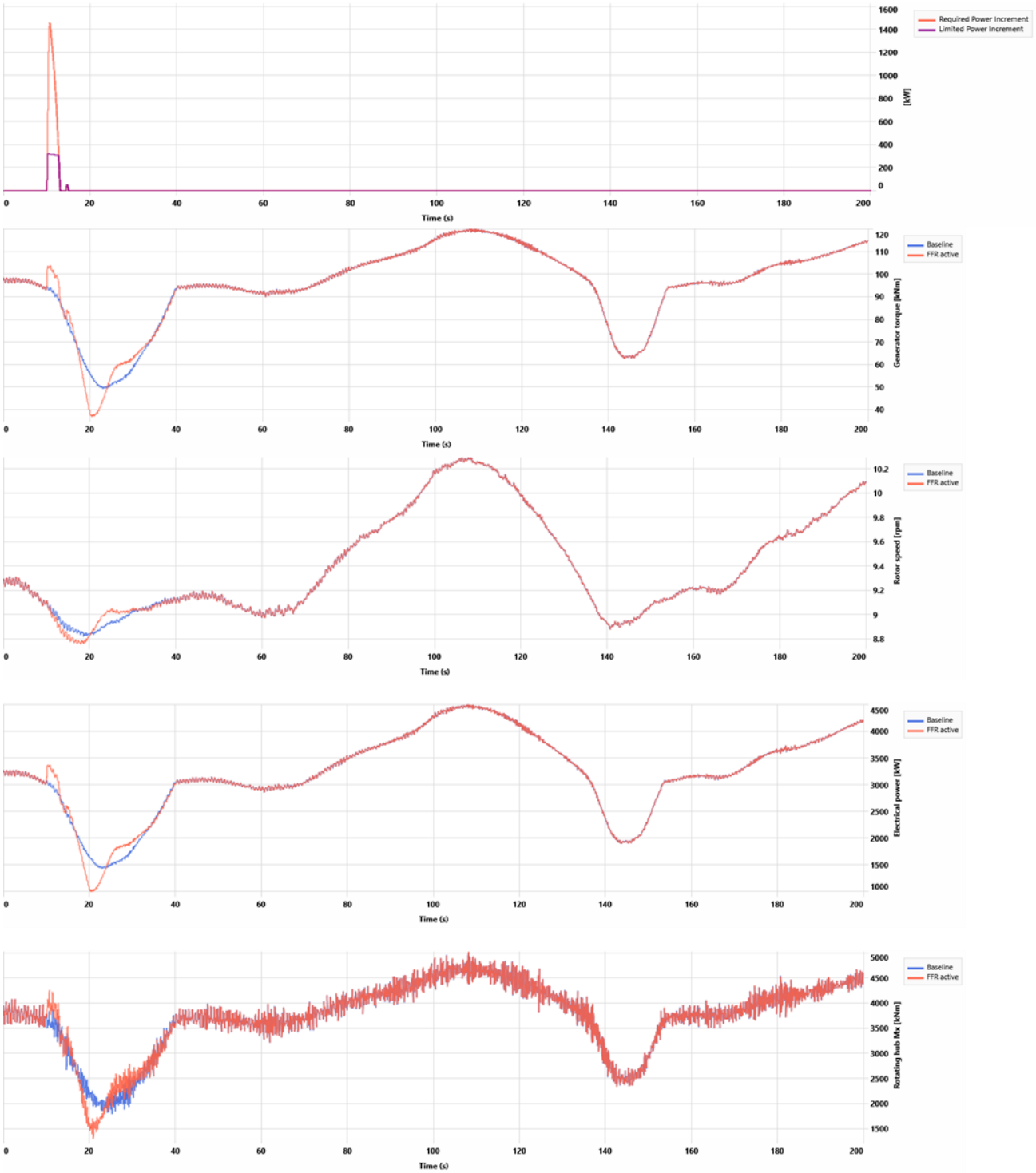

FIGURE 4-3 BLADED SIMULATION RESULTS AT 9M/S (NEAR RATED). FIRST PLOT SHOWS THE POWER INCREMENT, SECOND PLOT SHOWS THE GENERATOR TORQUE DEMAND, THIRD PLOT SHOWS THE ROTOR SPEED, FOURTH PLOT SHOWS THE OUTPUT POWER, AND FIFTH PLOT SHOWS THE ROTATING HUB MX LOADING

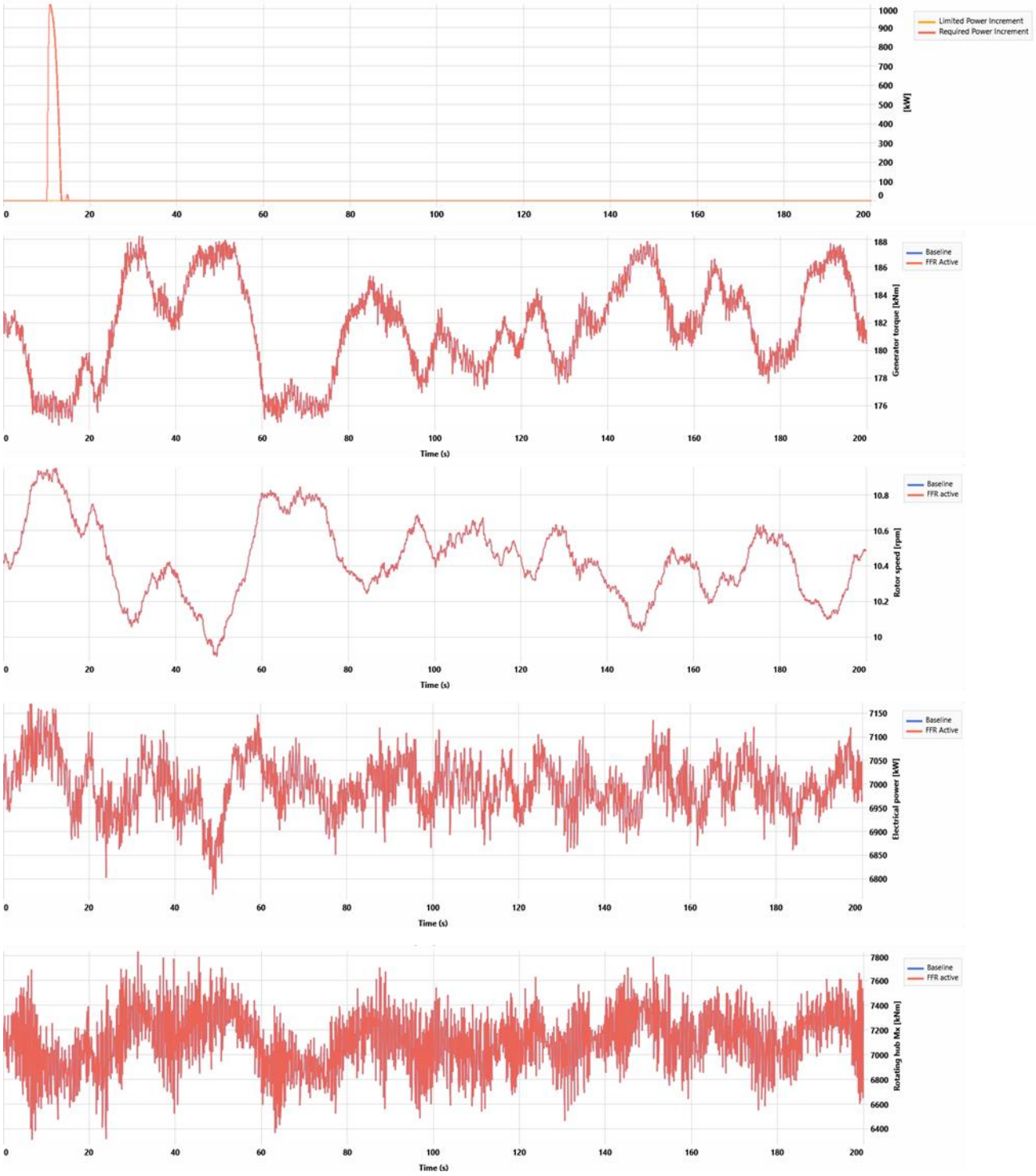

FIGURE 4-4 BLADED SIMULATION RESULTS AT 16M/S (ABOVE RATED). FIRST PLOT SHOWS THE POWER INCREMENT, SECOND PLOT SHOWS THE GENERATOR TORQUE DEMAND, THIRD PLOT SHOWS THE ROTOR SPEED, FOURTH PLOT SHOWS THE OUTPUT POWER, AND FIFTH PLOT SHOWS THE ROTATING HUB MX LOADING

For the below and near rated simulations, the power increment after the limitations are applied is implemented, showing a sharp increase in generator torque demand and resultant electrical output power. This results in a drop in the rotor speed as expected. The rotor speed then recovers, showing that stall was prevented, and the turbine returns to similar operation compared to the baseline. The rotating hub Mx loading shows an increase during the period of time that the FFR increment is being implemented, however the loading level is similar to that seen throughout the simulation and very much below the ultimate loading for the rotating hub Mx component. For the above rated simulation, the power increment is limited to zero so that the rated power of the machine is not exceeded. This results in no change to the operation of the machine compared to the baseline. Overall, the algorithm is working as expected.

5 CONCLUSIONS

DNV has implemented the FFR algorithm, developed in 2015, on the Samsung 7MW wind turbine controller and tested through Bladed simulations across the operational wind speed range of the machine. The algorithm worked as expected, producing an increased power output from the machine triggered by an emulated grid disturbance. The algorithm prevented the rotor from stalling and the turbine was able to return to normal operation after the grid disturbance event. The ultimate loading on the rotating hub Mx component was analysed and found to not be exceeded during the testing. DNV believe that the algorithm is safe to proceed to field testing.

6 REFERENCES

/1/ "Integrating renewables into the Japanese power grid by 2030", April 2019 , p22, Available: https://www.agora-energiewende.de/fileadmin2/Projekte/2018/Japan_Grid/148_Agora_Japan_grid_study_WEB.pdf

/2/ "The sequence of events of Friday 9th August 2019". August 2019. National Grid ESO. Available at: https://www.nationalgrideso.com/document/151061/download

/3/ "Generic grid frequency response capability for wind power plant", November 2015. Proc. European Wind Energy Association Conference. Ervin Bossanyi.

/4/ "Grid Frequency Stability with Wind Power: Irish Case Study Using a New Closed Loop simulation Environment". 2020. Proceedings of the 19th Wind Integration Workshop. Ervin Bossanyi, Wouter De Boer.

/5/ "Control algorithms for primary frequency and voltage support". 2020. Deliverable no. D4.1, Total Control. Ervin Bossanyi

APPENDIX 3: WAKE DEFLECTION LIDAR SCAN PLOTS

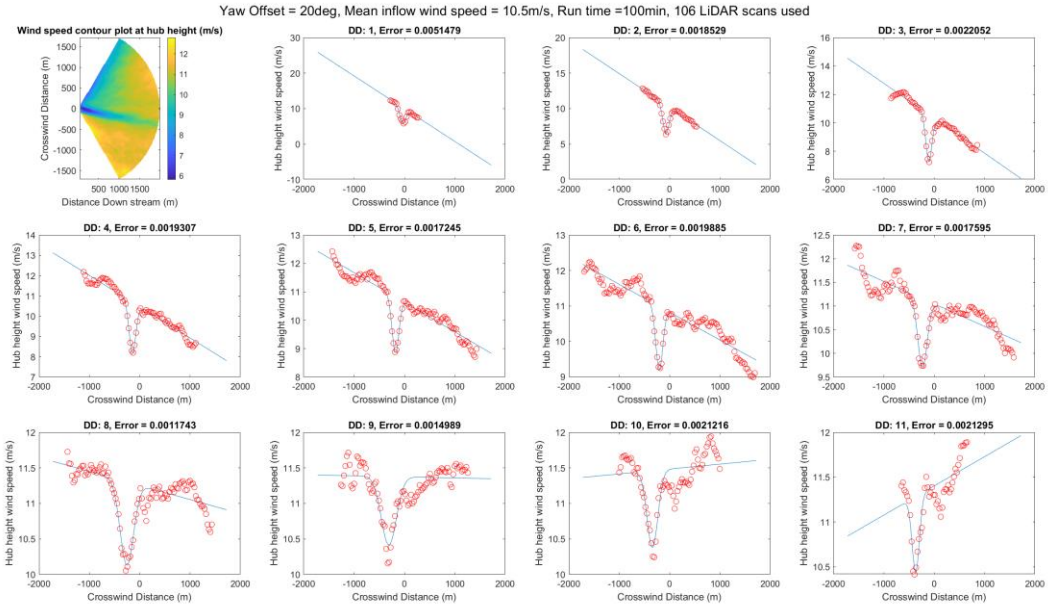

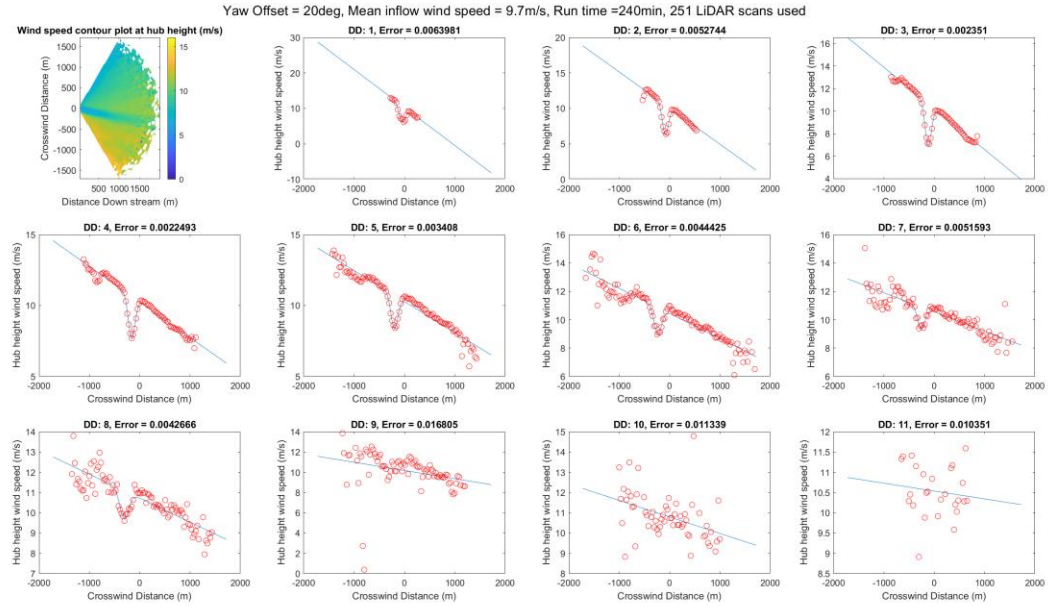

Yaw Offset = -20deg, Mean inflow wind speed = 11.3m/s, Run time =48min, 55 LiDAR scans used

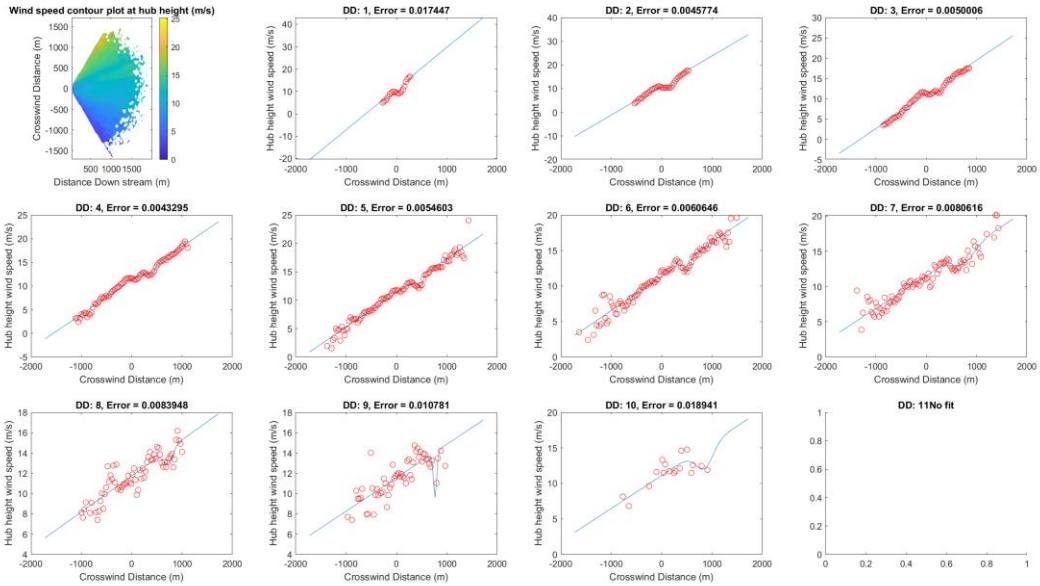

Yaw Offset = 20deg, Mean inflow wind speed = 9.8m/s, Run time =284min, 302 LiDAR scans used

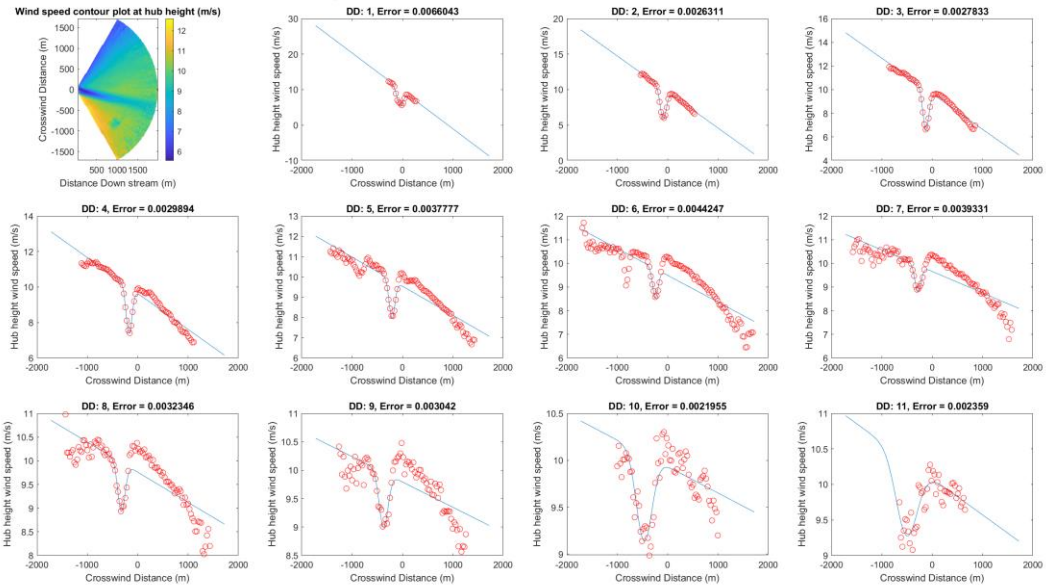

Yaw Offset = 10deg, Mean inflow wind speed = 9.5m/s, Run time =176min, 325 LiDAR scans used

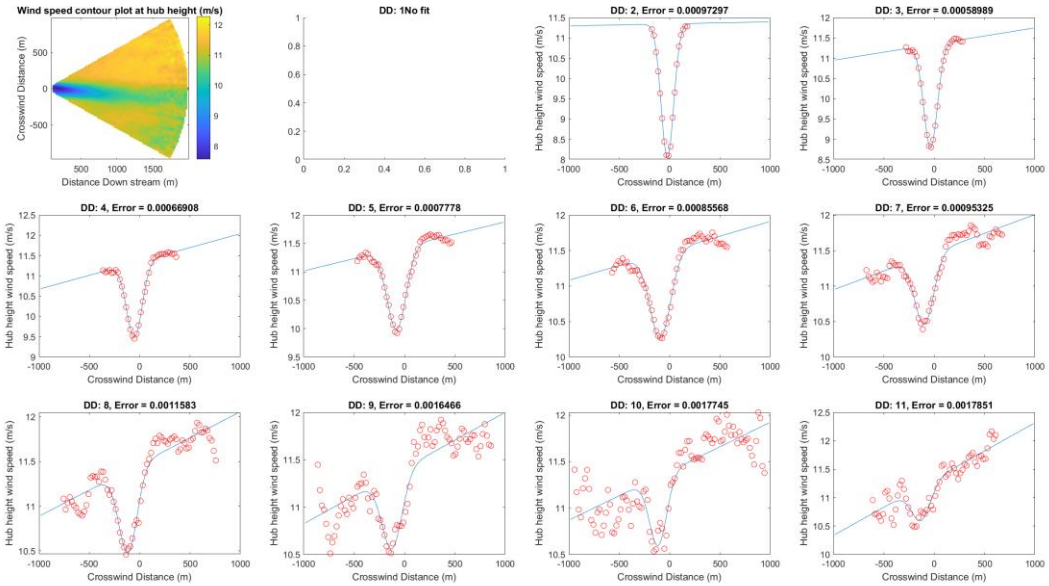

Yaw Offset = 10deg, Mean inflow wind speed = 8.6m/s, Run time =204min, 382 LiDAR scans used

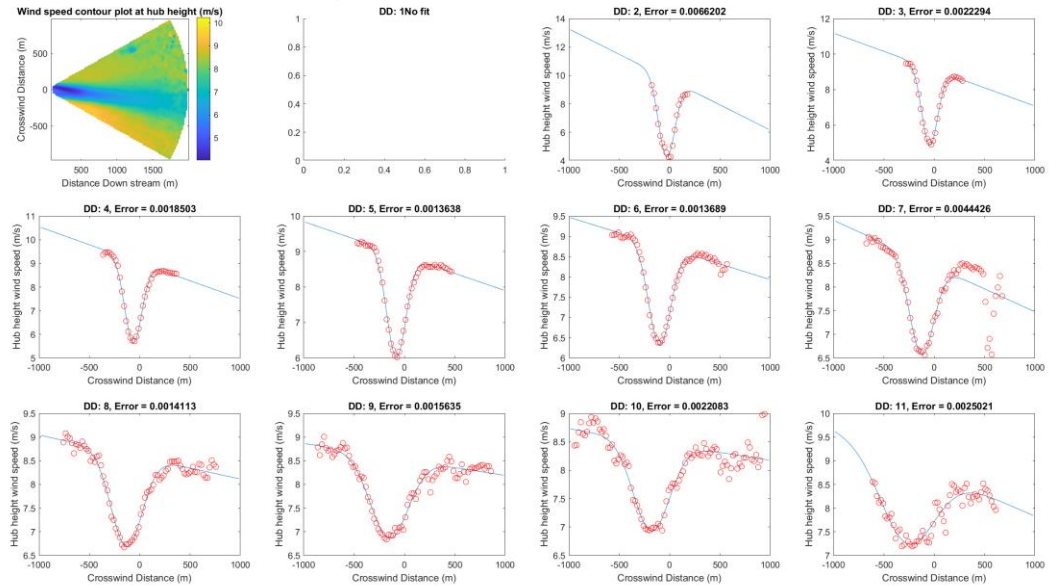

Yaw Offset = -10deg, Mean inflow wind speed = NaNm/s, Run time =17min, 20 LiDAR scans used

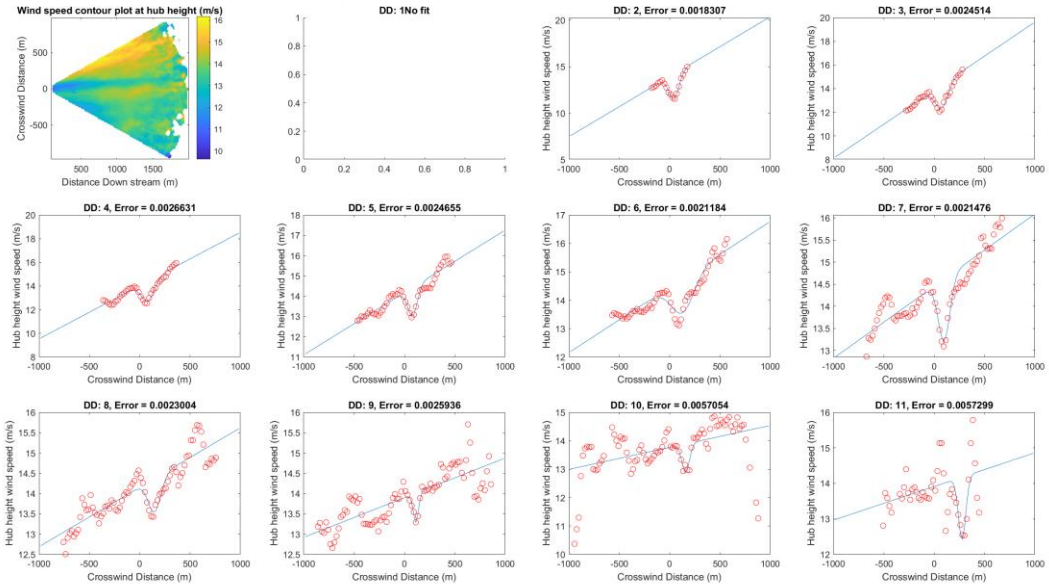

Yaw Offset = 10deg, Mean inflow wind speed = 9.2m/s, Run time =179min, 344 LiDAR scans used

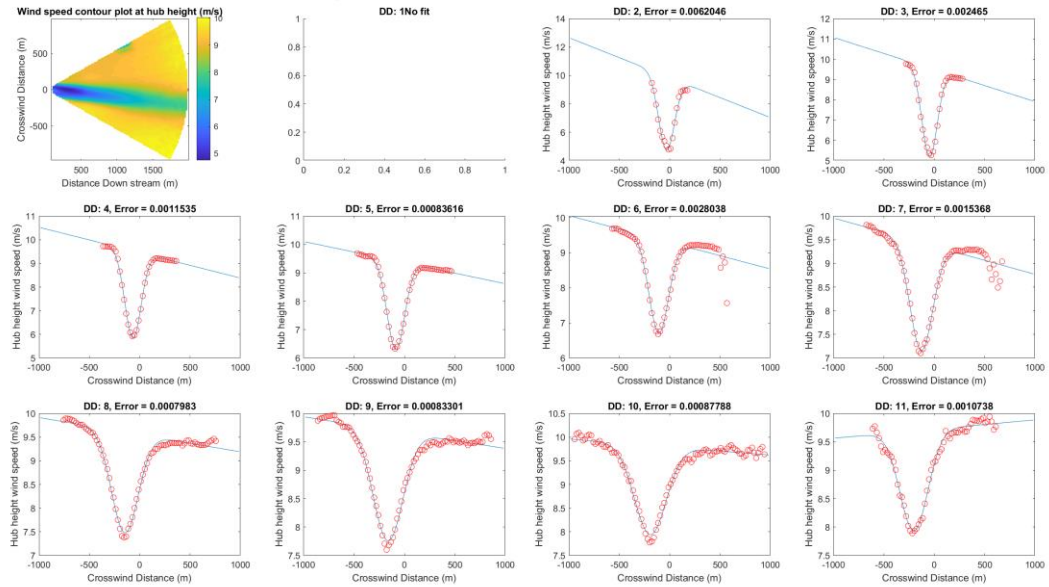

Yaw Offset = 10deg, Mean inflow wind speed = 8.6m/s, Run time =198min, 382 LiDAR scans used

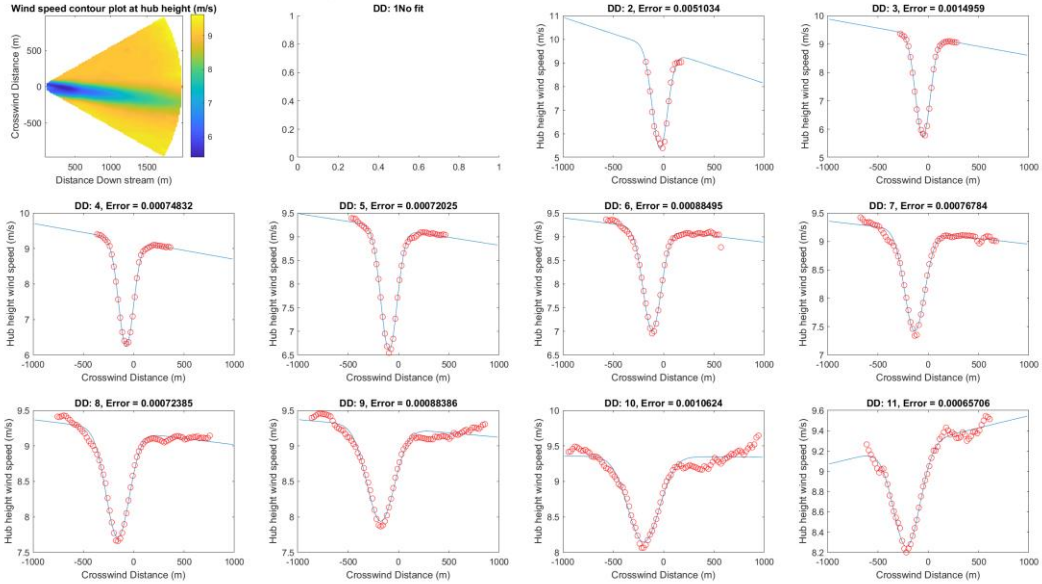

Yaw Offset = -10deg, Mean inflow wind speed = 7.3m/s, Run time =40min, 80 LiDAR scans used

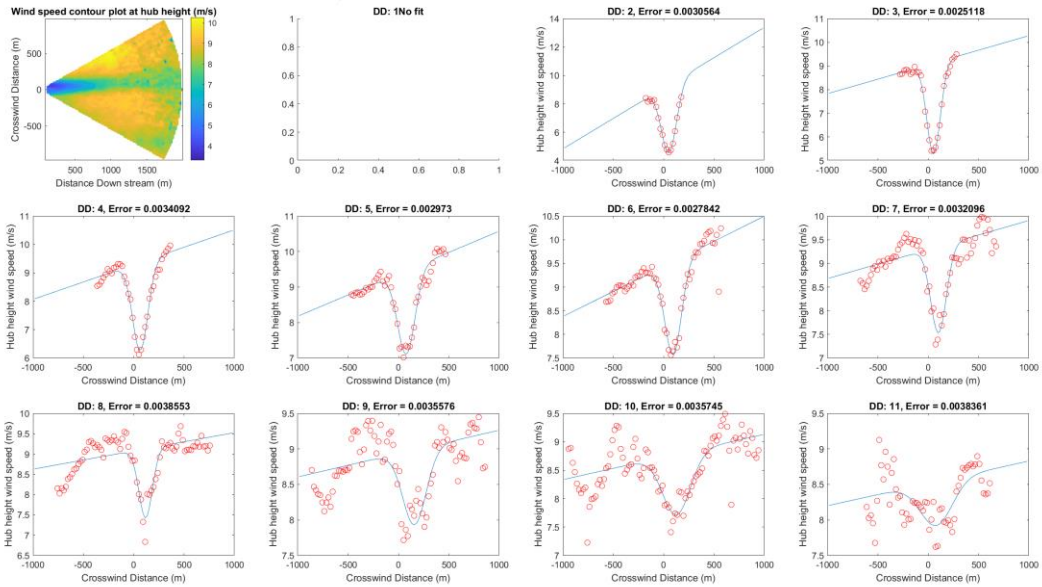

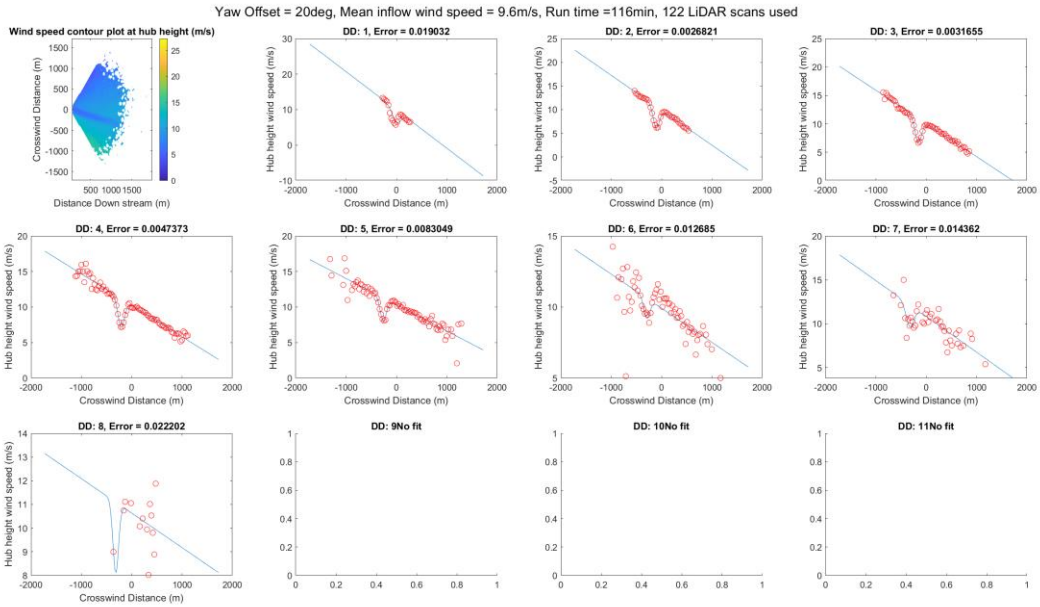
Yaw Offset = 20deg, Mean inflow wind speed = 9.6m/s, Run time =116min, 122 LiDAR scans used
Wind speed contour plot at hub height (m/s)
Crosswind Distance (m)
Distance Down stream (m)
DD: 1, Error = 0.019032
DD: 2, Error = 0.0026821
DD: 3, Error = 0.0031655
DD: 4, Error = 0.0047373
DD: 5, Error = 0.0083049
DD: 6, Error = 0.012685
DD: 7, Error = 0.014362
DD: 8, Error = 0.022202
DD: 9No fit
DD: 10No fit
DD: 11No fit
Hub height wind speed (m/s)
Crosswind Distance (m)